Overoxidized Polypyrrole-Osmium Telluride Quantum Dots Immunosensor for Prostate Specific Antigen - A Cancer Biomarker

By

Lerato Precious Nkuna
(BSc Honours)

A mini-thesis submitted in partial fulfilment of the requirements for the degree
of

Magister Scientiae in Nanoscience

Faculty of Science

University of the Western Cape

Bellville, Cape Town, South Africa

Supervisor: Prof Emmanuel I. Iwuoha

December, 2014

KEYWORDS

Biosensor

Immunosensor

Polypyrrole

$OsTe_2$ quantum dots

Cyclic voltammetry

Square wave voltammetry

Electrochemical impedance spectroscopy

Prostate cancer

Prostate specific antigen

Anti-PSA antibody

ABSTRACT

Prostate cancer is a deadly disease that occurs in the male's prostate gland. A prostate gland is a walnut structure that forms part of the male's reproductive system. Prostate cancer is caused by high level than normal of PSA (Gleason score > 4 ng ml^{-1}) in human blood. Some symptoms associated with high levels of PSA include blood in urine, pain when urinating, difficulty in getting and keeping an erection, blood in semen and pain in upper thigh. An immunosensor is a type of biosensor that has an antigen or antibody fragment as its biological recognition component. The specificity of the molecular recognition of antigen by antibodies to form a stable complex is the basis of immunosensor technology. In this work, overoxidized polypyrrole (OvoxPpy) was electrosynthesized as a novel sensor platform on glassy carbon electrode (GCE). The OvoxPpy was then doped with osmium telluride quantum dots (OsTe$_2$QDs) by drop-coating method to form OsTe$_2$QDs|OvoxPpy|GCE system. The morphology and the size of OsTe$_2$QDs|OvoxPpy|GCE nanocomposite were determined using scanning electron microscopy. The size of thioglycolic acid capped osmium telluride quantum dots (TGA-OsTe$_2$QDs) used as support material for the biosensor was about 2.289 nm. These quantum dots showed an excellent photo-absorption properties with an ultraviolet-visible (UV-Vis) photo absortion band occurring at 406nm associated with high band energy of 3.05 eV. The electrochemical immunosensor for PSA was prepared by immobilizing anti-PSA-antibody onto the OsTe$_2$QDs|OvoxPpy|GCE by drop-coating and allowing it to dry for 2 h. The nanocomposite sensor platform and the immunosensor were electrochemically characterised by voltammetric and impedimetric techniques. The phase shift in Bode diagram at maximum frequency was indicative of kinetic changes. Charge transfer resistance, R_{ct}, was used as the analytical parameter for measuring the interfacial kinetics which occurred as a result of the bio-recognition event between anti-PSA-antibody and PSA. The impedance of

the quantum dot electrode (TGA-OsTe$_2$QDs-Nafion|GCE) was lower (1.490 x 10^4 kΩ) than the impedance of the immunosensor platform (BSA-Anti-PSA-antibody|TGA-OsTe$_2$ QDs|OvoxPpy|GCE), 2.754 x 10^4. The R$_{ct}$ of the immunosensor was found to increase with increasing concentration of PSA. The linearity of the immunosensor at the very low concentration range (1.266 - 4.207 fg ml^{-1}) tested, confirms its high sensitivity for PSA.

DECLARATION

I declare that *Nanocomposite immunosensor for prostate specific antigen* is my own work, that it has not been submitted before for any degree or examination in any other university, and that all the sources I have used or quoted have been indicated or acknowledged as complete references.

Lerato P. Nkuna

Signed……………

ACKNOWLEDGEMENTS

LIST OF FIGURES

current ($\mathbf{p_c 1}$) for the CV's of TGA-OsTe$_2$QDs|OvoxPpy|GCE.

LIST OF TABLES

LIST OF SCHEMES

ACRONYMS AND ABRIVIATIONS

$I_{p,a}$	Anodic peak current
E_{pa}	Anodic peak potential
Anti-PSA antibody	Anti-prostate specific antigen antibody
BSA	Bovin serum albumin
$I_{p,c}$	Cathodic peak current
E_{pc}	Cathodic peak potential
CV	Cyclic voltammetry
EIS	Electrochemical impedance spectroscopy
GCE	Glassy carbon electrode
Ovoxppy	Overoxidized polypyrrole
PBS	Phosphate buffer saline
Ppy	Polypyrrole
PSA	Prostate specific antigen
SWV	Square wave voltammetry
TGA-OsTe$_2$ QDs	Thioglycolic acid capped osmium telluride quantum dots.

TABLE OF CONTENT

CHAPTER 1

1.0 BACKGROUND

1.1 Introduction

Label free impedimetric immunosensors have attracted considerable attention due to their simplicity, high sensitivity, selectivity and low cost. Based on these attractive characteristics, electrochemical impedance spectroscopy (EIS) based sensors are considered as good techniques for clinical and point-of-care diagnostic biomarkers [1]. Among other conductive polymers, polypyrrole is one of the mostly used polymers in electrochemical immunosensors due to its superior biocompatibility, simple synthesis and easy immobilization of different biomolecules [2]. In the label-free immunosensors, the electrochemical signal observed is the changes in the charge transfer resistance of the sensing interface due to the formation of immune-complexes between antibody and antigenic species to which it selectively binds. Usually the formation of immune-complexes inhibits electron flow and increased the charge transfer resistance of the sensing interface linearly, with the change in impedance being proportional to the concentration of the PSA antigen. The label-free micro-immunosensors are still faced with major challenges such as low detection limit and suffering from interferences due to unspecific bindings [3]. To overcome this problem, several strategies have been employed to enhance the immobilization of the biorecognition components, including incorporation of nanoparticles [4], use of porous material to increase the surface area [5] and the orientation-controlled antigen immobilization techniques. Furthermore, it was found that the sensitivity and selectivity of polypyrrole can be further enhanced by overoxidation and embedding metal nanoparticles into the porous polymer matrix to form a metal- polymer composite [6]. Current dissertation describes the application of overoxidized

polypyrrole and osmium telluride quantum dots as a novel matrix for the development of a label-free impedimetric immunosensor with anti-PSA antibody as the immobilized biological component. The overall emphasis of the immunosensor was for fast and accurate detection of prostate specific antigen in low concentrations, which can be used as a prostate cancer biomarker. Electrochemical impedance spectroscopy (EIS) has been considered to be a powerful tool for characterization of bulk and surface properties. This technique has already found analytical application in characterization of proteins immobilization on electrodes and for determination of affinity based antibody-antigen interaction [7]. For EIS measurements, small AC voltage signal perturbations of different frequencies are applied to the system and the current response is determined [8]. Hence, by applying cyclic voltammetry and impedance spectroscopy, the qualitative picture of antigen modified polymer platform during reaction with an antibody can be achieved.

1.2 Problem identification

Prostate cancer is a genetic disorder, with 1 in 23 men being positively diagnosed in South Africa. It is caused by high level than normal of prostate specific antigen (Gleason score > 4 ng ml^{-1}) in male serum. Prostate cancer occurs in the prostate gland which is a walnut structure that forms part of the male's reproductive system. It is a common cause of infertility in men. However, recognizing prostate cancer can be difficult since more of its symptoms are similar to those of benign prostate hypertension. As a result, prostate cancer is commonly under diagnosed or misdiagnosed.

The current clinical methods available for diagnosing prostate cancer include: digital rectal examination (DRE), transrectal ultrasound (TRUS). Magnetic resonance imaging (MRI) and a series of blood test. However, these methods are expensive, lack sensitivity and selectivity.

Most of these facilities are found in private health-cares, meaning that only men who have access to medical aid will afford them. Therefore there is a need of a point-of-care measuring device (immunosensor) for rapid quantification and accurate detection of prostate specific antigen in lower concentrations to aid in point-of-care analysis.

1.3 The aims and objectives of the research

- ❖ To electropolymerize pyrrole on glassy carbon working electrode
- ❖ To electropolymerize and characterize both pyrrole and overoxidized polypyrrole for the application as an immobilization platform of anti-PSA-antibody
- ❖ To immobilize osmium telluride quantum dots on the overoxidized electrode to form $OsTe_2QDs|OvoxPpy$ nanocomposite
- ❖ To evaluate the platform and immunosensor using cyclic voltammetry and electrochemical impedance spectroscopy.
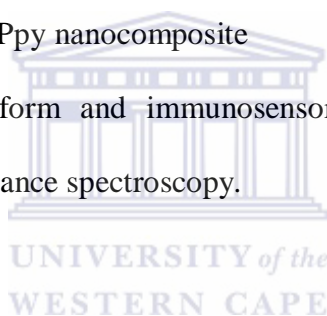
1.4 Motivation and Rationale

Available clinical methods for diagnosing prostate cancer and quantification of prostate specific antigen include a series of blood test, digital rectal examination, trans rectal examination and magnetic resonance imaging. However, these methods are less sensitive and specific, they require a skilled operator, they do not give real results on time and they are expensive. Therefore, faster and cheaper devices are highly desired for replacement of time-consuming laboratory analysis. The presence of PSA is highly suggestive of prostate cancer. Direct measurement of anti-PSA-antibody to PSA can now be done by immunoassay methods which are capable of direct and specific detection of proteins and peptides in 'real' samples like human serum and plasma. In most immunosensors the antibody is immobilized onto a conductive support and the electrical properties of the interface are modified when the

antibody reacts with antigen of interest. The prior literature survey information exemplified the fact that tedious methods of continuous blood testing for PSA together with lifelong fat-free diet, is an absolute necessity to ensure effective treatment, whilst concurrently reducing mortality. Hence, superior method for executing the task was shown to be label-free impedimetric immunosensors, in which appropriate miniaturization of bio-affinitive and transducer components for adequate antigen-antibody interaction, is expected to allow for fast and accurate diagnosis. Considering these aspects, the motive of the study was thus established.

1.5 Research framework

My thesis was designed to follow some sequential steps which were optimized over time. In line with the study objectives and the experimental procedure, a broad research design can be summarized in the diagram below:

```
┌─────────────────┐                              ┌─────────────────┐
│  Selection of   │◄────────────────────────────►│  Preparation of │
│  experimental   │                              │    chemicals    │
│   procedure     │                              │                 │
└─────────────────┘            │                 └─────────────────┘
                               ▼
          ┌──────────────────────────────────────────┐
          │ Electrode preparation:                     │
          │ ❖Pre-treatment of working electrode (GCE)  │
          │ ❖Preparation of overoxidized polypyrrole   │
          │ ❖Drop-coating OsTe₂QDs on OvoxPpy│GCE       │
          └──────────────────────────────────────────┘
                               │
                               ▼
┌─────────────────┐   ┌───────────────────┐   ┌─────────────────────┐
│ Surface         │◄──│  characterization │──►│ Cyclic voltammetry: │
│ morphology:     │   │                   │   │ Argon saturated PBS │
│ SEM             │   │                   │   │ (pH 7.0)            │
└─────────────────┘   └───────────────────┘   └─────────────────────┘
                               │
                               ▼
          ┌──────────────────────────────────────────┐
          │ Immunosensor fabrication:                  │
          │ ❖Anti-PSA antibody immobilization          │
          │ ❖BSA blocking                              │
          │ ❖PSA detection                             │
          └──────────────────────────────────────────┘
                               ▲
                               │
          ┌──────────────────────────────────────────┐
          │ Electrochemical measurements:              │
          │ Faradaic impedance measurements in 0.1     │
          │ M PBS (pH 7.0)                             │
          │                                            │
          └──────────────────────────────────────────┘
                               │
                               ▼
          ┌──────────────────────────────────────────┐
          │         Immunosensor evaluation            │
          └──────────────────────────────────────────┘
```

Scheme 1. Research framework

1.6 Thesis outline

The thesis will be presented as outlined below.

An introduction giving various aspect that contributes to the increased mortality rate with regard to undiagnosed or misdiagnosis of prostate cancer and the importance for adequate and continuous health assessment are raised in this chapter. Prostate cancer analysis, the disadvantages associated with current diagnostic methods, the risk associated with long term undiagnosed prostate cancer and the need for developing immunosensors for fast and accurate diagnosis of prostate cancer are also highlighted. The use and advantages of osmium telluride quantum dots that possibly lead to fabrication of the immunosensor platform in this study are discussed. The objective of this study, frame work and delimitations of this study are also discussed in this chapter.
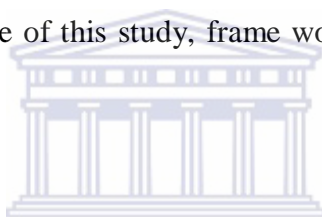
A literature review relating polypyrrole, the role of doped/undoped polypyrrole and overoxidized polypyrrole will be presented in Chapter 2. Furthermore, various aspects of biosensors, biomolecules as well as immobilization methods are presented in Chapter 2. This chapter also covers a brief introduction of conductive polymers containing metals as well as an introduction to overoxidized polypyrrole matrix for uniform incorporation of $OsTe_2QDs$ and its use as immobilization platform. Characterization methods, mainly electrochemical impedance spectroscopy, cyclic voltammetry and scanning electron microscopy are also briefly discussed in this chapter. In Chapter 3, information regarding the chemicals used, instrumentation and research design with an overview of all the sequential steps taken to solve the thesis problems are described.

In Chapters 4 and 5 results are presented and discussions are offered. Chapter 4 focuses on the characterization of the developed nanocomposite modified electrode, whereas, Chapter 5 highlights the immunosensor response after each consecutive incubation step based on electrochemical impedance spectroscopy. In addition, a detailed description of the immunosensor and its analytical characteristics such as stability, detection limit, selectivity, linear range and reproducibility is present. This chapter also features the results and discussion of the developed immunosensor response to various antigen concentrations.

Finally, Chapter 6 represents the conclusions.

UNIVERSITY *of the*
WESTERN CAPE

Chapter review

This Chapter provides a clear and brief survey of concepts, biosensor types and theory, a brief introduction to prostate cancer and diagnostic methods. The chapter also gives information about prostate specific antigen and anti-prostate specific antigen antibody, an insight on supporting materials used to fabricate the biosensor. This includes materials such as conductive polymers, quantum dots, types and applications. Furthermore, it covers a brief survey on enzymes and enzyme kinetics

2.0 Literature review

2.1 Polypyrrole

Recently polypyrrole (Ppy) received considerable application in bioanalytical applications particularly in developing electrochemical immunosensors [9]. Polypyrrole is a conductive polymer known for its unique chemical and electrochemical properties. It has good biocompatibility in vivo, good thermal stability, facile synthesis and high conductivity [10]. Ppy can be represented as a molecule containing a conjugation of double bonds (π-electrons) that can be oxidized or reduced electronically by dopants [11].
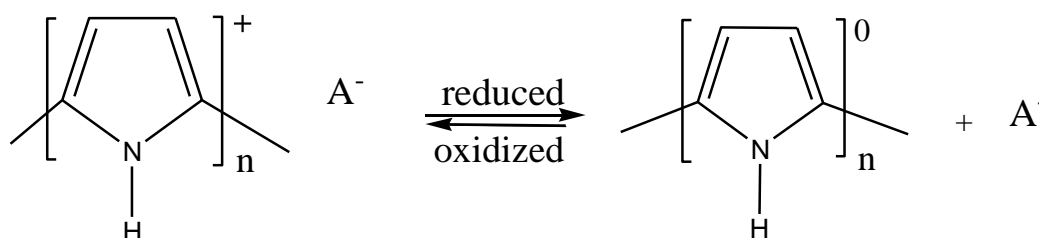
Scheme 2. Ion exchange behaviour of Ppy by oxidizing agent (p-doping) or reducing agent (n-doping).

Conducting polymers can be prepared chemically or electrochemically by polymerizing a monomer in aqueous solution. During polymerization process, ion exchange process between the polymer and the surrounding electrolyte solution is of great importance. Movement of ions in polymer depends on packing density of polymer chain and the strength between the polymer and the anions. Redox activity of conducting polymers depends on the doping level and reversibility of anions during redox cycle [12].

Chemical synthesis of polypyrrole involves oxidation of pyrrole monomer in the presence of oxidant. However, electropolymerization method is the most considered to produce better conductive polymers. Pyrrole monomer is electrochemically oxidized at the surface of the electrode [13]. The cation-radical mechanism indicates that alternation of single (σ)-bonds and double (π) bonds coupled with atoms that provide p-orbital continuous orbital overlap (Nitrogen atom) makes the polymer to be intrinsically conductive. Overlap of electrons causes charge delocalization along the polymer backbone. However conjugation alone does not make the polymer conductive. The polymer requires doping in order to facilitate electron movement [14].
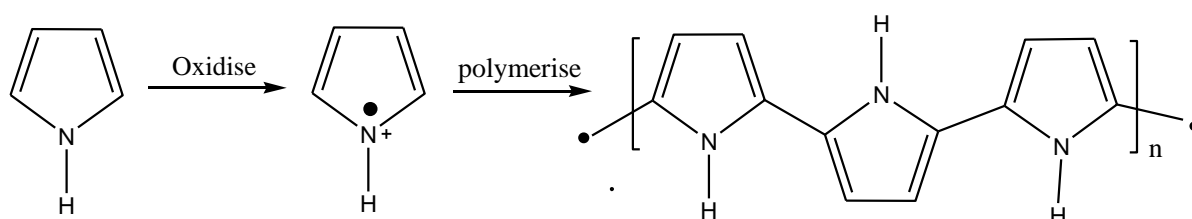
Scheme 3. Anionic synthesis of polypyrrole from pyrrole monomer.

2.2 Effect of dope-undope polypyrrole

Ion-exchange process plays an important role in the conductive ability of the polymer. During redox process, the polymer is kept neutral by repulsion of anions or by incorporating cations in the polymer. The ion exchange process depends on the nature of the dopant ions. Small dopant ions (ClO_4^-) are released by applying negative potential to the polymer that exhibits anion-exchanger behaviour [15]. Conductivity is achieved by p-doping (oxidation) or n-doping (reduction) followed by ion exchange process. Due to alternation of σ-bonds and π-bonds along the polymer backbone, charge species will be delocalized along carbon chain (Sp^2 hybridized) allowing electron transport thus becoming conductive [16].

Doping occurs when positive potential is applied to the polymer causing oxidation and anions in the aqueous solution are incorporated in the film. While in the undope process occurs when sufficient negative potential is applied to the polymer causing anions to be expelled and reducing the polymer charge to neutral state (Ppy^+ to Ppy^0) [17]. However, the effect of doping and undoping causes structural deformation of the polymer. Upon overoxidation, Ppy loses conductivity due to irreversible oxidation thereby creating pores on the film. This allows incorporation of nanoclusters. Due to their high electric conductivity, optical properties, electrocatalytic and biocompatibility, $OsTe_2$ quantum dots are considered best materials for electrochemical sensors and biosensor application [18].

2.3 Overoxidized polypyrrole

Overoxidation of polypyrrole (Ppy) occurs at high potentials causing degradation of polymer conductivity. During this process, doping ions are expelled from the film introducing oxygen containing groups such as carbonyls and carboxylic groups thereby destroying conjugation structure of the film. This occurs at high pH's and results in a porous film structure with

perm-selective properties [19]. Overoxidation is a slow process caused by nucleophilic attacks (water molecules) present at radical cationic counters. The rate of overoxidation is higher and has high selectivity as shown in Scheme 4 [20].

$$H_2O \longrightarrow 1/2\, O_2 + 2\, H^+ + 2\, e^-$$
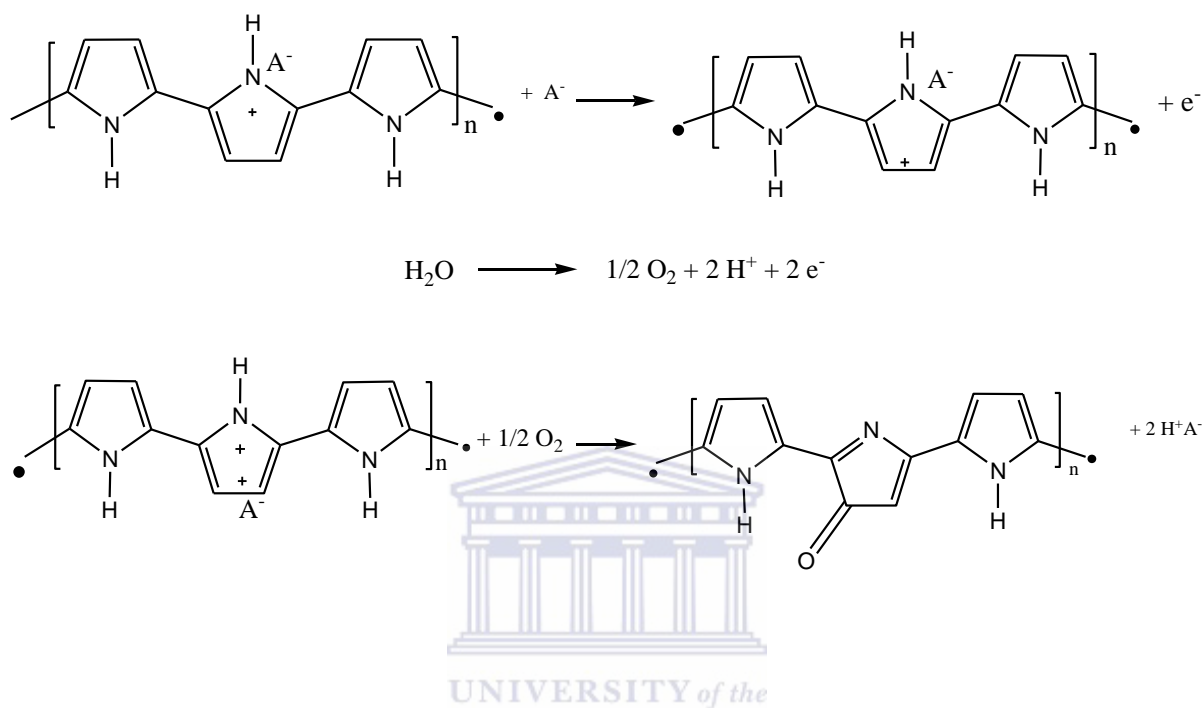
Scheme 4. Reactions that occurs during overoxidation of Ppy film.

2.5 Prostate cancer

Prostate cancer is a genetic disorder caused by abnormalities in activation of oncogenes and inactivation of tumor suppressor genes in the prostate [21]. Oncogenes or protooncogenes controls normal cell growth, signal transduction, modifies protein functions and other cell functions. Examples of oncogenes include ras family, c-myc, neu, c-fos, c-jun and bcl-2. At protein level, changes in oncogenes structure and concentration may lead to human tumors. Tumor gene suppressors (TGS) are important for developing biomarker for cancer detection [22]. Among other biomarkers, PSA is considered to be an important organ specific marker for detection of cancer. TGS helps in controlling the level of PSA in human serum. The Gleason score (tumor grading) is important for risk analysis and prognostication [23].

11

According to the Gleason, PSA levels of > 4 ng ml^{-1} are associated with prostate cancer [24]. Symptoms associated with high levels of PSA include blood in urine, pain when urinating, difficulty in getting or keeping an erection, blood in semen and pain in hips or upper thighs [25].

2.5.1 Diagnostic methods

Recently, PSA screening, digital rectal examination (DRE) and trans rectal ultrasound (TRUS) needle biopsy are used as diagnostic tools for the detection of prostate cancer [26]. PSA screening involves the evaluation of the amount of PSA in blood. However, this method alone lacks specificity because it can also be used to detect other diseases such as benign prostatic hyperplasia (BPH) (increase in size of the prostate) [27]. To validate PSA test, DRE is performed. DRE evaluates the size, shape and texture of the prostate through the rectum. However, DRE lacks sensitivity as many men might undergo unnecessary biopsy due to false positive results [28]. On the other hand, TRUS uses sound waves to image the prostate cells under video microscope. Some cells might not be normal but that does not mean that they are cancer cells. These suspicious cells might be due to prostatic intraepithelial neoplasia (PIN) which controls cell growth [29]. Since patients with prostate cancer have high PSA levels in the blood, a direct measurement of PSA using anti-PSA antibody can be done using immunoassay methods which are competent for direct and specific detections of proteins in serum. Therefore an anti-PSA antibody can be used as a screening test for prostate cancer. In such case a PSA test against anti-PSA antibody will be performed [30].

2.5.2 Prostate specific antigen: analytical biomarker for diagnosing prostate cancer

In 1981, PSA was considered to be a true marker for prostate cancer [31]. PSA is an androgen-regulated serine protease secreted by epithelial cells in the prostate gland. It is a

member of the Kallikrein tissue family and it is used to cleave semenogelins in the seminal coagulum [32]. PSA is composed of single chain of glycoproteins which consist of 93% peptide and 7% carbohydrates and alsoan isoelectric pH of 6.9 [34]. It exhibits proteolytic activity like chymotrypsin and has molecular weight of 33-34 kDA estimated by sodium dodycyl sulphate polyacrylamide gel electrophorisis (SDS-PAGE) [33].

In blood PSA occurs as both unbound free PSA (fPSA) and complexed PSA (PSA-ACT) that is bound to either alpha-antichymotrypsin or alpha-macroglobulin. Major portions of PSA in serum are PSA-ACT and only a small portion is fPSA. Over the years, total PSA (tPSA) has been used as a marker for early detection of cancer. However, it has limitations in differentiating between BPH and prostate cancer [35]. Studies show that tPSA can be used to measure free-to-total PSA (f/tPSA) ratio because it is easy to differentiate between BPH and cancer using f/tPSA ratio than using tPSA alone [36]. fPSA is low in patients with prostate cancer [37].
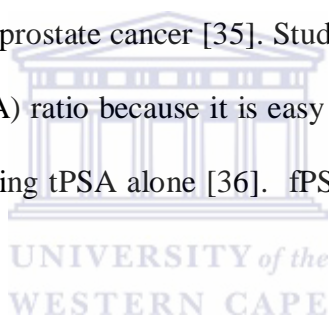
2.5.3 Anti-PSA antibody

Anti-PSA antibody (IgG) has a very high affinity for immunoreactive fPSA and alpha-antichymotrypsin complexed PSA [38]. IgG recognizes the six epitope regions of PSA. Immunological cross reactivity of these two proteins can help in determining the levels of PSA during prostate cancer diagnosis [39].

5.5.3.1 Electrochemistry of antibody modified electrode

Immobilization of biomolecules onto a modified electrode is a key factor in developing an immunosensor [40]. Antibody molecules are immobilized onto a conductive support to interact with the antigen molecules forming antibody-antigen complex [41]. When the

antibody is directly adsorbed onto the surface, they generally adopt random orientations which hinder their *in vivo* or *in vitro* immunoaffinities. To overcome this problem i.e. preserving their binding activity and specificity, antibodies are attached to a solid support [42].

Excellent properties of conducting polymers allow them to supply a suitable interface for attaching biomolecules onto a micro-sized surface [43]. Direct immobilization of antibodies onto a conductive solid support hampers their sensitivity and signal background. Due to steric hindrance and random orientation of antibodies onto a solid support, impedance spectroscopy is considered an important tool for interrogating interfacial mechanism for antibody-antigen reaction. Antibody-antigen bindings are validated by detection in shift in impedance and change in capacitance of the electrode interface. Therefore EIS is the best technique to study antibody-antigen interactions at conductive electrode [44].
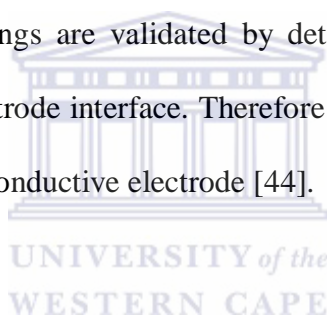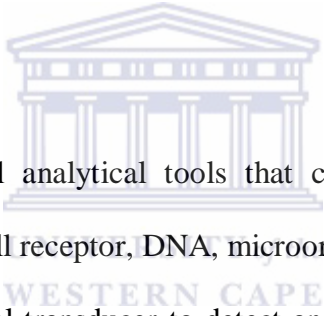
2.5.3.2 Immobilization and non-specific adsorption of proteins

Antibody immobilization techniques must have the following characteristics in order to be suitable for immunosensor design. i) Substrate used for immobilization should be inert to nonspecific adsorption of proteins. ii) They should prevent protein denaturing and unspecific binding of other proteins in the assay. This will avoid false positive and negative results of the assay and increases sensitivity of the matrix. iii) The antibody must be covalently bonded to the modified substrate to increase selectivity and to make the antibody confined in a defined orientation. iv) The method should allow rapid reaction between small amount of the antibody and the modified support to minimize solvent evaporation. v) The method should also be able to control antibody density, to ease steric interactions of neighboring proteins and ensures reproducibility of immobilized antibody [45]. Biocatalytic efficiency can be

14

improved by manipulating the structure of the carrier material for antibody immobilization. Reducing the size of protein-carrier material can improve the efficiency of immobilized biomolecules [46]. In the case of surface attachment, small nanoparticles can provide large surface area for biomolecules attachment.

Bovine serum albumin (BSA) is efficient for blocking unspecific adsorption of proteins onto a modified electrode. The adsorption mechanism of BSA involves random sequential adsorption [47].In this study BSA was utilized as a blocking agent after antibody immobilization. This is a constructive method to prevent non-specific bindings and false positive results [48].

2.6 Biosensors

Biosensors are defined as small analytical tools that combine a biological recognition component (enzyme, antibody, cell receptor, DNA, microorganisms, organelles, nucleic acids etc) with a physicochemical signal transducer to detect an analyte with the generated signal being proportional to the analyte concentration. A biosensor is composed of two parts: the biological and the transducer part. The biological part consists of enzymes or antibodies that interact with the analyte particle causing physical changes to the particle. The transducer part converts biological information to a measurable signal. During analysis, specific biological part is immobilized onto a transducer allowing specific and efficient interaction with analyte molecules [49]. Advantages of biosensors over other detection methods include high specificity and selectivity towards biological objects [50]. According to the interaction mode, there are two types of biosensors: biocatalytic-based biosensor and bioaffinity-based biosensor. Biocatalytic-based biosensor uses enzymes (as biological compound) to catalyze

biochemical reaction. Bioaffinity-based biosensor monitors specific bindings of proteins, antibodies, membranes, cells and receptors for biomolecular recognition [51].

2.6.1 Electrochemical biosensor

The basic principle for electrochemical biosensor is that chemical reactions between immobilized biomolecules and target analyte produces or consumes ions or electrons which affect measurable electrical properties of the solution such as electrical current or potential [52]. Operative principle of electrochemical biosensors utilizes potentiometric, amperometric and impedimetric transducers to convert chemical information into measurable signal [53].
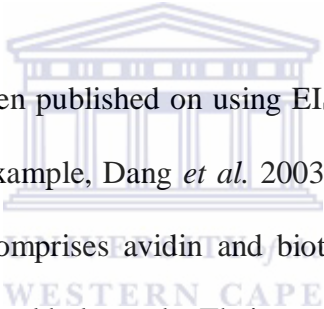
2.6.1.1 Potentiometric biosensor

Potentiometric biosensor is made up of an ion-selective electrode that transduces biological recognitions into electrical signal. Other potentiometric transducers include glass electrode, ion-selective field effect transistor and two-terminal microsensor. Potentiometric transducers measures potential differences across as ion-selective membrane that separates tow solution at near zero current. However, this type of biosensor has the following drawbacks: high detection limit, inactive response to solution of low analyte concentration, risk to interferences, expensive to fabricate and unstable [54].

2.6.1.2 Conductometric/ impedimetric biosensor

Impedimetric biosensors are based on enzyme reactions which involve consumption or production of charged species leading to change in ionic composition of analyte sample. Advantages of impedimetric biosensors include (a) the use of thin film electrodes, (b) the fact that the transducers are not light sensitive, and (c) the techniques involves the use of low voltage which decreases power consumption. However, the problem with impedimetric biosensors arises from their lack of sensitivity [55].

During immunosensor construction, the antibody is immobilized onto a solid support and allowed to interact with antigen of interest. Surface organizations of antibodies play a vital role in immunosensor fabrication. Characterizing immobilization of the antibody with its stability and ability to interact with a specific antigen optimizes the catalytic performance of the immunosensor (i.e. stability, selectivity and response time). The formation of antibody-antigen complex is used to study biomolecular recognition process by measuring resistive and capacitive change in the reaction. The binding event between antibody and antigen was studied using EIS and the results indicated that covalent binding of antibody on the electrode surface is required for successful impedance-based immunosensor [56].

Several literature articles have been published on using EIS to monitor surface properties of developed immunosensors. For example, Dang *et al.* 2003 [50] used EIS to characterize the growth of multilayer film that comprises avidin and biotin labeled antibody formed on a mercaptopropionic acid modified gold electrode. Their results indicated that electron transfer resistance in directly proportional to the number of avidin/biotin antibody layer. Zayats *et al.* 2002 [57] fabricated an ion sensitive field effect transistor (ISFET) to monitor antibody-antigen binding process and used EIS to interrogate the thickness of different films formed on ISFET.

2.6.2.1.3 Amperometric biosensor

Amperometric biosensors measure current resulting from electrochemical redox (reduction and oxidation) reactions of enzyme systems. It detects concentration-dependent current generated during redox reaction of electroactive species at the electrode surface to which specific antibody-antigen interactions occurs at constant current potentials. During antibody-

antigen detection, current potential is directly proportional to the antigen-antibody specific bindings [58]. This is due to the mass transfer rate of the detecting species in the reaction and faradaic kinetic or charge transfer at the electrode surface. Mass transfer process occurs through (a) ionic migration as a result of current potential gradient, (b) concentration gradient, and (c) bulk transfer by natural or force convection [59]. Signal transduction is achieved by controlling current potentials at the working electrode and monitor current as a function of time. The resulting current reflects on the rate of recognition event and it is proportional to the analyte concentration [60].

The rate of enzyme reaction depends on temperature, pH, ions, cofactors and competitive or non-competitive inhibitors present in the analyte solution. Redox compounds such as oxygen, ascorbate, thiols or certain drugs may interfere with the reaction. Thus, to overcome this problem, mediators such as chemical electron-acceptors are employed, scheme 4. For example, ferrocen-ferricinium redox system can be utilized to mediate electron transfer from glucose oxidase to graphite electrodes [61].
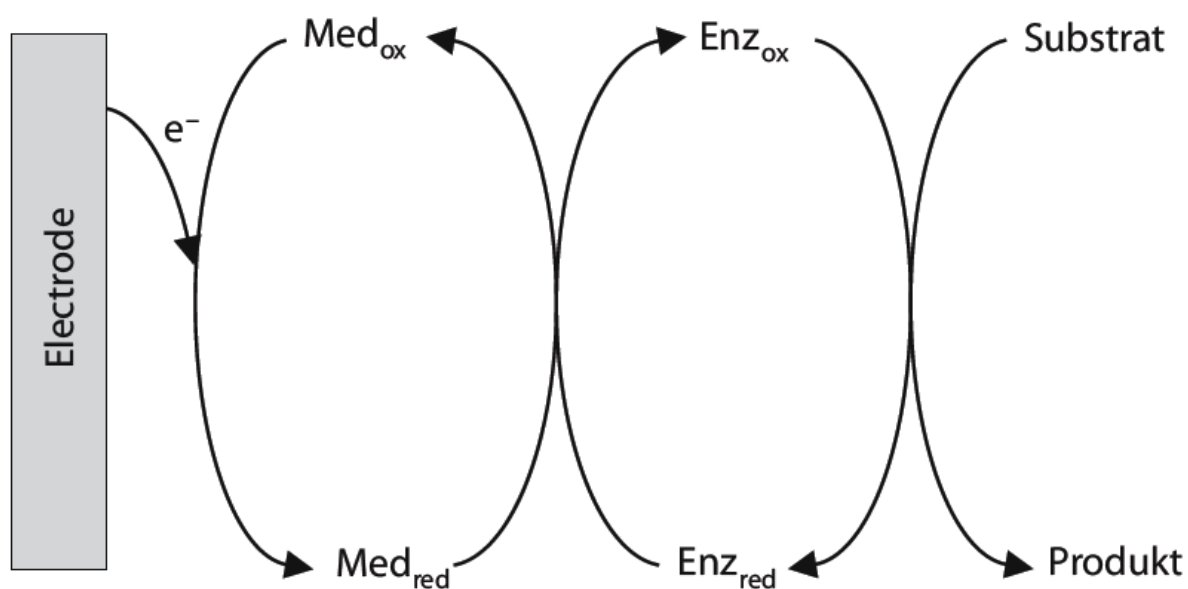
Scheme 5. Reaction mechanisms for enzyme-linked amperometric biosensor.

2.7 Electrochemical immunosensors

Electrochemical immunosensors are based on specific reaction between antibody and antigen that occurs directly on the electrochemical transducer. Electrochemical immunosensors can be performed both with labels and without labels (label free) [62]. Direct detection of the label free immunosensor can be performed by cyclic voltammetry, chronoamperometry, impedimetry and by measuring current during potential pulse (pulsed amperometry) impedimetry. These methods can detect change in capacitance and resistance of the electrode induced by binding of proteins. Electrical capacitance and ion diffusion of the antibody-antigen complex affects electrochemical impedance of the electrode. Therefore EIS is the best method for interrogating label-free detections of antibody-antigen interaction in real life [63]. Common used enzyme labels include peroxidase, glucose oxidase, alkaline phosphatase or catalase. Enzyme labels have high stability [64].
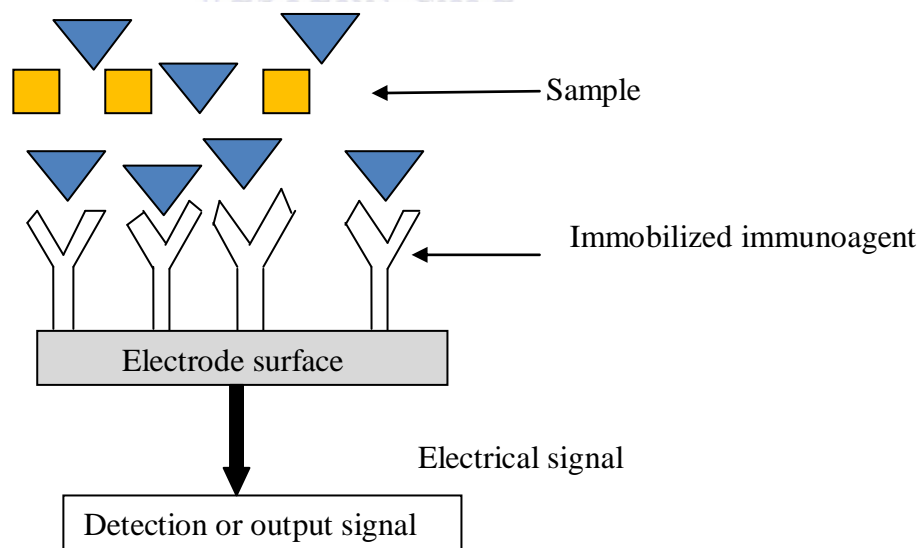
Scheme 6. Schematic representation of a working principle of an immunosensor.

2.7.1 Enzymes

Enzymes are proteins in nature and functions as catalyst that accelerates reactions by lowering that activation energy. They are also known to be biological catalyst that accelerates chemical reactions without changing equilibrium. Enzyme catalysis is important to make biochemical reactions precede at faster speed in physiological conditions. Enzymatic reactions occur on a substrate [65]. When an enzyme (*E*) bind to their substrate (*S*), an enzyme-substrate complex (*ES*) is formed. The substrate binds to the specific site of the enzyme called an active site. After the formation of enzyme-substrate complex, the substrate changes into the product (*P*) of the reaction which is then released from the enzyme.

$$E + S \leftrightarrow ES \leftrightarrow E + P \qquad (1)$$
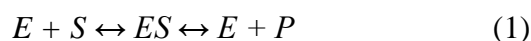
Enzymes differ from other ordinary biomolecular catalyst in that, a) they are specific i.e. they react on specific substrate producing a specific product unlike chemical catalyst that reacts with a variety of substrate. For example hydroxide ions can catalyze formation of double bonds and also hydrolysis of esters, b) enzyme activity occur under mild conditions such as room temperature (25 °C), standard pressure, and pH (5 − 9), c) enzymes are steriospecific i.e. during catalysis of water by enzymes, either the D or L isomer can be formed but not both. In contrast, chemical catalyst forms both products in a 50:50 ratio, d) enzymes are regulated by concentration of the substrate [66]. Enzyme activity is affected by cofactors and coenzymes. Cofactors are non-protein substances that ensure that enzyme-controlled reactions occur at an appropriate rate. Examples of cofactors may include inorganic metal ions such as iron, magnesium or zinc. Coenzymes are non-protein substances that bind to the active site of the enzyme for a short period of time. Some examples of coenzymes include organic compounds such as NAD^+, $NADP^+$ and FAD^+. These organic compounds are involved in the electron transfer and hydrogen release during catabolic pathways [67].

Enzymes that can be studied using electrochemistry must have one surface exposed to the redox center which facilitates electron transfer from the electrode. Enzymes can be used as labels during the construction of immunosensors. Enzyme-labeled antibodies can be used for quantitative determination of antigens in solution in immunosensors [68].

2.7.2 Antibody structure

Antibodies are also known as immunoglobulin (Ig) and have a "Y" shaped structure. Immunoglobins are composed of five major classes (isotypes) namely immunoglobin G (IgG), Immunoglobins A (IgA), Immunoglobins M (IgM), immunoglobin D (IgD) and immunoglobin E (IgE). They consist of two light chains (L) and two heavy chains (H). The (L) chain contains the variable region (V_L) (which is responsible for recognition of antigens) and the constant region (C_L). On the other hand, the heavy chain consists of one variable and 3 constant (C_H) domains (C_H1, C_H2, C_H3). The variable regions are responsible for antigen binding while the constant regions are responsible for different biological functions such as binding to cell surface receptors [38]. The C_H2 domain is involved in the activation of complement system. C_H1 and C_H2 are known as the hinge regions of the heavy chains. C_L and C_H1 are linked by disulphide bonds.

The variable region is composed of 110-130 amino acids. It is subdivided into the hypervariable (HV) and framework (FR) regions. There are three HV regions, namely HV1, HV2 and aHV3. These regions are indirect contact with the antigen surface hence they are sometimes referred to as complementary determining regions (CDR). The FR regions are more stable and form a beta-sheet structure which helps to keep the HV region in place for contact with the antigen [39].

The isotypes IgG, IgA, IgM, IgD, and IgE are differentiated by their heavy chains γ, α, μ, ε, δ respectively. Each of the IgD, IgE and IgG antibodies consist of a single structure unit., whereas IgA antibodies consist of two units and IgM antibodies consist of five disulfide-liked structural unit. On the other hand the IgG antibodies are divided into four isotypes (IgG 1, IgG 2, IgG 3, IgG 4). Proteolytic enzyme such as pepsins and papains cleaves IgG into specific fragments. When IgG is treated with pepsin, F (ab')$_2$ fragments are generated which encloses the two Fab regions linked by the hinge region. F(ab')$_2$ molecule is bivalent and is capable of precipitating an antigen. Papain cleaves IgG molecule in the hinge region between C_H1 and C_H2 domains producing an identical Fab fragment which retains their antigen-binding ability and one non-antigen-binding fragment (FC) region. FC region helps in distinguishing different types of antibodies from one another [69].
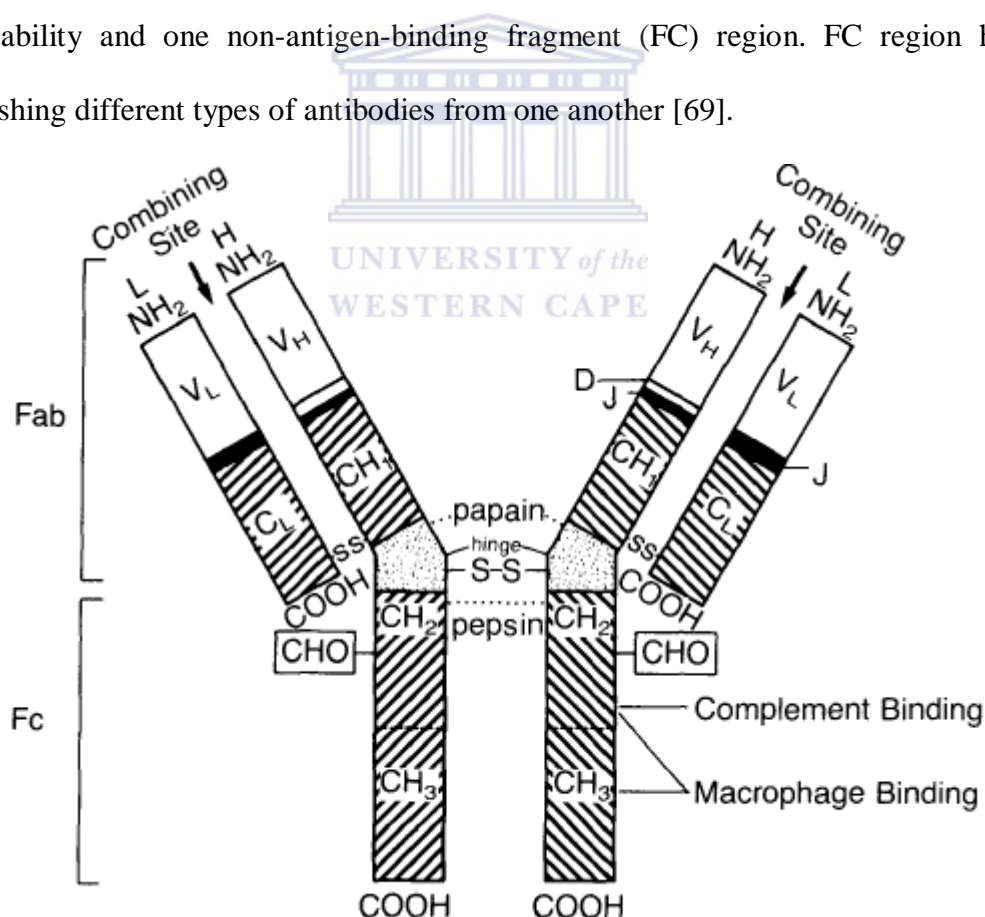
Scheme 7. Schematic representation of immunoglobins with heavy chains (H) and light chains (L).

2.7. 3 Antibody production and properties

When foreign substance enters the immune system, they are said to be antigens. This causes problems with the immune system leading to illness and infection. When the immune system detects an antigen, cells work together to recognize the antigen, thereby triggering the B lymphocytes to produce antibodies. Antibodies are characterized by features such as solubility in strong salt solutions, electrolytic charge and isoelectric point, molecular weight (150000-180000 molar mass per monomer unit) and antigenicity. The antibodies continue to protect and exist in the body in case there are more antigens present. The antibody and their responding antigens fit together in a lock and key model. The duty of the antibody is to detect the antigen but not to destroy it. Specific T cells, also known as the "killer cells", destroy the antigen that is tagged by the antibody. T cells also helps in signaling other cells of the immune system to do their work. Antibodies can also neutralize toxic substances produced by different organisms. They can activate a group of proteins known as complement that assist in killing bacteria, viruses and other infected cells.
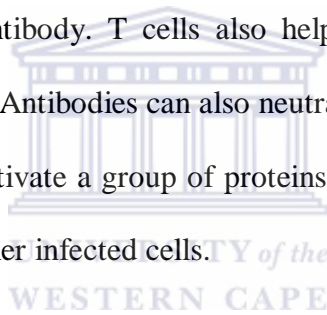
Each B-cell has $\sim 10^5$ antibody molecules in its plasma membrane. Each antibody is non-covalently associated with invariant set of trans-membrane polypeptide chains that are involved in passing the signal to the cell interior when the antigen attaches itself. This invariant polypeptide chain is coupled to the antigen receptor on the B-cell to the tyrosine protein kinase thereby activating phosphorylation cascade during antigen attachment to the antibody [70].

2.7.4 Antibody-antigen interaction

This process is mediated by a sum of different weak forces that are effective when the antigen is in close proximity with the complementary regions of the antibodies. These forces include,

hydrophobic and hydrogen bonds, van der Waals forces and ionic forces. The corresponding two identical antigen binding sites are known as a determinant. The reversible reaction between an antigen with a single antigenic determinant (*Ag*) and antigen binding site (*Ab*) can be expressed as:

$$Ag + Ab \Leftrightarrow AgAb \qquad (2)$$

Equilibrium point of this reaction depends on both the concentration of Ag and Ab and the strength of their interaction. The strength of their interaction is expressed as the affinity constant or association constant (K_a):

$$K_a = \frac{[AgAb]}{[Ag][Ab]} \qquad (3)$$

The K_a value ranges between 5 x 10^4 to 10^{11} l mol^{-1}. An antibody with K_a values less than 10^4 is said to be biologically effective. The affinity of the antibody to bind to the antigen is independent of the number antigen binding sites. Antigen having multiple copies of the same antigenic determinant combines with a multivalent antibody causing an increase in the binding strength of the antigen-antibody bond. If the affinity of the antigen binding in an IgG and IgM molecules is the same, the IgM molecule will have highest overall strength of the antigen-antibody binding than IgG. The difference in the overall strength of the antibody-antigen binding, that is, 10^4 fold or more, is important because antibodies that are produced early in the immune system have low affinities than the ones that are produced later. Since IgM has the high overall strength of the antibody-antigen binding, it can function effectively even when each of its binding sites has a low affinity [71].

2.7.5 Immobilization of biomolecules

Enzyme immobilization is a procedure which involves the confinement of enzymes onto a support material leading to their restricted mobility. Immobilizations of enzymes have proven

to be a valuable method due to the fact that it improves enzyme stability and allows enzymes to effectively work in different environments. Furthermore, immobilization methods should allow enzymes to maintain their active conformation, catalytic flexibility and conserve catalytic residue of enzymes [67,68]. Brena B.M *et al.* 2006 [72], classified the immobilization methods into two categories: reversible and irreversible enzyme immobilization methods. Reversible enzyme immobilization promotes and completes desorption of enzymes away from the support when enzyme derivative becomes inactive. In this method, the support can be recovered fully intact but the enzyme will be wasted [73]. Reversible enzyme immobilization method include, adsorption, affinity binding and metal binding. On the other hand, during irreversible enzyme immobilization process, the enzyme can be detached from the support without destroying both the enzyme activity and the support. The most common methods of irreversible enzyme immobilization includes, covalent coupling, entrapment, and cross-linking method [74].
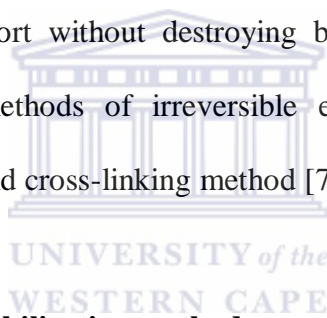
2.7.5.1 Reversible enzyme immobilization methods

2.7.5.1.1 Adsorption

Adsorption immobilization is the simplest method of immobilization. It is based on the physical adsorption of the enzyme on the matrix through hydrogen bonds, van der Waals forces, hydrophobic interactions and hydrogen bonds. Although the method is easy in preparation, the weak interactions between the enzyme and the support may cause the enzyme to leak into the solution. It may also cause unstable bindings, low reproducibility and uncontrollable reloading of support.

2.7.5.1.2 Affinity binding

During affinity binding process, the enzyme is linked to the support matrix through specific interactions. This immobilization procedure is divided into two methods. In the first method, the support matrix contains affinity ligands that must be activated prior to enzyme loading. This method is convenient in that the enzyme is not exposed to harsh conditions. The second method involves the modification of the enzyme by another molecule which has the ability to bind with the matrix.

2.7.5.1.3 Metal binding

In metal binding immobilization, the metal salts are precipitated on the surface of the support by heating or neutralization method. Due to steric factors, the metal salts cannot occupy all the coordination position of the support leaving some of the free positions to coordinate the enzymes. This is a simple method, however, the results are not easily reproducible due to the un-uniform adsorption of the metal salts on to the support and the metal ions may leak into the solution [75].

2.7.5.2 Irreversible enzyme immobilization method

2.7.5.2.1 Covalent coupling

Covalent binding is based on the formation of covalent bonds between the enzyme and the support which prevents the enzyme from leaking from the support into the solution. During this process, electrophilic groups are generated on the support that will react with the nucleophiles on the protein. Binding occurs via amino acid chain, thiol groups and carboxylic groups. Several advantages of this process include unlimited contact between the enzyme and the support since there is no barrier between the enzyme and the support. The method also gives high enzyme stability. However, the challenge faced with this method is making sure

that the active site of the amino acid does not bind to the support during immobilization. This factor determines the usability of the method.

2.7.5.2.2 Entrapment

During entrapment, enzymes are occluded with a polymer matrix that allows the substance to pass through but retain the enzymes. This method differs from the covalent binding in that the enzyme is not bound to the matrix. In this method, matrix pore size is a deciding factor for the usability of ready probes. That is, when pores are too small, adsorption occurs on the external surfaces, however, when the pores are too big, enzymes will leak into the solution causing a decrease in loading capacity. Other drawbacks include, cost of immobilization, diffusion limitations, deactivation of enzymes during immobilization and damaging the support during usage [76].
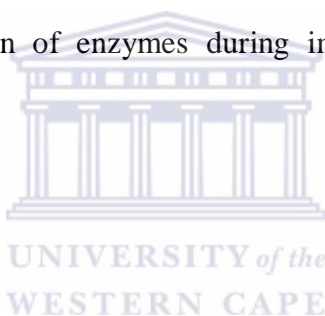
2.7.5.3 Cross-linking method

Cross-linking method does not require any support. Immobilization of enzymes occurs by intermolecular cross-linking of enzymes, either to other proteins or to functional groups of the insoluble support. Generally, this method is best used in conjunction with other methods such as covalent binding. It stabilizes adsorbed enzymes and prevents leakages from the support [77].

2.7.6 Practical consideration

For biosensor fabrication, optimum response can be obtained by immobilizing the enzyme alone or by mixing the enzyme with other proteins such as bovine serum albumin on the transducer or on a polymer matrix. Covalent binding and cross-linking method or combination of both methods are more complicated than entrapment method but they are

more useful in the case where sensors are small and the support is produced directly on the transducer. In small sensors combination of cross-linking method and covalent binding provides stable and reproducible performance, long term stability and the enzyme will cross-link in three dimension lattice.

2.8 Supporting Material

Apart from the immobilization methods discussed above, selection of adequate support material is a crucial step in fabrication of a biosensor. In this context, support materials used in fabrication a biosensor include materials such as $OsTe_2$-QDs and polymer-polypyrrole. In order to choose an adequate support material for an electrochemical biosensor system, the major requirement is that the material should produce an optimum electrode response for its given application. As stipulated previously in electrochemical immunosensors (section 2.7), one studies reduction and oxidation reactions occurring at the electrode surface. One can also study critical aspect such as physical stability of the support material, rate of electron transfer, product sensitivity and conductivity of the support material on the electrode surface. Other critical aspects include the cost and lifetime of support material for any electrochemical enzyme biosensor platform. The following paragraphs highlights the supporting material used during the development and fabrication of biosensor in this project [77,78]

2.8.1 Quantum dots

2.8.1.1 Quantum dots for enzyme stabilization

Among other nanomaterials, quantum dots have attained considerable attention in recent years. Colloidal semiconductor quantum dots are nanocrystals with size in the nanometer range (1 – 100 nm) [79]. Unique properties of quantum dots are due to quantum confinement which is caused by the restriction of electrons and holes in three dimensions. Quantum

confinement is an effect arising in nanocrystals smaller than their Bohr exciton radius. Semiconducting nanomaterials possess a valence band a conduction band. In quantum dots, these bands are quantized with energy values directly proportional to the nanocrystals size. This quantization of energy results in discrete size dependent emission wavelength of a single quantum dot. During excitation, the electrons absorb energy causing it to move from the valence band to the conduction band thereby creating a hole at the valence band. Upon recombination of the electron with its hole, light of certain wavelength is emitted which correspond to certain band gap. The adsorption and luminescent properties of quantum dots can be tuned from the UV to the infrared region by changing the quantum dots size and composition [80].

2.8.1.2 Types of quantum dots

Quantum dots are made from a combination of atoms of the periodic table. The most studied types of quantum dots are from:

Group II and VI (examples include CdSe, CdS, ZnO).

Group III and V (examples include InAs, InSb, GaAs).

Group IV and VI (examples include PbSe, PbS).

Other types of quantum dots include a combination of transition metal atoms and group IV non-metal such as ZnS and ZnSe quantum dots. QDs can be prepared in different media, from atomic deposition on solid phase to colloidal synthesis in aqueous solution. However, the most facile method of preparing quantum dots for biosensors application is using the aqueous approach (discussed in Chapter 3) [81,82]. Quantum dots based optical biosensors are also referred to as photoluminescence biosensor due to their good photo electronic properties. The principle of these biosensors is based on the interaction of the substrate biomolecules with QDs. The interaction between the QDs ad the biomolecules causes

quenching and a decrease in intensity of photoluminescent of QD. Furthermore, many parameters such as detection limit and biosensor efficiency can be determined [83].

2.8.1.3 Other quantum dots application: in solar cells

With the energy cries in the world and greenhouse gas emission solar cells have attracted significant attention [84]. Photovoltaic cells are believed to be the cleanest ways in achieving greenhouse gas. However, effort must be made to make photovoltaic cells cost effective than other energy producing technologies. Therefore, Emin *et al.* 2011[85] showed how the integration of QDs in photovoltaic solar cells will improve energy efficiency and cost of photovoltaic solar cells. Operational procedure of typical voltaic cell that uses QDs: begins at the valence band: sun light excites the electrons causing them to move from the valence band to the conduction band. Then, the electrons accumulate on the conduction band resulting in the generation of electricity [86].
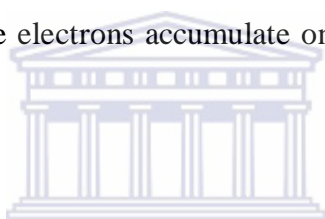
2.8.2 Conductive electroactive polymers

2.8.2.1 Polypyrrole used as a platform in electrochemical immunosensors

Among other conductive electroactive polymers, polypyrrole is the most studied polymer in the field of sensors and actuators. This is due to their fascinating properties such as good electrical conductivity, good environmental stability, relative ease of synthesis and potential to co-polymerize without affecting its electroactivity [87]. In recent studies, Singh *et al.* 2013 [88], determined a method for incorporating cholesterol esterase (ChEt) and cholesterol oxidase (ChOX) in polymer layers. Polypyrrole electrodes were prepared galvanostatically by polymerizing pyrrole form aqueous solution containing ChEt and ChOX on a polished indium tin oxide (ITO) electrode. Pt nanoparticles were electrochemically deposited between two layers of polypyrrole onto ITO electrode. This was to enhance electroactive surface area and to create a favorable microenvironment for immobilization of ChEt and ChOX. The

impedimetric response indicates that the ChEt and ChOX do interact with the sensing bilayer while no response was obtained with polypyrrole without incorporating ChEt and ChOX. This method was further used by Moon *et al*. 2014[89], who prepared a label-free electrochemical immunosensor for PSA detection. In their study, polypyrrole was electropolymerized on a three-dimension Au nanowire array. PSA was then directly detected on the Au|Ppy backed anodic aluminum oxide template. Differential pulse voltammetry (DPV) and cyclic voltammetry (CV) indicate that polypyrrole not only acted as a conductive platform to enhance electron transfer for biorecognition but also allowed incorporation of large amounts of the antibody.

Due to its inherent electrical conductivity, polypyrrole has the ability to form biologically compatible polymer matrix on electronic surface to produce an analytical signal [90]. Another interesting property of polypyrrole is that, it has the ability to switch its redox (oxidation or reduction) of analyte or product from an enzymatic reaction involving the analyte [91]. In cases were no electroactive species are present, biomolecular interaction of interest may give rise to a change in electronic properties (conductivity or capacitance) of a polymer and the electrochemical switching properties of the polymer [92].

Among other methods of synthesis, electrochemical synthesis of polypyrrole is the most facile method of obtaining a highly conductive polymer. An advantage of electrochemical synthesis includes ease of preparation, clean procedure and fast method. Electrochemical synthesis of polypyrrole also allows direct grafting of polypyrrole onto the surface of the electrode while simultaneously trapping the protein molecule. It is easy to control special distribution of the immobilized enzymes, polymer thickness and modulate enzyme activity by changing the polymer state [93,94].

2.8.2.2 Effect of polymer thickness on cation permselectivity of overoxidized polypyrrole film.

In literature, the use of modified electrode has received considerable attention in recent years [95]. This is to enhance selectivity and sensitivity of the electrode. Selectivity enhancement may be brought about selective binding of analytes, electrocatalysis of slow reactions and exclusion of interfering species from the electrode surface by using a protective barrier [96]. Several studies have been presented in literature demonstrating the effect of doping on the properties of polypyrrole film, which depends on the dopant material and electropolymerization conditions [97]. Electropolymerization of polypyrrole film onto a conductive electrode facilitates the doping of polypyrrole with specific anions. During this process, the polymer is in its oxidized state (positively charged) with a polymer thickness < 5 μM [98].

During overoxidation, carboxylic groups are introduced into polypyrrole backbone. High electron density of the carbonyl group acts as a barrier to hinder the anion diffusion in the film. Previous investigations indicate that overoxidized film (thickness ~ 0.1 μM) have excellent cation permselectivity. A thinner ion-selective film is always desirable due to expected fast response time and higher sensitivity. Film permeability is expressed by the following equation:

$$P_m = \frac{\alpha D_m}{\delta_m} = \frac{D_{app}}{\delta_m} \qquad (4)$$

Where P_m (cm s^{-1}) is the film permeability, α is the membrane partition coefficient, D_m (cm^2 s^{-1}) is the diffusion coefficient within the film, D_{app} is the apparent diffusion coefficient and δ_m (cm) is the film thickness. According to eq. 4, film permeability increase as δ_m decreases.

High P_m will allow analyte to reach the surface easily hence fast response time and high sensitivity can be achieved [99].

2.8.2.3 Quantum dot-polymer Nanocomposite

Nanocomposites are engineered by incorporation of optically active materials such as semiconducting and metal nanoparticles into polymer film. Combination of two or more different constituent material allows the manipulation of nanocomposite to exhibit new properties such as good mechanical properties, electrical properties, thermodynamic properties and chemical properties. Due to the above mentioned properties, nanocomposite of quantum dots and electroactive conjugated polymers have studied intensively and found multiple of applications in optical amplification, photovoltaics, photodetection, sensing and plasmonics [100]. Several methods have been outlined on the synthesis of polymer-quantum dot nanocomposite. These methods includes: surface passivation, chain end attachment and layer by layer assembly. Some of these methods require quantum dots to have certain surface properties like hydrophilic or hydrophobic property [101]. Thus by combining quantum dots and polymer film, one can intrinsically design polymer-quantum dot nanocomposite with combinations of conductivity, chemical stability, mechanical stability posed by polymers together with electronic, photo-electronic properties and biocompatibility posed by quantum dots [102].

During this project, a new polymer-quantum dot architect of OvoxPpy:TGA-OsTe$_2$ QDs was developed and successfully characterized by techniques such as Ultraviolet –Visible spectrophotometry (UV-Vis), Cyclic Voltammetry (CV), Electrochemical Impedance spectroscopy (EIS), Fourier Transform Infrared spectrometry (FT-IR), Scanning Electron Microscopy (SEM) and Transmission Electron Microscopy (TEM), in order to interrogate the

new characteristics exhibited by combination of these two materials. This newly composite material was successfully used as the electron mediator for one the biosensors developed during this project.

CHAPTER 3

3.1 Experimental section

Chapter review

The chemicals used in this project are enlisted in this chapter and the instrumentations involved are explained. This chapter also describes preparation procedures of different electrolyte solutions and buffer solutions as used for biosensor application and characterization. Secondly, the chapter accentuates on the synthesis and characterization of TGA-OsTe$_2$ QDs, preparation of overoxidized polypyrrole doped thioglycolic acid osmium telluride quantum dots (TGA-OsTe$_2$ QDs|OvoxPpy) composite, characterization and applications of biosensor (anti-PSA-antibody|TGA-OsTe$_2$QDs|OvoxPpy|GCE), preparation procedure for the analyte PSA. This experiment section also includes the procedure for preparation of samples for characterization and brief discussion on characterization techniques used during the project.

3.1.1 Chemicals and instrumentation

3.1.1.1 Chemicals

All chemicals used in this study were of analytical grade purchased from sigma Aldrich. This includes sodium dihydrogen phosphate, disodium hydrogen phosphate, and osmium tetrachloride (99%), and lithium perchlorate (99%), sodium hydroxide (99%), sodium borohydride tellurium powder (99%), thioglycolic acid (TGA), pyrrole (98%), bovine serum albumin (BSA), and purified human prostate specific antigen, purified rabbit anti-prostate specific antigen-antibody (from Abcam). The 0.1 M phosphate buffer solution was prepared from 0.05 M sodium dihydrogen orthophosphate (NaH$_2$PO$_4$) and 0.05 M disodium hydrogen orthophosphate (Na$_2$HPO$_4$) with the pH adjusted by mixing adequate volumes of each

solution. 0.05 M of NaH_2PO_4 and 0.05 M Na_2HPO_4 solutions were prepared in double-distilled water filtered by Millipore[TM] filtering system.

3.1.2 Instrumentation

All electrochemical experiments were carried using a BAS Epsilon intergrated and automated electrochemical work station from Bio Analytical Systems (BSA) Lafayette, USA. All voltammogram of cyclic voltammetry, square wave voltammetry and steady-state amperometry were recorded with a computer interfaced to the Epsilon electrochemical workstation. A 10 ml electrochemical cell with conventional three electrode setup was used. The electrodes used in this study were: (1) Glassy carbon electrode (working electrode, diameter 3 mm), (2) platinum wire acted as a counter electrode, (3) Ag/AgCl (reference electrode, 3 M NaCl) from BAS. Transmission electron microscopy (TEM) analysis of materials dispersed and spread on a copper coated TEM grid, were done using a Tecnai G2F2OX-Twin MAT 200 kV field Emission Transmission Electron Microscope from FEI (Eindhoven, Netherlands). Screen printed carbon electrode with surface area of 0.1257 cm^2, from Dropsens, Spain were used as working electrodes to prepare samples from SEM analysis. The SEM images were taken using Hitachi Model X-650 Scanning Electron Micro analyzer from Tokyo, Japan coupled to Energy Disperse X-ray Analyzer. Alumina micro polish and polishing pads were obtained from Buehler, IL, USA and were used for polishing the glassy carbon electrode before any modification. All FT-IR spectra were recorded on PerkinElmer spectrum 100, FT-IR spectra spectrometer on a NaCl pill. The FT-IR spectrum analysis was done on liquid sample of TGA-OsTe$_2$QDs, overoxidized polypyrrole and TGA-OsTe$_2$ QDs|OvoxPpy film respectively. The films were placed in between two NaCl plates of about 2.5 cm diameter, and FT-IR spectrum was recorded from a frequency range of 4000 cm^{-1} to 750 cm^{-1}. Impedance measurements were measured with Zahner (IM 6ex), impedance

measurement unit. The impedance measurements were performed at a frequency range of 0.5-1000 Hz, with a sinusoidal potential modulation of $\pm$ 100 mV superimposed on the applied dc potential. Impedance measurements were performed in 0.1 M PBS (pH 7.0) at a bias potential of 200 mV using a three-electrode cell with a volume 1 M. The data obtained from impedance was fitted to an equivalent circuit using the implemented THALES software.

3.1.2 Synthesis and preparation procedure

3.1.2.1 Synthesis of thioglycolic acid capped $OsTe_2$ quantum dots

Water soluble osmium telluride quantum dots were prepared by the same approach used by Wang *et al.* 2012 [104], with some modification. In a 250 ml three neck flasks, 0.29 g (0.01 M) of osmium tetrachloride ($OsCl_4$) was dissolved in 100 ml distilled water and 184.2 μL (0.02 M) was added while stirring followed by adjusting the pH to 11.2 with 1.0 M NaOH solution. The solution was bubbled under nitrogen gas for 45 min at 25 °C. After which a fresh solution containing (0.02 M) tellurium ions (i.e prepared by chemical reduction of 0.02 M tellurium powder by 0.04 M sodium borohydride ($NaBH_4$) in 100 ml distilled water under nitrogen gas for 30 min at 0 °C) was introduced drop wise until a brownish-red color was obtained indicating the formation of TGA capped $OsTe_2$ quantum dots solution (TGA-$OsTe_2$ QDs) was then transferred in the refrigerator at -20 °C for 5 min to quench size escalation. The TGA-$OsTe_2$ QDs solution was finally capped in room temperature in a dark until used [103]. The following reaction mechanism indicates the formation of quantum dots:

$$4NaBH_4 + 2Te + 7H_2O \rightarrow 2NaHTe + Na_2B_4O_7 + 14H_2 \tag{5}$$

$$OsCl_4 + SHCH_2COOH + 2NaOH \rightarrow CH_2SCOOOs + SHCH_2COOH + Na_2Cl_4 + 2H_2O \tag{6}$$

$$2NaHTe + CH_2COOHS\text{-}Os \rightarrow OsTe_2\text{-}SCH_2COOH \tag{7}$$
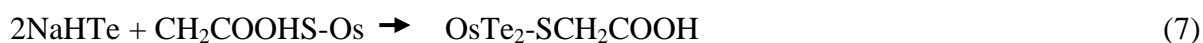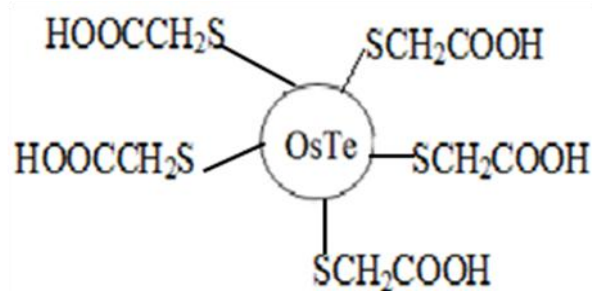
Scheme 8. Structural representation of the desired TGA-OsTe$_2$ QDs.

Equation (6) demonstrate the slightly basic solution for the formation of Os (TGA)$^{4+}$ complex. On the other hand, reaction (5) illustrates the reduction of Te^0 to Te^{2-} in NaBH$_4$ at 0 °C. Equation (7) demonstrate the reaction of the Os(TGA)$^{4+}$ with Te^{2-} ions to form a quantum dot. Scheme 8 shows the structure of the as prepared TGA-OsTe$_2$ QDs.

3.1.2.2 Preparation of anti-PSA-antibody|TGA-OsTe$_2$QDs|OvoxPpy||GCE immunosensor

3.1.2.2.1 Electrochemical polymerization of polypyrrole film on GCE

Before modification, glassy carbon electrode (GCE, diameter 3 mm) was polished with 1, 0.3, and 0.05 μM aluminum slurry, rinsed with double-distilled water and henceforth sonicated in absolute ethanol and distilled water for minimum of 5 min. This was to remove any adsorbed substances on the electrode surface. Finally the electrode was air-dried and ready for use [105].

To polymerize pyrrole film, GCE was placed into deaerated solution containing of 0.1 M LiClO$_4$ and 0.1 M (70 μL) pyrrole. Electropolymerization was performed potentiodynamically by sweeping the potential anodically from -1400 to 700 mV (vs. Ag/AgCl) at scan rate 50 mV s^{-1} for 10 cycles under argon gas. The electrode is denoted Ppy||GCE [105].

3.1.2.2.2 Preparation overoxidized polypyrrole film on GCE

The modified electrode obtained in Section 3.1.2.2.1 denoted Ppy||GCE, was rinsed with double-distilled water and transferred to 0.1 M NaOH. Conductive polypyrrole film was electrochemically overoxidized at constant potential 1000 mV for 420 s until current decreases. The obtained electrode denoted OvoxPpy||CE was removed from the solution and gently rinsed with double-distilled water to remove non-adsorbed species [106].

3.1.2.2.3 Preparation of nanocomposite: TGA-OsTe$_2$QDs|OvoxPpy||GCE

In order to incorporate semiconducting nanoparticles in the overoxidized polymer film, an aliquot (20 µL) of the TGA capped OsTe$_2$ QDs was drop-coated onto OvoxPpy||GCE and air dried in an oven (temperature 50℃) for 15 min. The electrode denoted TGA-OsTe$_2$QDs|OvoxPpy||GCE was then gently rinsed with deionized water and characterized by CV, SWV and EIS [107].
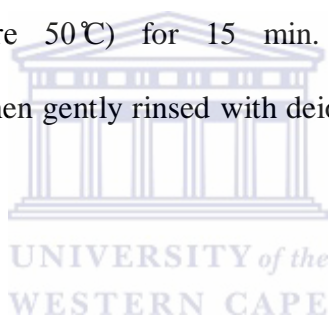
3.1.2.2.4 Fabrication of the immunosensor

After preparing the nanocomposite platform as denoted in Section 3.1.2.2.3 (TGA-OsTe$_2$QDs|OvoxPpy||GCE), 40 µL of anti-PSA-antibody solution was immobilized on the platform for 2 h at 25 °C. The unbound ati-PSA-antibody was then removed by gently rinsing the electrode with PBS pH 7. The unspecific and residual binding sites were blocked by immobilizing 40 µL of BSA (2 mg mL^{-1} prepared in PBS) for 1 h. The electrode was now denoted as BSA|anti-PSA-antibody|TGA-OsTe$_2$QDs|OvoxPpy||GCE. The prepared electrode was now ready to be used as immunosensor for the detection of PSA. The immunosensor was then transferred to a solution of PBS and analyzed by electrochemical impedance spectroscopy [108].
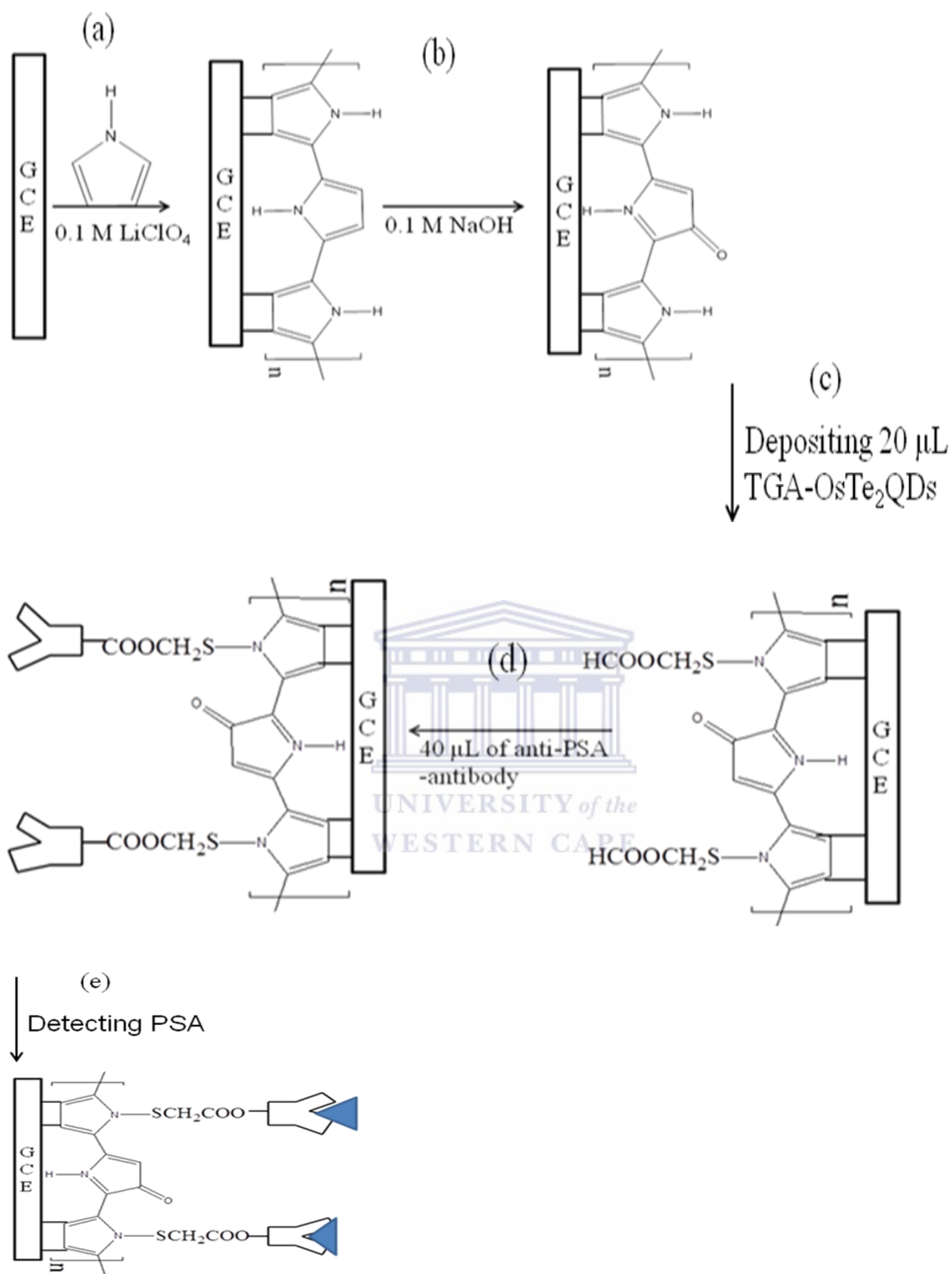
Scheme 9. Stepwise fabrication of the immunosensor: (a) electropolymerization of pyrrole monomer, (b) overoxidation of polypyrrole, (c) deposition of TGA-OsTe$_2$QDs, (d) immobilization of anti-PSA antibody and (e) detection of PSA.

3.2 Antigen Preparation

Antigen solution was prepared by diluting the required concentration of the antigen in 1000 μL PBS (pH 7.0). Concentration ranges were used (1.266 – 4.207 fg ml^{-1}) since prostate cancer is noted at very low concentrations of PSA.

3.2.1 Stability studies

Storage stability of the immunosensor was investigated over a period of 7 days. When the electrode was not in use, it was suspended above 0.1 M PBS at 4 °C. The change in R_{ct} was then monitored by running EIS over the 7 days.

3.3 Analytical Techniques

3.3.1 Electrochemical techniques

Electrochemical techniques are robust techniques that offer high sensitivity, precision as well as large linear dynamic range. There are two types of electrochemical methods: potentiometric (no current, equilibrium potential) and voltammetric (current is applied as a function of applied potential). In the present study, voltammetric techniques will be considered to test the immunosensor since current will be measured as a function of potential.

Voltammetry is an electro-analytical technique that measures current flowing through an electrode dipped in a solution containing electroactive species, while potential scanning is imposed on it. A typical voltammetric cells consist of reference electrode, counter electrode (platinum electrode) and a working electrode (gold, platinum or glassy carbon electrode). The working electrode has a very little surface in order to assume quickly accurately the potential imposed by the electrical circuit. Voltammetry is a versatile technique for research purpose; it

allows the search into several aspects of electrochemical reactions, namely, those reactions in which electron exchange are involved between reagents and products. Voltammetric techniques have wide variety of applications in analysis of physical properties of material for their application in electric resistors, capacitors, transistors and sensors [109,110].

Basic concept of electrochemistry: Suppose that a working electrode is dipped in a solution containing an electroactive species, A_{ox}, that can be reduced to A_{red} when known potential (V) is applied. The following reaction mechanism applies:

$$A_{ox} + ne \rightarrow A_{red} \qquad\qquad (8)$$

The basic concept of electrochemistry is that the reactions occur at the surface of the working electrode based on the chemical changes resulting from the flow of ionic species from the electrolyte solution to the surface of the electrode [111], as shown in Scheme 10 [112].
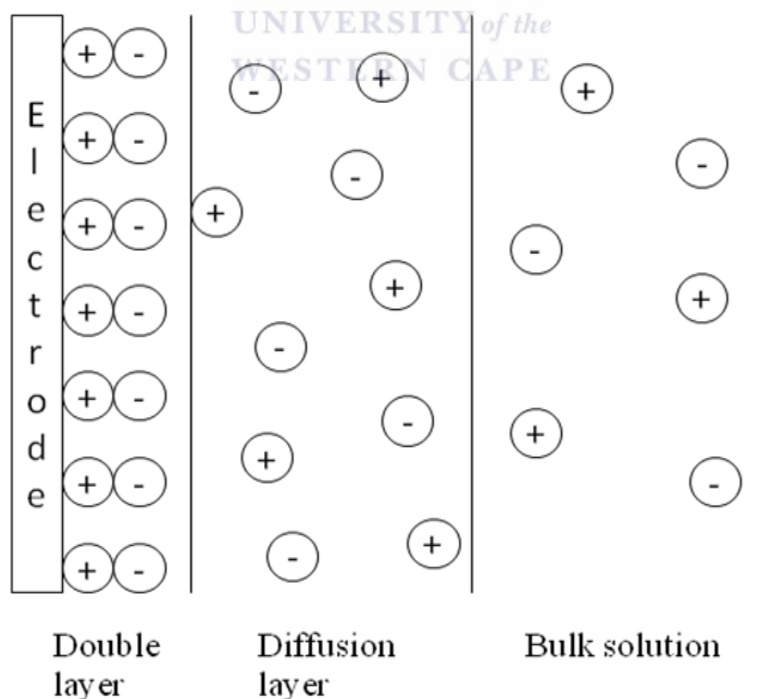
Scheme 10. Schematic representation of the interfaces that describes the electrode/solution system at positively charged electrode.

Movement of electroactive species from bulk solution or electrode to another area, arises either from difference in electrical or chemical potential at two locations or from movement of species from high concentration in the solution to lower concentration. Generally, mass transfer of electroactive species can be classified into three types:

I. Migration: movement of charged species in response to local electric field. During migration process, total flux is proportional to the charge of ions, ion concentration, the diffusion coefficient and the magnitude of the electrical field gradient experienced by ions.

II. Conventional: it is a forced movement of species in solution by mechanical (stirring) or other means. In this case movement of fluid is described by hydrodynamics.

III. Diffusion: spontaneous movement of ions in bulk solution from high concentration regions to low concentration regions. The main aim for diffusion movement is to minimize concentration gradient [112].

3.3.1.1 Cyclic voltammetry

Cyclic voltammetry (CV) is a simple and direct electroanalytical technique used to clarify the kinetics of electrochemical reactions taking place at the electrode surface [113]. In principle, CV is performed by sweeping the potential of the working electrode (from starting value E_i to a final value E_f then return back to the starting potential at constant potential sweep) and measuring the resulting current. The concentration of electroactive species is directly proportional to the measured current. Cyclic voltammetry can be used to determine qualitative information about electrochemical processes under different conditions such as the presence of intermediates in oxidation-reduction reactions and reversibility of the reaction. It

can also be used to study the electron stoichiometry of the system, the diffusion coefficient of the analyte and the reduction potential (which can be used as an identification tool).

Figure 1 represents a typical cyclic voltammogram of an electron transfer reaction in which the rate is governed by the diffusion of the electroactive species to the electrode surface [114].
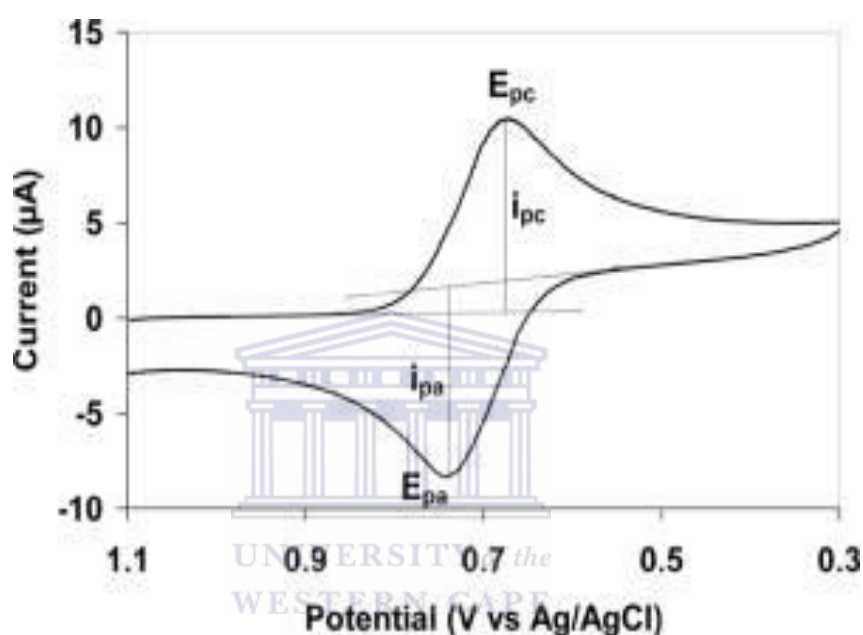
Figure 1. A typical cyclic voltammogram of reversible redox process.

From the cyclic voltammogram illustrate in Figure 2, critical parameters such as the magnitude of the anodic peak (I_{pa}), cathodic peak (I_{pc}) and their corresponding potential peak, E_{pa} and E_{pc} can be exploited further to understand reaction kinetics occurring at the working electrode. The positions and location of the above mentioned parameters provides information about the reversibility and electron transfer kinetics of a system [115].

I. Reversible: is defined as a system in which both redox species exchange electrons with the electrode. For a reversible system, the peak current is given by the Randel-Sevčik equation:

$$I_{pc} = -(2.69 \times 10^5) n^{\frac{3}{2}} A D_o^{\frac{1}{2}} C_o^* v^{\frac{1}{2}} \qquad (9)$$

where I_{pc} is the cathodic (reduction) peak current, n is the number of electrons passed, A is the area of the electrode (cm^2), D is the diffusion coefficient of the redox species ($cm^2\ s^{-1}$), v is the scan rate in $mV\ s^{-1}$ and C_o is the concentration of the redox species ($mol\ cm^{-3}$). Equation10 shows that the peak current id directly proportional to the concentration of bulk analyte and increases with the square root of scan rate, v. It can also be shown that in reversible process, peak-to-peak separation between the anodic peak and the cathodic peak can be represented as:

$$\Delta E_p = E_{pa} - E_{pc} = \frac{59}{n} \qquad (10)$$

where ΔE_p represent peak-to-peak separation in mV. On the other hand, the formal potential (E^o), can be expressed as the average of two peak potentials:

$$E^o = \frac{E_{pa} + E_{pc}}{2} \qquad (11)$$

II. Irreversible: in an irreversible system, the size of the peak currents are reduced and the peak potentials depends on the potential scan rate as they shift away from the formal potential as scan rate increases. The peak current for irreversible system is defined by:

$$I_p = (2.6 \times 10^5) \alpha^{\frac{1}{2}} n^{\frac{3}{2}} A C D^{\frac{1}{2}} v^{\frac{1}{2}} \qquad (12)$$

where i_p is the peak potential, α is the transfer coefficient, n is the number of electrons involved in charge transfer step, A is the area of the working electrode, C is the concentration of the redox species and D is the diffusion coefficient. Thus, E_p occurs at potentials higher

than E^o, with E^o related to k^o (standard rate constant) and α. For irreversible process, the relationship between E^o and E_p can be expressed as:

$$E_p - E^o = \frac{48}{\alpha n} \qquad (13)$$

Equation 5 indicates that as the number of electrons transfer increases, α also increases resulting in more drawn out voltammogram.

III. Quasi-reversible: is a system that shows reversibility at low scan rate and irreversibility at high scan rate. The shift from reversible to irreversible is caused by slow mass transfer rate than the electron transfer rate at the surface of the electrode. Table 1 summarizes the kinetic parameters at the working electrode [116].

Table 1. Summary of parameters for diagnosis of reversible, irreversible and quasi-reversible.

Parameters	Cyclic voltammetry process		
	Reversible	Quasi-reversible	Irreversible
E_p	Independent of v	Shifts with v	Shifts cathodically by $\frac{30}{\alpha n}$ mV
$E_{pa} - E_{pc}$	$\frac{59}{n}$ mV at 25°C and independent of v	-	Many approaches $\frac{60}{n}$ mV at low v but increases with v
$I_p/v^{1/2}$	Constant	Virtually independent of v	Constant
I_{pa}/I_{pc}	Equals to 1 and independent of v	Equal to 1 only when α is 0.5	No current on the reverse side

3.3.1.2 Square wave voltammetry

Square wave voltammetry (SWV) is a pulse voltammetry technique that offers unique advantages in terms of high sensitivity, great speed and low detection limit. In SWV, the excitation signal consist of symmetrical square wave pulse of amplitude E_{sw}, superimposed on a staircase waveform of step height ΔE where the forward pulse of the square wave coexist with the stair case step. The forward pulse gives cathodic current, Ψ_c, while the reverse pulse gives Ψ_a. The net current (Ψ_{net}) is then given by the difference between the Ψ_c and the Ψ_a and from this a voltammogram is obtained. SWV indicates that the peak height is directly proportional to the concentration of the electroactive species in solution and direct detection limit can be as low as 10^{-8} M. The peak current can be expressed by:

$$I_p = kn^2 D^2 \Delta E_A C \qquad (14)$$

where I_p is the peak current, k is a constant, n is the number of exchange electrons, D is the diffusion coefficient of the analyte, ΔE_A is the pulse magnitude and C is the concentration of the analyte [117]. Figure 2 indicates a typical square wave voltammogram [118].
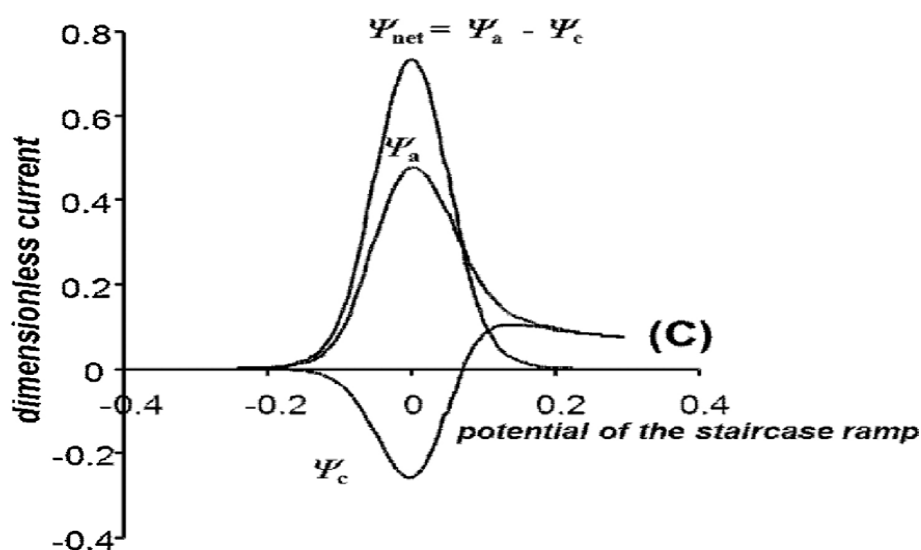
Figure 2. A typical square wave voltammogram consisting of the forward (anodic, Ψ_a),

backward (cathodic, Ψ_c) and the net (Ψ_{net}) current.

3.3.2 Ultraviolet –visible spectroscopy

Ultraviolet – visible (UV-vis) spectroscopy is an analytical technique that uses light in the

visible region (400 – 700 nm) and ultraviolet regions (185 – 400 nm) for quantitative

determination of different analytes in solution. The basic principle of UV-vis spectroscopy is

well known. That is, when light of specific wavelength is passed through the uv active

substance, some of the light may be absorbed by the substance and the remainder being

transmitted through the sample. Transmittance, which is defined by as a ratio of light

intensity entering the sample (I_o) to that exiting the sample (I_t), can be expressed as a

percentage.

$$\%T = \frac{I_o}{I_t} \times 100 \qquad (15)$$

Absorbance (A) of a sample can be expressed as the negative logarithm of transmittance:

$$A = -\log T \qquad (16)$$

The important principle in absorption spectroscopy is the Beer-Lambert law. The law is used

to determine the concentration of specific analyte in the sample at specific wavelength.

$$A = \varepsilon \times l \times c \qquad (17)$$

where ε is the absorbtivity of the substance, c is the concentration and l is the path length.

The law states that absorbance of light is directly proportional to the concentration of analyte

species [119]. During absorption, the analyte of interest absorbs energy causing changes in

the electronic energy of the molecule. As molecules absorb energy, electrons are promoted

from the highest occupied molecular orbital (HOMO, usually a non-bonding n or bonding π

orbital) to the lowest unoccupied molecular orbital (LUMO, an antibonding π^* or σ^*). Thus the energy resulting from the electronic transitions can be determined by using Plank's law:

$$\Delta E = h v = h \left(\frac{c}{\lambda_{max}} \right) \qquad (18)$$

where ΔE is the energy of light, h is a Plank's constant (6.626×10^{-34} J s^{-1}), v is the frequency of light, c is the speed of light (3.0×10^8 m s^{-1}) and λ_{max} is the maximum wavelength (nm). The energy level diagram depicting different types of electronic transitions are shown in Scheme 11 [120].

Scheme11. Different energy levels and types of electronic transitions.

The * indicates an excited state of σ, π and n indicates the type of orbital involved. UV-vis spectroscopy is a complementary technique for fluorescence spectroscopy. In fluorescence, detectors measure emission of light from a substance, as it loses energy and transmit from excited state to the ground state. In this study, both these instruments will be used to study a series of compounds and substances for transition metal, organic complexes and charge transfer complexes [121].

3.3.3 Scanning electron microscopy

SEM is one of the most versatile techniques used to determine structural morphology and chemical composition. In principle, a beam of electrons (produced by the electron gun) is focused at the sample specimen through electromagnetic lenses in an electron column. When these electrons interact with the sample specimen, secondary electrons (low energy electrons) and backscattered electrons (high energy electrons) are produced. Secondary electrons are the most common electrons used for investigating surface morphology [122]. It produces images by recording different signals resulting from interactions of electron beam with sample specimen as it is scanned in a raster pattern across the sample surface. These image sizes can be obtained in a few nanometers (10^{-9}) range in 1D, 2D and 3D. These features of SEM have intrigued many researchers to develop new materials and to study existing materials in depth. Scientist often used this technique to investigate the shape, volume, cracks and voids with a set of materials [123]. In this study, SEM technique will be used to study a series of materials such as TGA-OsTe$_2$QDs and OvoxPpy-TGA-OsTe$_2$QDs composite.
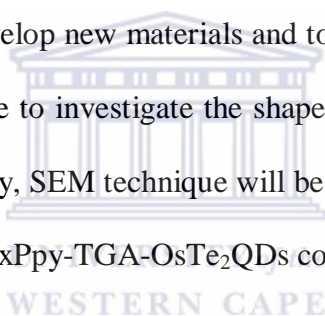
3.3.4 Fourier transform infrared spectroscopy

The underlying principle of FT-IR spectrometer is the separation of an incoming infrared light beam into two individual beams using an optical path splitter, followed by variation of the optical path difference between the two beams using a movable mirror for one beam and a fixed mirror for the other and by recombination of the two separate beams using an optical combiner so that interference can occur. The interference path that depends on the optical path difference is produced and can be measured using standard infrared detector [124]. FT-IR is a powerful tool to determine the infrared absorption spectrum, information about the structure and nature of the chemical bonds in a molecule. It is currently applied to the analysis of solids, liquids and gases [125]. In this study, FT-IR was used to study the

structural properties of newly developed TGA-OsTe$_2$ QDs together with the composite OvoxPpy-TGA-OsTe$_2$ QDs nanocomposite.

3.3.5 Electrochemical impedance spectroscopy

Electrochemical impedance immunosensing have attracted considerable attention for quantifying the interaction between the antibody and the antigen. Impedance immunosensing provides a general method to follow the procedure of antibody-antigen reaction at the modified electrode surface.

Studies by Xiao *et al.* 2007 [126] showed that EIS is a powerful tool for predicting the surface activity of an immunosensor. The impact of immobilization of the antibody-antigen binding on to polypyrrole-streptavidin revealed a covalent attachment of the antibody to the modified electrode surface and a successful impedance-based immunosensor.
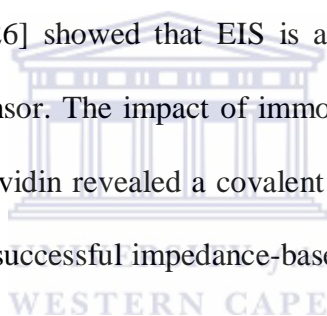
3.3.5.1 EIS measuring parameters.

The fundamental principle of EIS method is to apply a small amplitude sinusoidal excitation signal to the system under investigation and measure the response (current or voltage). A low amplitude sine wave ΔE_{sin} *(ωt),* of a particular frequency is superimposed on the dc polarization voltage, $E_{polarization}$.

$$E_{(t)} = E_{polarization} + \Delta E_{\sin}(\omega t) \qquad (19)$$

where $E_{polarization}$ is the base potential of the working electrode measured against a suitable reference, ΔE is the amplitude of the sine wave and ω is the frequency of the signal in rad s^{-1}.

If the system is linear, the sinusoidal current response of the same frequency but different amplitude and phase from the same voltage can be expressed as:

$$I(t) = \Delta I \sin(\omega t + \Phi) \qquad (20)$$

In this instant, $I_{(t)}$ is the current, ΔI is the current amplitude and Φ is the phase shift angle.

The ratio which is known as the impedance modulus (in Ω) can be calculated using the ohm law as:

$$Z = \frac{\Delta E_{(\omega)}}{\Delta I_{(\omega)}} = \frac{\Delta E \sin(\omega t)}{\Delta I \sin(\omega t + \Phi)} \qquad (21)$$

Impedance modulus of the system is a complex quantity with a magnitude and phase shift which depends on the frequency of the signal. The impedance modulus also consists of the real ($Z^{'}$) and imaginary ($Z^{''}$) components. These components give information about the kinetic and mass transport properties of the cell, as well as its capacitive properties.

$$Z' = |Z|\cos\theta \text{ and } Z'' = |Z|\sin\theta \qquad (22)$$

The real components of impedance correspond to a resistance in-phase with the applied voltage, while the imaginary component corresponds to a reactance $90°$ out - of –phase with applied voltage. The reactance is caused by capacitance charging in the cell [127].

3.3.5.2 Electrode

A minimum of three electrodes configuration is the most common for typical electrochemical application. The system consists of the electrode under investigation (working electrode), the reference electrode which is used to determine the potential of the working electrode precisely and the counter electrode which is necessary to close circuit. All three electrodes are usually immersed in a liquid electrode [128].

3.3.5.3 Instrumentation in EIS

A potentiostat imposes a desired command voltage between the solution and working electrode while simultaneously measuring the current flow between them. EIS analyzers are potentiostat designed especially for measuring AC impedance and have typical frequency ranges of 10 MHz – 100 kHz. A computer control ubiquitous for both potentiostats and EIS analyzers. Digital post processing is commonly employed to amplify the signal and to eliminate background noise [128].

3.3.5.9 Faradaic vs. non-Faradaic

Faradaic EIS requires the addition of redox-active species and DC bias conditions such that it is not depleted. In contrast, no additional reagent is required for non-faradaic process, rendering non-faradaic schemes somewhat more amenable to point of care application [127,128].
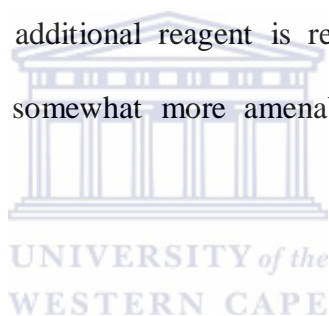
3.3.5.10   Data fitting

  The measured impedance data can be used to extract equivalent values and capacitance if a circuit model is assumed a priori, though there is not a unique model or even necessarily a one-to-one correspondence between circuit elements and the underlying physical process. Figures 3 (a) and (b) shows typical circuit models and Figures 4 (c) and 4 (d) shows impedance data.

It is not always necessary to fit the data to a model and even the best models of the electrode-solution interface do not perfectly fit data or else require so many fitting parameters as to be useless. Sometimes the raw impedance data is fit to a model and changes in model elements are reported as the sensor out-put. Alternatively, the impedance at a particular frequency is

used. Depending on the values of the respective model circuit parameters, data at a particular frequency can contain information about various circuit elements or be dictated primarily by one element [128].

3.3.5.11   Circuit models

Figure 3 shows the two most common models used to fit impedance biosensor data, depending on whether a faradaic or non-faradaic measurement is made. The solution resistance R_{sol} arises from the finite conductance of ions in bulk solution and thus is not generally affected by binding. The capacitance between the electrode and the ion solution, C_{surf} can be modeled as a series combination of the surface modification capacitance and the double layer capacitance. The component due to surface modification depends on the thickness and dielectric constant of the surface modification depends on the thickness and dielectric constant of the probe layer. It can be thought as a parallel plate capacitor, whose capacitance is given by $C = \varepsilon_r \varepsilon_0 \dfrac{A}{t}$ where $\varepsilon_r \varepsilon_o$ is the relative dielectric constant, A is the electrode area and t is the insulator thickness. The capacitance C_{surf} is often modelled by a constant phase element instead of a pure capacitance. In parallel with this capacitance there is a resistive path modelled by R_{leak} for non Faradaic sensors or the series combination of Z_w and R_{ct} for Faradaic sensors. For an ideal insulator or when no redox species is present, R_{leak} is theoretically infinite. The Warburg impedance (Z_w), is only of physical significance in Faradaic EIS, represents the delay arising from diffusion of the electroactive species to the electrode. It is only appreciable at low frequencies, is affected by convection (and thus may be invalid for experimental time scales), and has a phase shift of 45°. The charge transfer resistance (R_{ct}) is a manifestation of two effects (1) the energy potential associated with the oxidation or reduction event at the electrode (i.e. the over potential) and (2) the energy barrier

of the redox species reaching the electrode due to electrostatic repulsion or steric hindrance. The two circuit elements most commonly used as indication of affinity binding are C_{surf} for non-Faradaic biosensors and R_{ct} for Faradaic ones [128].

3.3.5.12   Constant phase

The impedance of solid electrodes usually deviates from purely capacitative behaviour, this is empirically modelled as a constant phase element (*CPE*).The complex impedance of a *CPE* is given by $\dfrac{1}{J\omega A}$ where *A* is analogous to a capacitance, ω is the frequency expressed in rad s⁻¹ and 0.5 < m < 1 (m = 1) corresponds to a capacitor and m = 0.5 corresponds to a Warburg element; m for C_{surf} modelling is typically 0.85 and 0.98). This introduces a sub 90° phase shift, or equivalently a frequency-dependent resistor in addition to a pure capacitor. *CPE* behaviour can be explained mathematically by dispersion in local capacitance values. Microscopic chemical inhomogenities, ion adsorption and inhomogeneous current distribution contribute to *CPE* behaviour. Since solid electrodes can be expected to have a certain amount of intrinsic *CPE* behaviour, modelling the electrode-solution interface as purely capacitative is often an over simplification which can reduce the quality of the data fit [127].

3.3.5.8 Double Layer Capacitance

When an electrode is polarized relative to the solution, it attracts ions of opposite charge. This tendency is countered by the randomizing thermal motion of the ions, but results in a local build-up of excess ions of opposite charge. Thus, any electric field arising at the electrode or within ionic solution decays exponentially because the excess ions screen the field. The characteristic length of this decay or Debye length is proportional to the square root

of ion concentration. This effect creates a capacitance called double layer capacitance or diffuse layer capacitance. Ions adsorbed at bare electrodes also increase the capacitance in accordance with the Gouy-Chapman-Stern. The double layer capacitance is voltage dependent because increasing the electrode voltage attracts the diffuse ion layer, increasing capacitance. If an insulator (e.g. an insulating probe layer) covers the electrode, forming a capacitance, the double layer capacitance appears in series with it. In impedimetric biosensors, the ionic double layer usually plays a minor in the overall measured impedance since it is so large relative to series capacitance of the probe layer for non Faradaic sensors and because the parallel path through Z_w and R_{ct} dominates at relevant frequencies for Faradaic sensors [128].

(a)
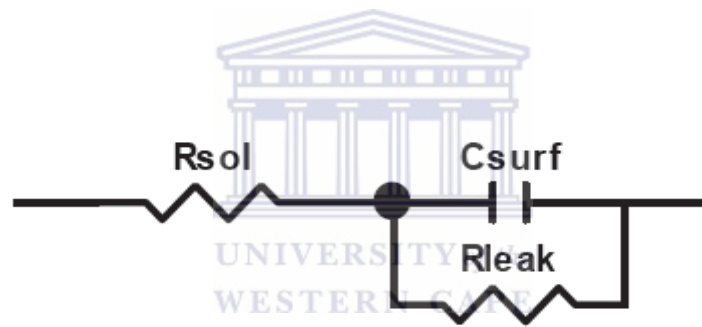
(b)
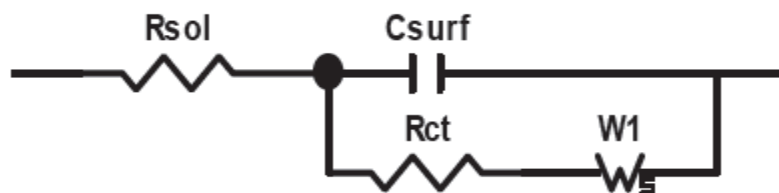
(c)
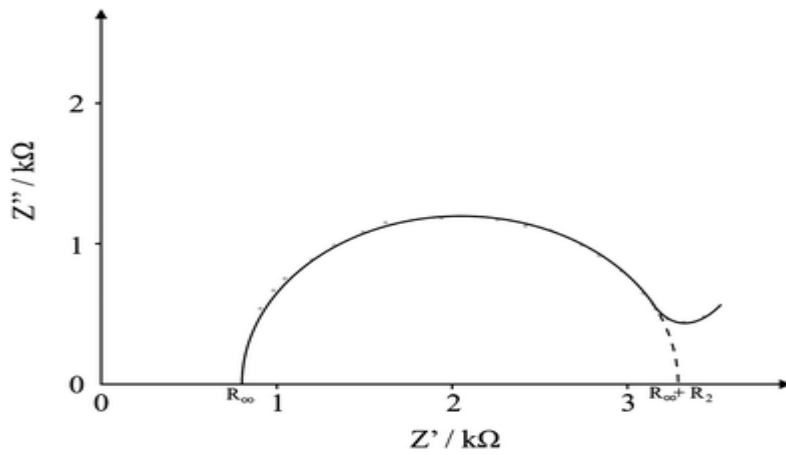
(d)
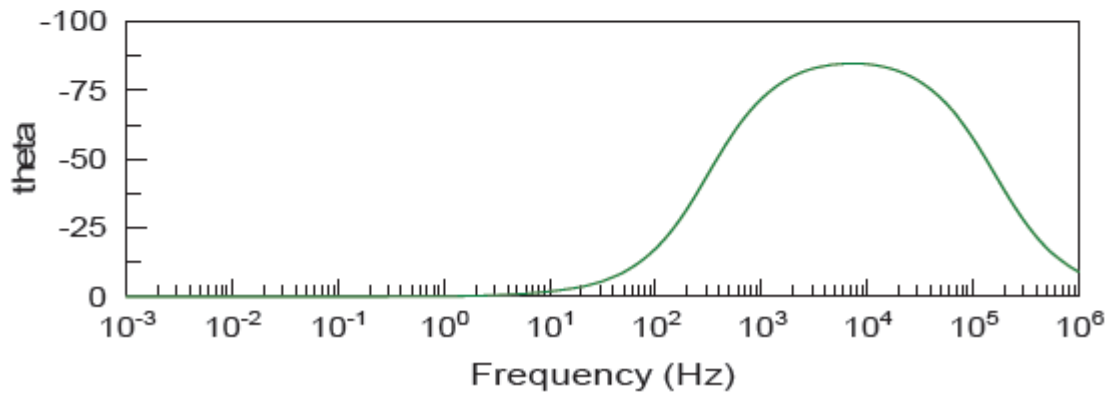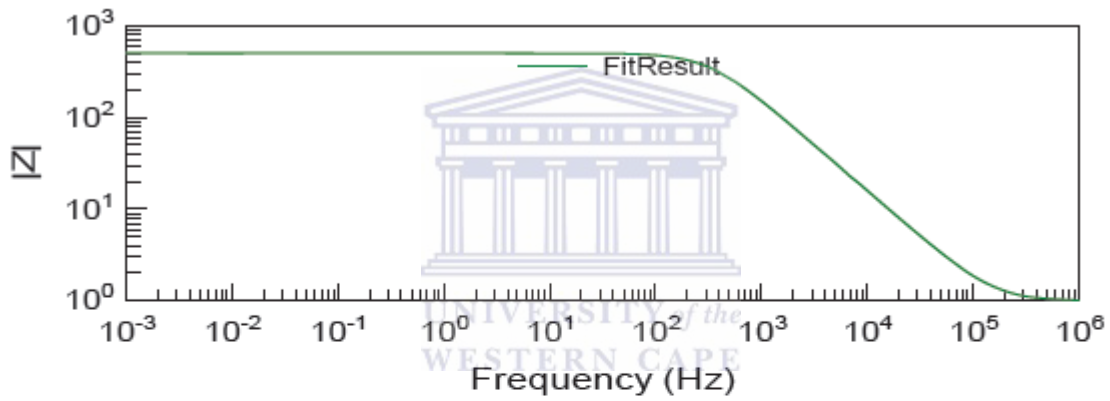
Figure 3. Common circuit models for (a) non-Faradaic (b) Faradaic interfaces. (c) Non Faradaic impedance data in Nyquist representation. (d) Faradaic impedance data in magnitude/phase representation (Bode plot) [129,130].

CHAPTER 4

Chapter review

This chapter, discuses the characterization of the TGA-OsTe$_2$ QDs by techniques like: UV-vis spectroscopy, XRD, FT-IR and HR-TEM. It also discusses the electro-analysis of TGA-OsTe$_2$ QDs based immunosensor by analytical techniques such as CV and EIS in 0.1 M PBS (pH 7.0).

4.1 Results and Discussion

4.1.1 Characterization of TGA-OsTe$_2$ quantum dots

4.1.1.1 Optical studies of TGA-OsTe$_2$ quantum dots

The measurements of the absorption spectrum were carried out at different refluxing times as shown in Figure 4. This was to reveal the effect of refluxing time on the optical and electrical characterization of the TGA-OsTe$_2$ QDs. During the first 10 min of refluxing, no excitonic peak is observed because there are more monomers in the reaction mixture and nucleation occurred right after the reaction mixture was heated at prolonged times (20, 30 and 40 min). The absorption spectra of TGA-OsTe$_2$ QDs were recorded from 250 nm to 600 nm. The spectrum indicated an intense peak at 406 nm and the peaks became broader at 417nm as the refluxing time was increased. The spectrum also indicates that absorption wavelength shifted slightly to longer wavelength (red-shift) as the reaction times increased. However, the intensity of the absorption peak decreased with its red-shift.
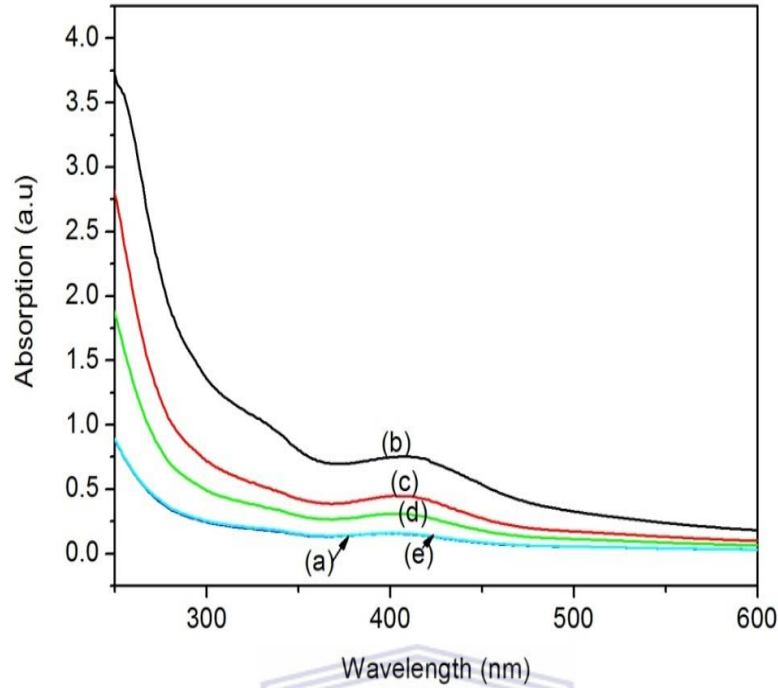
Figure 4. Time dependence of the absorption spectra of obtained during the synthesis of TGA-OsTe$_2$ QDs: (a) 10 min, (b) 20 min, (c) 30 min and (d) 40 min
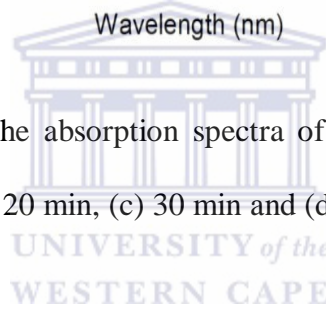
So, the growth mechanism of TGA-OsTe$_2$ would be best described by the Ostwald ripening process as smaller particles dissolve in the process of producing large particles. The peak at 406 nm was deduced to be associated with electron transition of d valence electron from Os (bonding) to Os* (antibonding or excited state). The energy associated with the deduced electronic transition was estimated using equation no. 15, Plank's law:

$$\Delta E = h v = h \left(\frac{c}{\lambda_{max}} \right) \qquad (18)$$

Table 2 bellow shows how band gap energies are associated with the wavelength and QD size. From the table it is observed that as the size of the TGA-OsTe$_2$ increases, the band gap energy decreases. The QD size was estimated according to the following equation:

$$E_g = \frac{h^2}{8\gamma^2}\left(\frac{1}{m_e} + \frac{1}{m_h}\right) \qquad (19)$$

where E_g = band gap energy (eV), γ = particle size, h = Plank's constant, m_e = electron mass ($0.451m_o$), m_h = hole mass ($1.717\ m_o$) (m_o is the electron mass = 9.1095 x 10^{-3} kg) [131,132]. Structural properties and the size of TGA-OsTe$_2$ QDs was also confirmed using X-ray diffraction (XRD) spectroscopy.

Table 2. Size and band gap energies of TGA-OsTe$_2$ QDs synthesized at different refluxing times

Time (min)	Wavelength (nm)	E_g (eV)	Size, γ (nm)
20	406	3.05	2.289
30	410	3.02	3.67
40	414	2.95	4.38

4.1.1.2 X-ray Diffraction spectroscopy analysis for TGA-OsTe$_2$QDs

The XRD pattern of the synthesized TGA-OsTe$_2$ hallow spheres is shown in Figure 5 which indicates a phase structure. It is notable that all the diffraction peaks correspond to the (1 1 1), (2 0 0), (2 1 1) and (2 2 0) of a cubic (zinc blended) OsTe$_2$ (JCPDS no. 5-592) at 2θ = 22.9 ° 27.6 °, 31.7 ° and 38.4 ° At 20 min, the diffraction peak at (2 1 1) is broader with the average crystal size was estimated from the half-width of the diffraction peak of (2 1 1) using the Debye-Scherrer's formular:

$$D = \frac{k\lambda}{\beta\cos\theta} \qquad (20)$$

where D is the crystal size, k is a constant (0.9), λ is the X-ray wavelength (1.5405Å), β is the full width at half maximum (FWHM)of the diffraction line and θ is the diffraction angle.
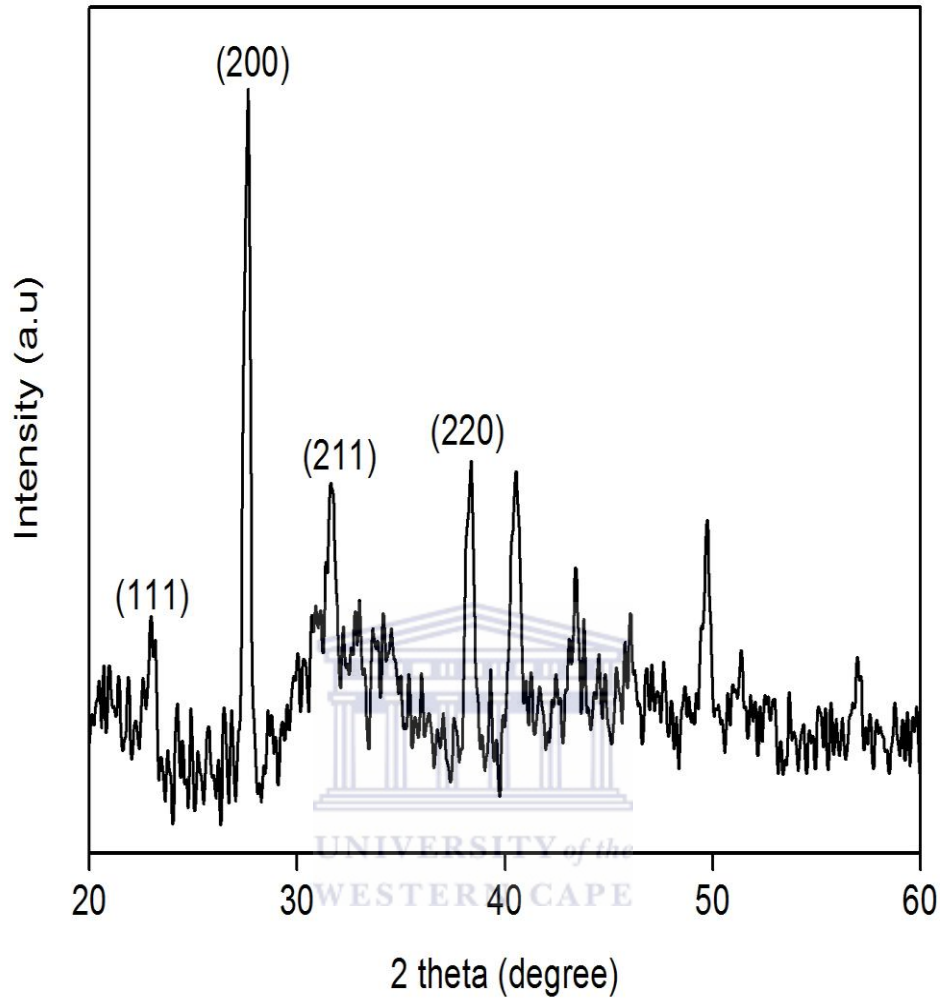
Figure 5. Patterns of XRD analysis related to TGA-OsTe QDs.

The strong and intense reflection peaks in the XRD pattern indicate that $OsTe_2$ products were well crystallized. Among all peaks, the intensity of (2 0 0) was much higher than that of (2 1 1) and (2 2 0) which suggest a high growth rate at (2 0 0) facet in comparison to (2 1 1) and (2 2 0). The lattice constant parameter ψ was found by calculating the interplanar crystal spacing as follows:

$$d_{hlk} = \frac{\lambda}{2\sin\theta} \qquad (21)$$

$$\varsigma = d_{hlk}\sqrt{\left(h^2 + k^2 + l^2\right)} \qquad (22)$$

The table bellow summarizes the crystal size, crystal spacing and the lattice constant. Values of the lattice constant α were very close to the standard card value 6.39680 nm (JCPDS no. 5-592) [133]. XRD analysis really confirmed the TGA-OsTe$_2$ QDs as discussed in UV-vis spectroscopy, section 4.1.

Table 3. Values for crystal size, d-spacing and lattice constant for TGA-OsTe$_2$ QDs

Crystal size, D, (nm)	d-spacing (nm)	Lattice constant, ς (nm)
2.3	2.8	6.2531

4.1.1.3 HR-TEM characterization of TGA-OsTe$_2$ QDs

HR-TEM was used to acquire direct morphological information about the size of TGA-OsTe$_2$ QDs synthesized by aqueous method. Figure 6 evidently shows the HR-TEM images of QDs on Cu grids. Figure 6 shows a good monodispersed QDs with size (2 nm) and close to the Bohr radius. The corresponding EDS spectra, Figure 7, give the signal of Os and Te from quantum dots. The Na might from the reducing agent; the C, O and S are from the capping agent HSCH$_2$COOH. The Cl is from the OsCl$_4$ precursor. The Os:Te ratio of these nanoclusters was 1:2 which consistent with the stoichiometry ratio of OsTe$_2$. From the TEM analysis, the smallest size QDs will be used for electrochemical characterization and immunosensor fabrication because small quantum dots have high surface area [134].
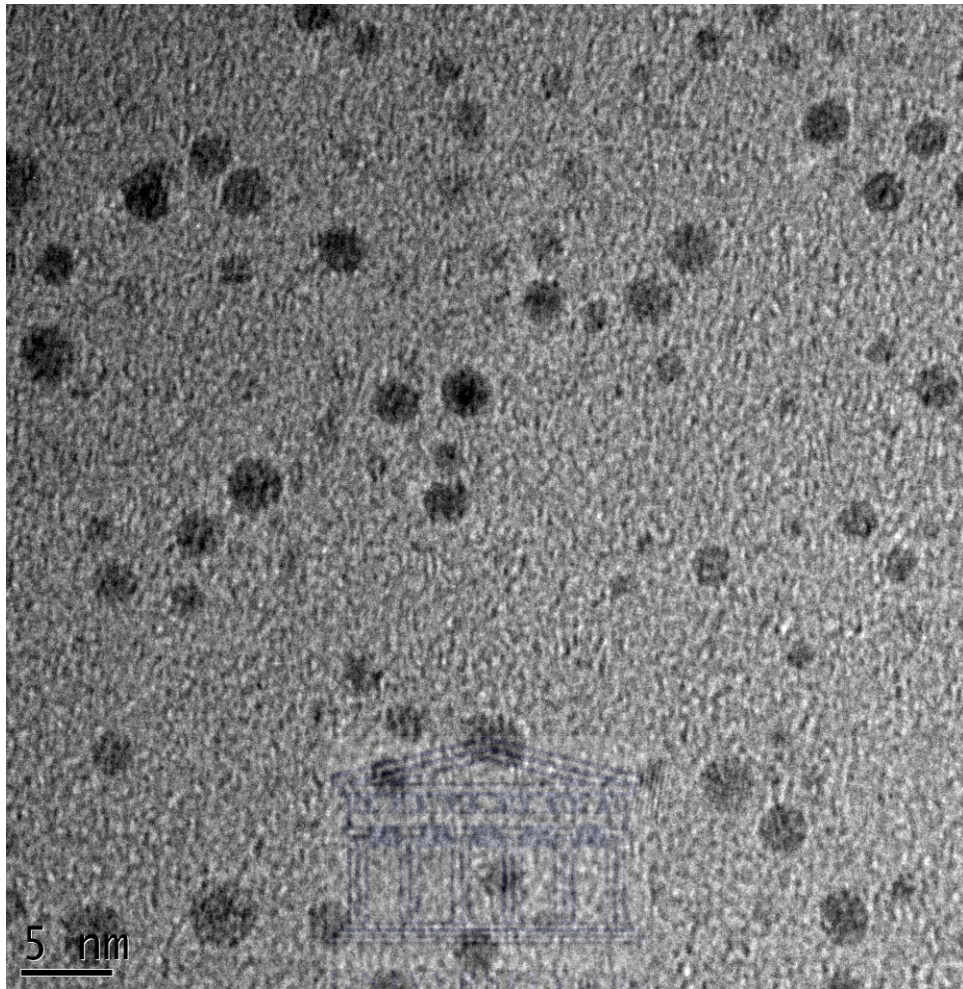
Figure 6. HR-TEM images of TGA-OsTe$_2$QDs.
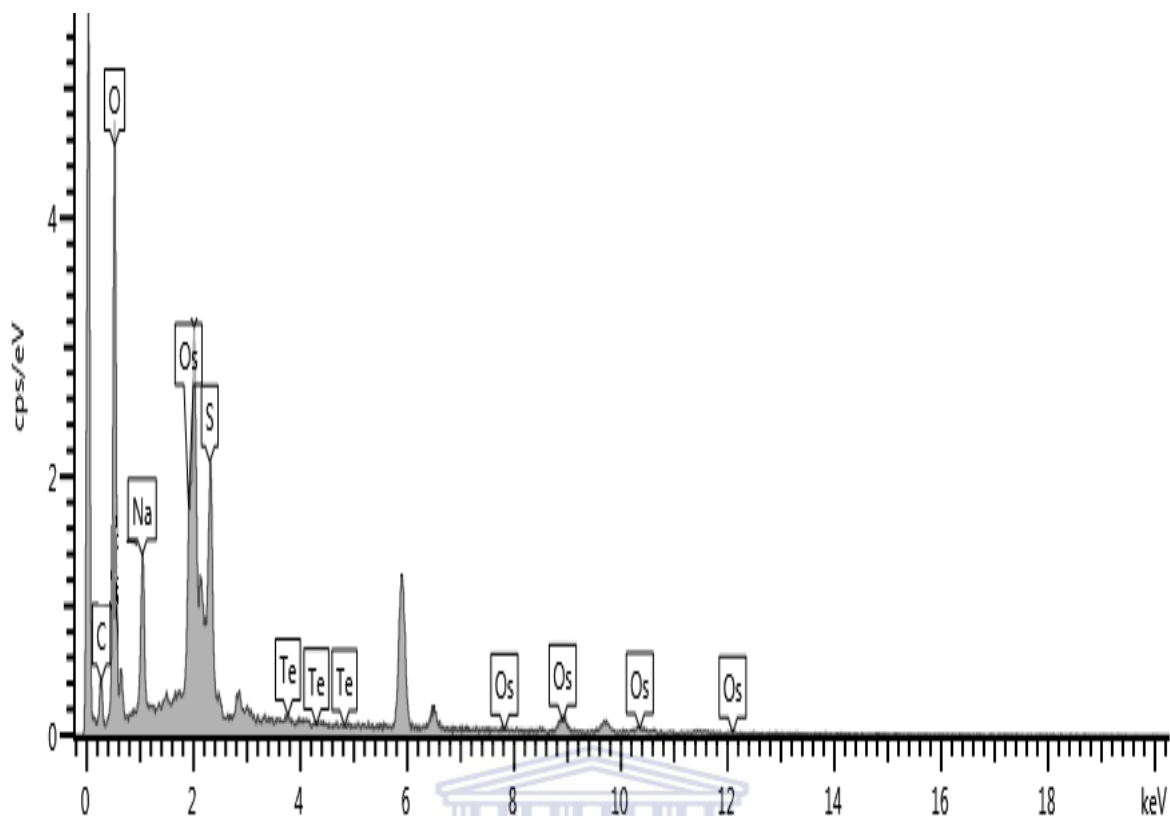
Figure 7. EDS spectrum of TGA-OsTe$_2$ QDs.

4.1.1.4 FTIR characterization of TGA-OsTe$_2$ quantum dots

Figure 8 depict the FT-IR spectra of (a) TGA and (b) TGA-OsTe$_2$ QDs. The band at 3247 cm^{-1} corresponds to the –OH stretching, the band at 1623 cm^{-1} mainly due to C=O stretching and the peak at around 1384 cm^{-1} arises from C-OH. Both C-O stretching (1145 cm^{-1}) and C-S stretching (619 cm^{-1}) were also detected from the FT-IR spectra. In addition, no S-H bond stretching appears at 2568 cm^{-1} in figure 8 (curve b) which implies that the sulfhydryl (-SH) has bound to Os atoms forming a TGA-Os complex and the polar carboxylic acid groups retains the surface of OsTe$_2$ quantum dots [135].
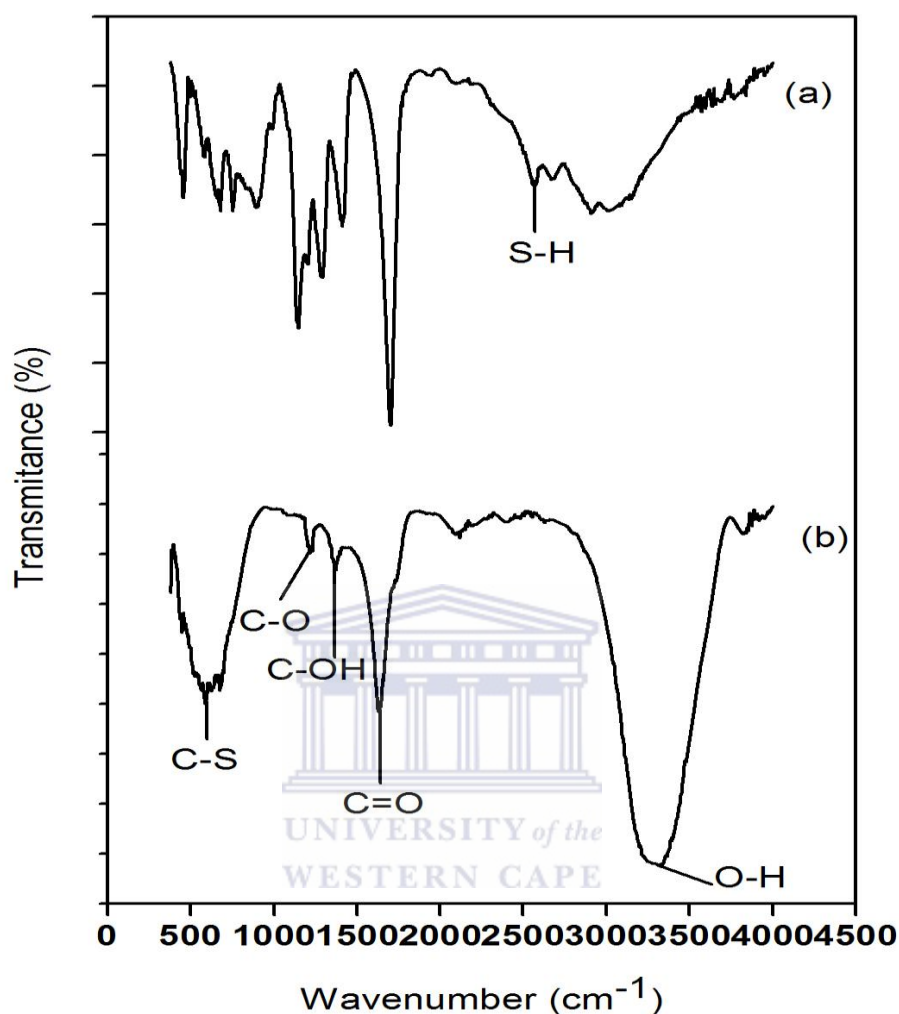
Figure 8. FT-IR spectra of (a) TGA and (b) TGA-OsTe$_2$QDs.

4.1.1.5 Electrochemical characterization of TGA-OsTe$_2$ quantum dots.

Figure 9 compared the electrochemical response of bare GC electrode (curve a), nafion at bare GCE denoted as Nafion|GCE (cure b) and TGA-OsTe$_2$QDs at bare GCE surface using nafion denoted TGA-OsTe$_2$QDs|Nafion|GCE (curve c). Curve (a) and curve (b) indicated that there are no redox peaks observed on a bare GC electrode and Nafion|GCE. However, the bare GCE appears to have high background current compared to Nafion|GCE. This was due to the fact that nafion prepared in water possesses low conductivity [136]. However, nafion

consist of acid ionic groups that hang from a fluorocarbon backbone making it stable matrix for immobilizing quantum dots. Curve (c), which shows the cyclic voltammogram of TGA-OsTe$_2$ QDs-Nafion|GCE, suggests that the electrochemical behavior of the quantum dots made a moderate contribution to the bare GCE. The anodic peak potential (E_{pa}) and the cathodic peak potential (E_{pc}) are located at 449.6 mV and -233.47 mV, respectively. The peak separation (ΔE_p) was found to be 108.06 mV indicating that TGA-OsTe$_2$ QDs immobilized on nafion|GCE displayed a one electron transfer. These results shows that the TGA-OsTe$_2$ QDs|nafion is surface controlled not diffusion controlled [137].
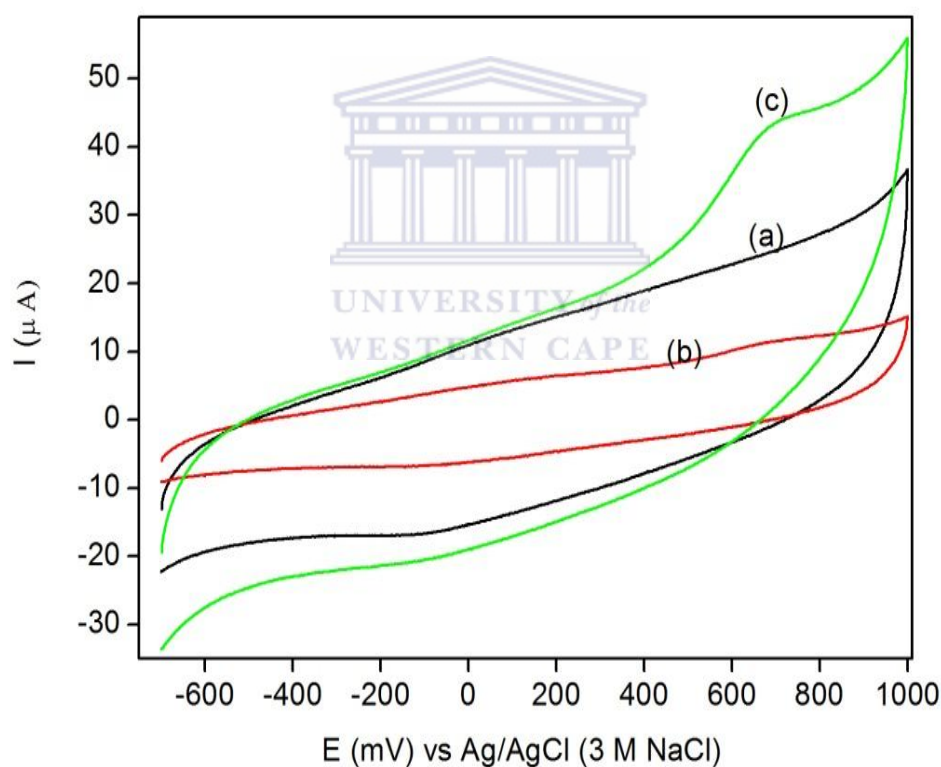

Figure 9. cyclic voltammograms of (a) bare GCE, (b) Nafion|GCE and (c) TGA-OsTe$_2$ QDs-Nafion|GCE in 0.1 M PBS. Scan rate = 50 mV s^{-1}.

Furthermore, the effect of scan rate on current peak was interrogated by running a series of cyclic voltammogram at different scan rates, Figure 10. The results from CV shows that the

anodic peak current varies linearly with the scan rate and the oxidation peak potential shifts to more positive values with increasing scan rate. A plot of anodic peak against the scan rate (Figure 11) is almost a straight line with linear regression I_{pa} (μ A) = 0.0256 x (-2.97) and a correlation coefficient R^2 = 0.9962. The dependence of anodic peak current on scan rate indicates the redox system of surface adsorbed species [138,139].
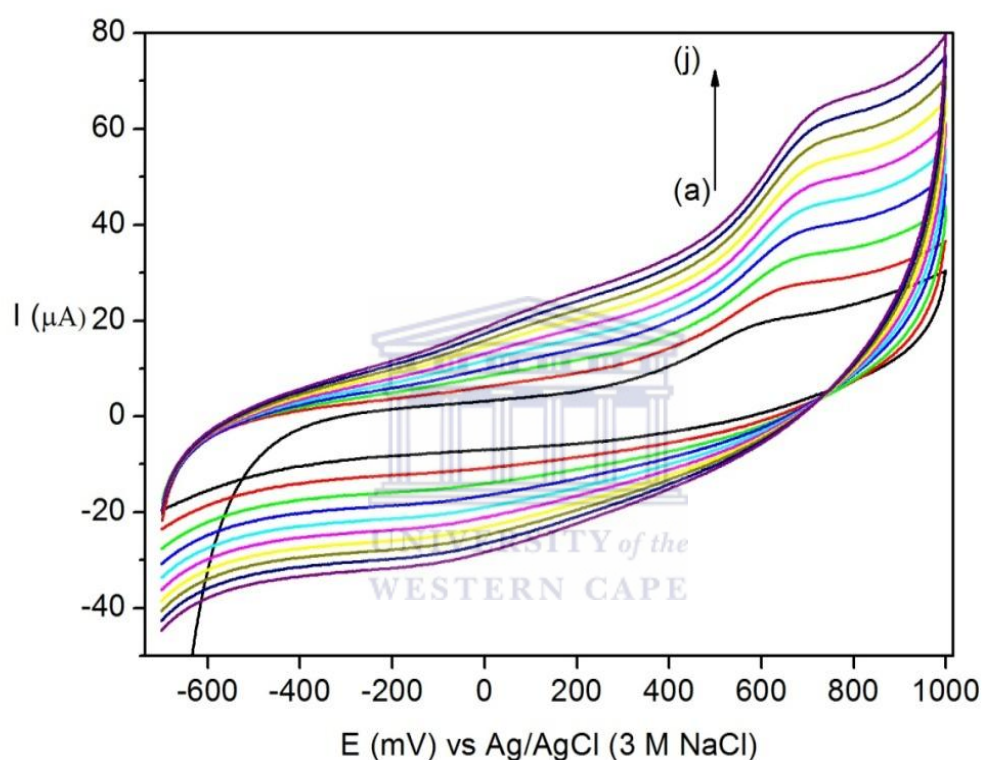

Figure 10. Cyclic voltammograms of TGA-OsTe$_2$ QDs-Nafion|GCE in 0.1 M PBS at (a) 10, (b) 20 , (c) 30 , (d) 40, (e) 50, (f) 60, (g) 70 , (h) 80 , (i) 90 and (j) 100 mV s^{-1}.

4.1.1.5.2 Impedimetric characterization of TGA-OsTe$_2$ QDs.

To further investigate electrochemical reaction mechanism and to determine the most reliable electrochemical circuit, electrochemical impedance spectroscopy (EIS) was utilized. The Nyquist plots of bare GCE (a), Nafion|GCE (b) and TGA-OsTe$_2$ QDs-Nafion|GCE are shown in Figure 12. The Nyquist plot consists of two parts namely: the semicircle part and the linear

part. The semicircle part appears at higher frequencies and it corresponds to the electron transfer limited process and the diameter of the semicircle is equivalent to the electron transfer resistance (R_{ct}). The linear part which appears at lower frequencies corresponds to the diffusion limited process.

From the EIS spectra, the initial charge transfer resistance (R_{ct}) of the bare GC electrode was 1.9079×10^6 kΩ and decreased to 2.3898×10^5 kΩ and 1490 kΩ for Nafion|GCE and TGA-OsTe$_2$ QDs respectively, as shown in (Figure 12 insert).S The change in R_{ct} values is caused by the negatively charged and/or partially negative (carboxyl, carbonyl and hydroxyl) groups localized on GCE surface. These groups hinder the diffusion of electrons towards the electrode surface. The R_{ct} values also indicate that TGA-OsTe$_2$ QDs are semiconducting. The electron transfer reaction monitored by EIS at TGA-OsTe QDs-Nafion|GCE surface is in agreement with a standard Randle's circuit model (Figure 13) in high frequency range. The impedance parameters (Table 4) were obtained by fitting an equivalent circuit that consist of solution resistance (R_s), charge transfer resistance (R_{ct}), constant phase element (*CPE*) and the Warburg resistance (W_s), Figure 9 [140].
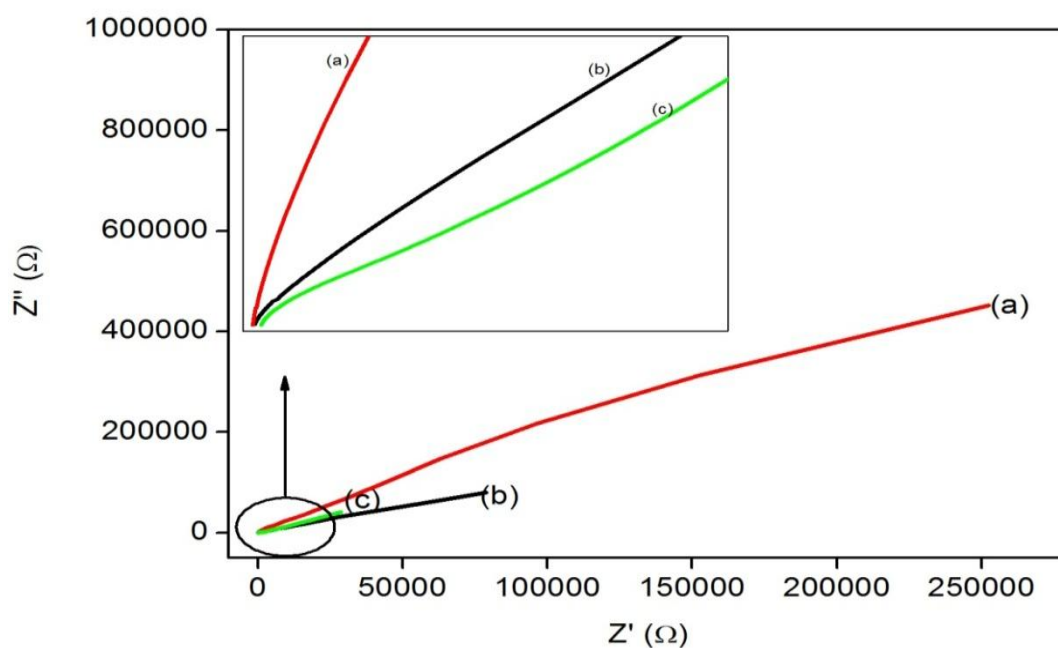
Figure 12. Electrochemical impedance spectra of (a) bare GCE, (b) Nafion|GCE and TGA-OsTe$_2$ QDs-Nafion|GCE within a frequency range from 100 mHz to 100kHz in 0.1 M PBS (pH 7.0).
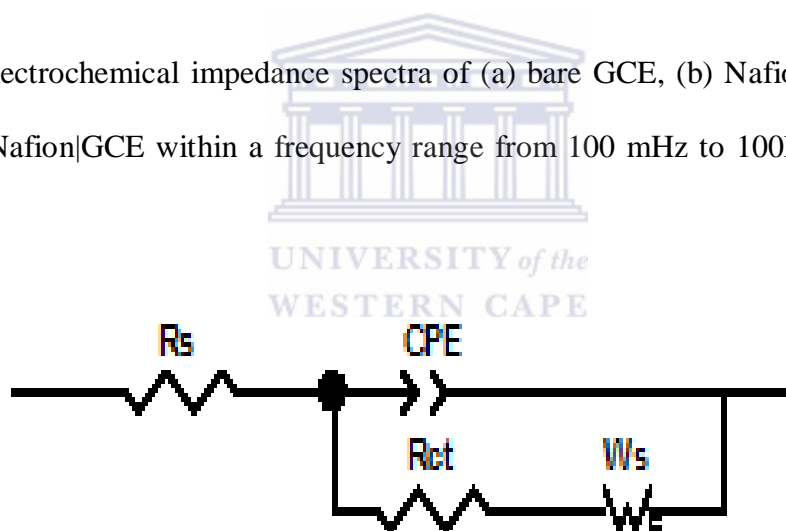

Figure 13. Randles circuit of TGA-OsTe$_2$ QDs-Nafion|GCE.

Table 4. EIS parameters of modified GCE in 0.1 M PBS (pH 7.0).

Electrode	R_{ct} (k Ω)	C_{dl} (μF)	R_s (kΩ)	W_s (kΩ s$^{-0.5}$)
Bare GCE	1.9079 x 10^6	4.9704 x 10^{-7}	222.6	367.15
Nafion|GCE	2.3898 x 10^5	8.5079 x 10^{-6}	31.7	224.69
TGA-OsTe$_2$QDs-Nafion|GCE	1490	4.2032 x 10^{-6}	842	65.79

From ω_{max} (frequency at maximum imaginary impedance of the semi circle), important information about kinetic parameters of electron transfer such as time constant τ (cycle life), and exchange current (I_o) and the heterogeneous rate constant k_{et} [141,142] were calculated from the following equations:

$$\omega_{max} = \frac{1}{R_{ct}C_{dl}} \tag{23}$$

$$\tau = R_{ct}C_{dl} \tag{24}$$

$$I_o = \frac{RT}{nFR_{ct}} \tag{25}$$

$$k_{et} = \frac{I_o}{nFAC_o} \tag{26}$$

where $\omega_{max} = 2\pi$F, C_{dl} is the double layer capacitance or constant phase element, $R = 8.314$ J K^{-1} mol^{-1}, $F = 96486$ C mol^{-1}, $n = 1$, C_o is the concentration of PBS (pH 7.0) = 0.1 mol cm^{-3}. The maximum frequency (f) values obtained from Figure 12, were 13.792 Hz, 24.746 Hz and 67.654 Hz for the bare GCE, Nafion\|GCE and TGA-OsTe$_2$ QDs-Nafion\|GCE respectively.

Table 5. Electro-kinetic parameters bare and modified GCE.

Electrode	ω_{max} (rad s^{-1})	τ (s rad^{-1})	I_o (A)	k_{et} (cm s^{-1})	F_Φ (Hz)
Bare GCE	1.0545	9.483×10^{-1}	1.345×10^{-5}	4.6497×10^{-8}	1.38×10^{2}
Nafion|GCE	4.918×10^{-1}	20.332×10^{-1}	1.0745×10^{-4}	3.7121×10^{-7}	2.47×10^{2}
TGA-OsTe$_2$QDs-Nafion|GCE	1.59×10^{3}	6.2627×10^{-3}	1.72×10^{-2}	5.942×10^{-5}	6.76×10^{2}

From the Table, it is observed that the bare GCE has lower exchange current (1.3459×10^{-5} A) compared to TGA-OsTe$_2$ QDs-Nafion\|GCE with 0.0172 A. A high exchange current at the modified electrode, TGA-OsTe$_2$ QDs-Nafion\|GCE, indicate that there is an increase in electron transfer. The increase in electron transfer at the modified electrode is cause by the TGA-OsTe$_2$ QDs [13]. The surface cover of TGA-OsTe$_2$ QDs on GCE was calculated using the following equation:

$$\theta = 1 - \frac{R_{ct}^{TGAOsTe_2QDS}}{R_{ct}^{bareGCE}} \qquad (27)$$

From the above equation and the R_{ct} values in Table 4, the surface coverage of TGA-OsTe$_2$ QDs onto GCE was 0.9992 (99.92 %) which indicates a good coverage [143]

4.2 Synthesis and characterization of Ppy|GCE

Electrochemical polymerization of pyrrole monomer was performed by cyclic voltammetry in 0.1 M LiClO$_4$ in the potential range -800 mV to 400 mV through 20 cycles. As shown in Figure 14, at the first scan, there is a cathodic peak at 50 mV. By continuing electropolymerization through the second scan, another anodic peak was observed at 70 mV indicating the formation of polypyrrole [144].
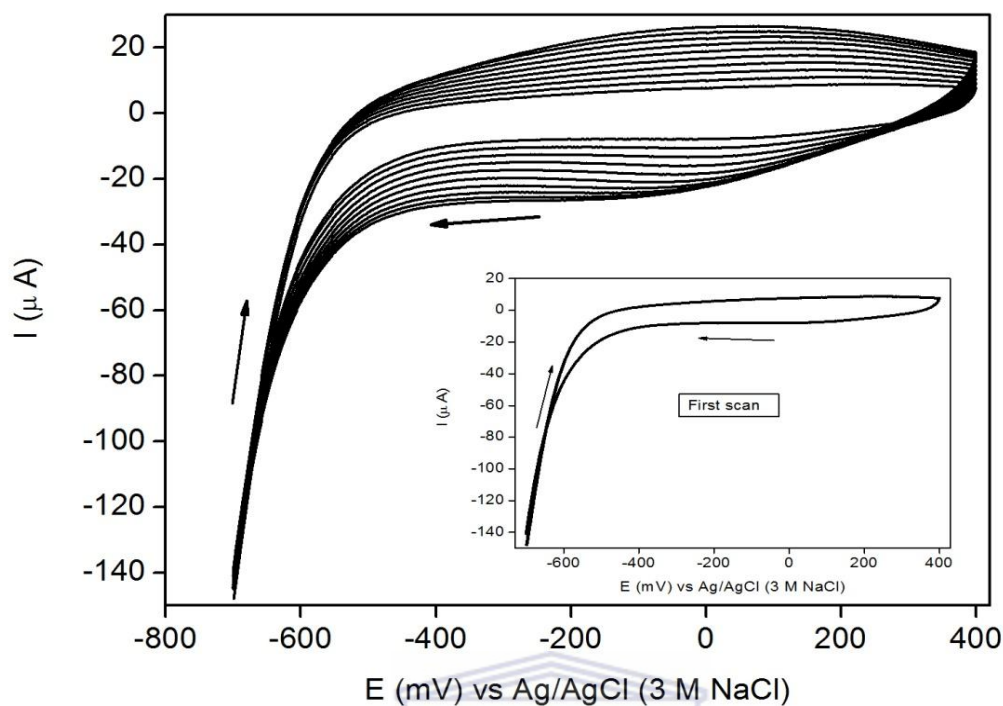
Figure 14. Polymerization of pyrrole monomer in 0.1 M LiClO$_4$ at 50 mV s^{-1}.
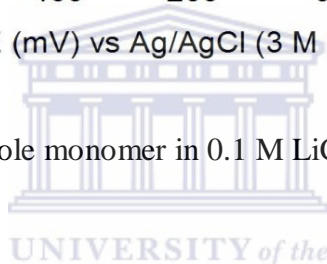
4.2.1 Characterization of Ppy|GCE in 0.1 M PBS (pH 7.0)

Cyclic voltammetry was used to study the reversibility of electron transfer in Ppy film because the oxidation and reduction peaks of Ppy film can be monitored in the form of current - potential diagram. The multiscan voltammogram, Figure 15, shows two well defined redox peaks (a) and (b) for Ppy|GCE. The anodic and cathodic peaks for Ppy|GCE are observed at 224 mV and 560 mV respectively. Both peak potential and the corresponding peak currents varied indicate that the polymer was electroactive and diffusion of electrons was taking place along the polymer chain [145,146].
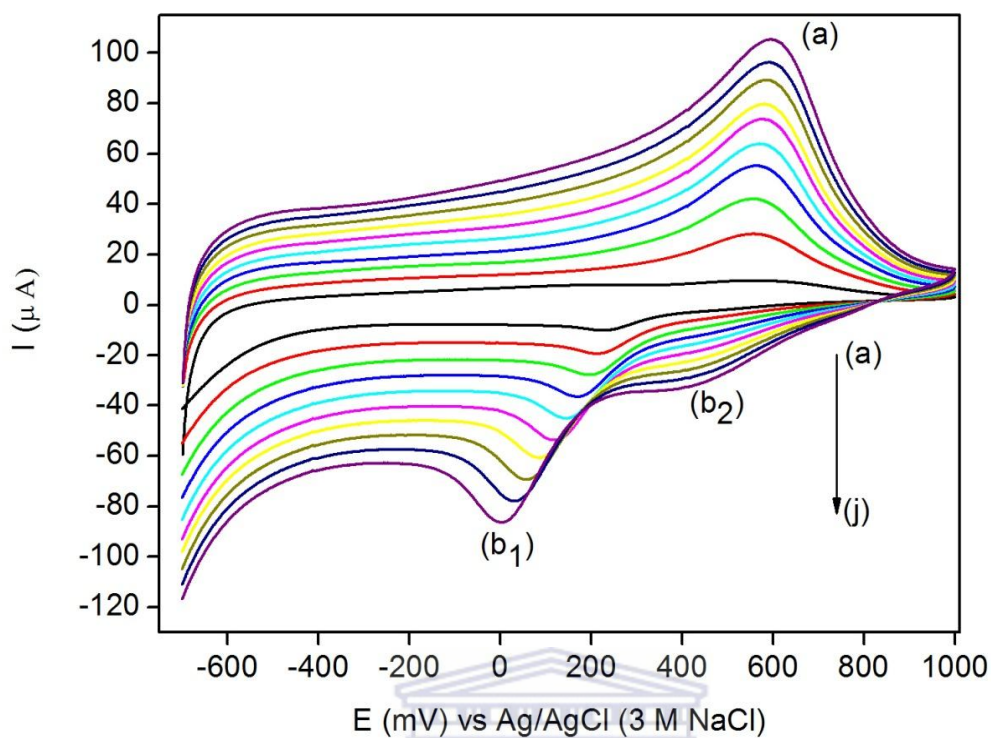
Figure 15. Multiscan voltammograms of Ppy obtained in 0.1 M PBS (pH 7.0) at scan rate of : (a) 10 , (b) 20 , (c) 30 , (d) 40 , (e) 50 , (f) 60 , (g) 70 , (h) 80 (i) 90 and (j) 100 mV s^{-1}.

The multiscan voltammograms of Ppy|GCE in Figure 15 also indicates that as the scan rate is increased, the anodic peak potential shifts to more negative potential values. In the range of 10 mV s^{-1} to 100 mV s^{-1} the reduction peak current of Ppy increases linearly with the square root of scan rate in Figure 16, demonstrating that the electron transfer of Ppy is diffusion defined (rapid reversible electron transfer reaction) [147].
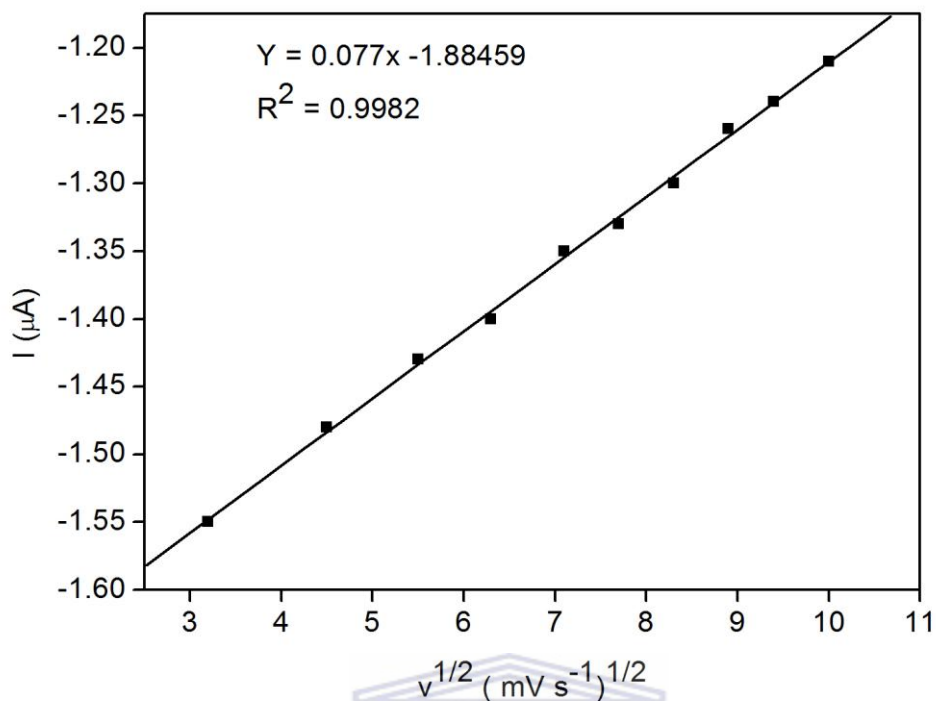
Figure 16. Randel-Sevčik plot of polypyrrole electrochemistry in 0.1 M PBS (pH 7.0).

The oxidation or reduction of polypyrrole requires two simultaneous processes: (i) the transfer of electrons either from or to pyrrole and (ii) the diffusion of the counterion or cation into or out of polypyrrole film to maintain charge neutrality. The redox mechanism of polypyrrole is described by one electron transfer:

Ppy   Ppy⁺
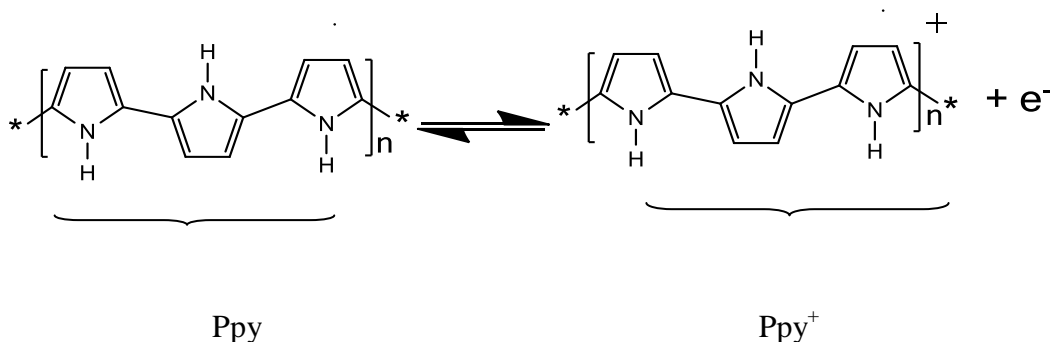
where Ppy is the neutral species and Ppy$^+$ is the radical cation species or polarons (one positive charge localized over three or four monomer units). The polaron can be further be oxidized:

Ppy⁺   Ppy⁺⁺
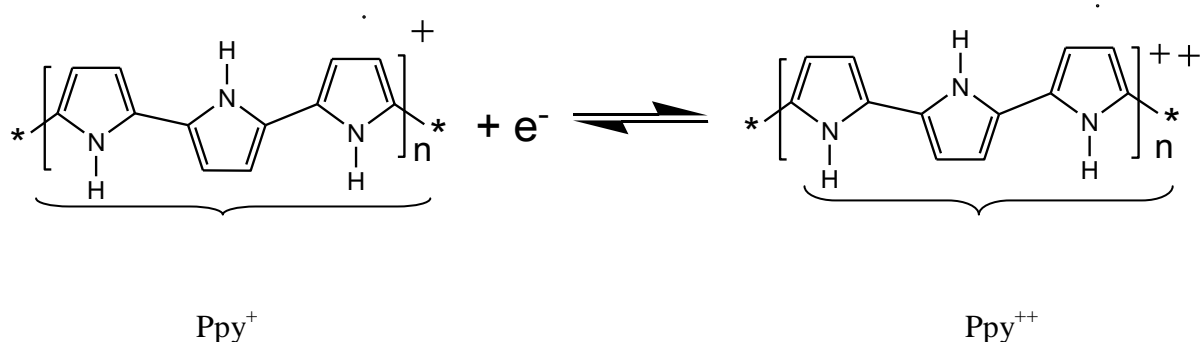
where Ppy is the dicationic species or bipolarons (two positive charges localized over three or four monomer units). This explains the existence of intense reduction peak in Ppy, one strong peak at Figure 15 (curve (a)) when characterized in 0.1M PBS (pH 7.0). On the cathodic scan, the bipolaron species (Ppy^{++}) was reduced to the radical cation species (Ppy^+) which is responsible for Peak (a) (Figure 10) while the radical cationic species was further reduced to the natural Ppy species. In the reverse scanning (cathodic scan), the neutral Ppy was oxidized to the dicationic species Ppy^{++} denoted by peak b_1 (Figure 15). This corresponds with the previous literature [19]. However at high scan rate, a second oxidation peak was observed (Figure b_2) as a result of the polaron (Ppy^+). It is evident that both polarons and bipolarons were present in the film containing $LiClO_4$. The $LiClO_4$ was used as a dopant during electropolymerization (as reported in Section 3.1.2.2.1) to enhance electrical neutrality during polymerization. The surface coverage (Γ^*) of Ppy film onto GCE was estimated using Brown-Anson model [148].

$$I_p = \frac{n^2 F^2 \Gamma^*_{Ppy} A v}{4RT} \qquad (29)$$

where $n = 2$ is the number of electrons, F is the faradays constant (96584 C mol^{-1}), Γ^*_{Ppy} is the surface coverage of Ppy film (mol cm^{-2}), A is the area of glassy carbon electrode (0.03 cm^2), v is the scan rate (mV s^{-1}), R is the gas constant (8.314 J mol^{-1} K^{-1}) and T is the temperature (298 K). The surface coverage Γ^*_{ppy} was estimated to be 3.2995 x 10^{-10} mol cm^{-2} as confirmed by literature [148].

The electrochemical behavior of Ppy|GCE was investigated to elucidate the electron transfer in 0.1 M PBS (pH 7.0). The cyclic voltammograms of the bare GCE and Ppy|GCE which are shown in Figure 17, were recorded in the presence of 0.1 M PBS (pH 7.0) at a scan rate 50 mV s^{-1}. At the bare GCE (Figure 17, curve a) no redox peaks were observed. However, at Ppy|GCE, a pair of well-defined redox peak was observed with a peak-to-peak separation (ΔE_p) of 360 mV. This improved electrochemical behavior can be attributed to good electrical conductivity of Ppy on GCE surface. The increase in both the anodic and cathodic peak currents also shows that the conducting Ppy increased the electroactive surface area of the electrode and enhanced faster electron transfer between the solution and the electrode compared to the bare GCE. Based on the conductivity of the electrodeposited Ppy, the possibility of the polymer being overoxidized was ruled out because overoxidized Ppy is not conductive [149]. Therefore it was of great importance to overoxidize Ppy.
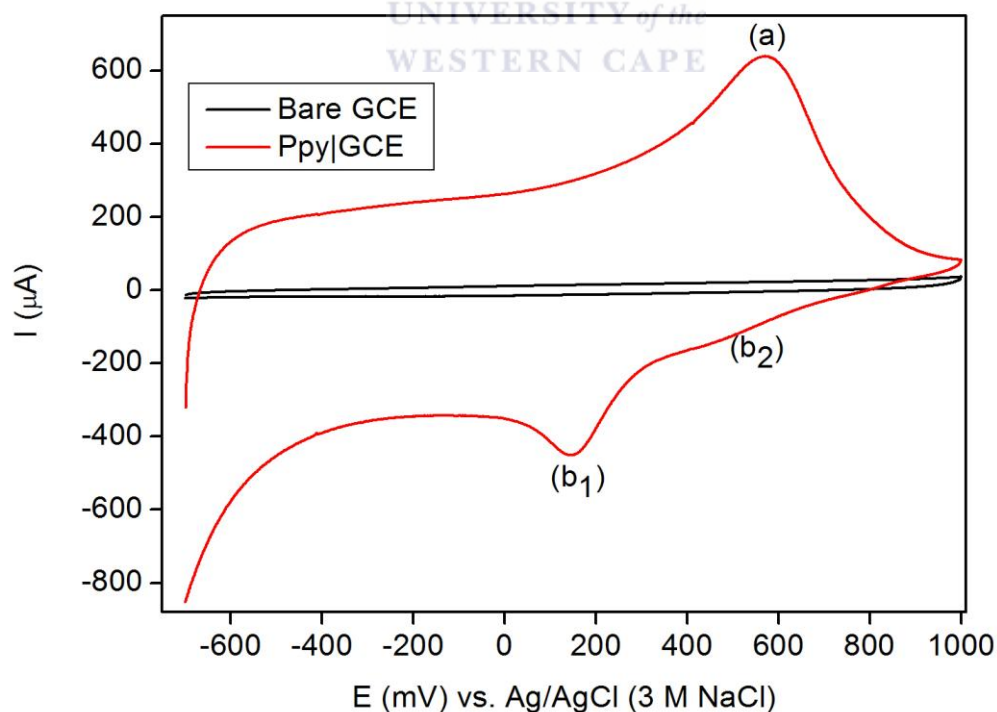
Figure 17.Cyclic voltammograms of (a) bare GCE and (b) Ppy|GCE in 0.1 M PBS (pH 7.0) at 50 mV s^{-1}.

4.3 Overoxidation of polypyrrole

Overoxidation of polypyrrole was performed in 0.1 M NaOH at potential of 1000 mV for 420 min indicated in Figure 18. The voltammogram shows current reduction response as reported by Paramo-Garcia *et al.* 2012 [150].
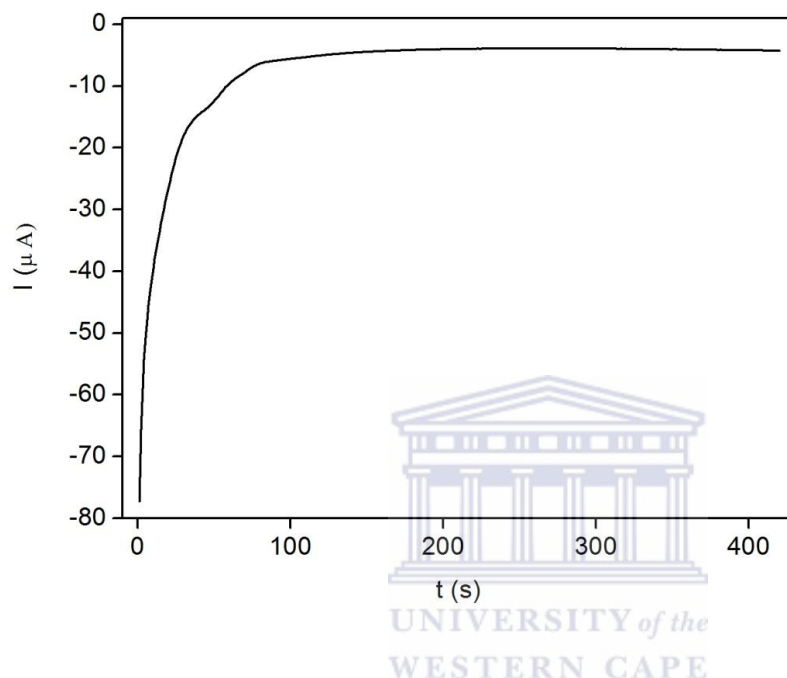
Figure 18. Overoxidation of Ppy in 0.1 M NaOH for 420 s.

During overoxidation, pours are created on polypyrrole film thus allowing the accumulation of nanoparticles. TGA-OsTe$_2$ QDs were immobilized on the overoxidized Ppy modified electrode denoted as TGA-OsTe$_2$ QDs|OvoxPpy|GCE and was characterized in 0.1 M PBS (pH 7.0) to test the conductivity of the prepared electrode, to confirm that whether polypyrrole was overoxidized and to investigate the catalytic effect of the quantum dots on the overoxidized polypyrrole as shown in Section 4.4.

4.4 Morphological characterization of the electrode assembly

The morphologies of the as-obtained polymers have been investgated by SEM, and the morphological changes of Ppy, OvoxPpy and TGA-OsTe$_2$ QDs|OvoxPpy are shown in Figure 19. As can been in Figure 19 (a), Ppy has a dense packing plate-like structure. Comparatively, when Ppy was overoxidized (Figure 19 (b)), nanopores were created on the polymer surface making it a suitable matrix for immobilization of quantum dots. As quantum dots were immobilized on the surface of OvoxPpy, the structure of Ppy film changed to a cauliflower-like structure (Figure 19 (c)).

(b)

| 200 nm | EHT = 5.00 kV | Signal A = InLens | Date :5 Mar 2014 | ZEISS |
| | WD = 4.5 mm | Mag = 50.00 K X | Time :14:34:29 | |
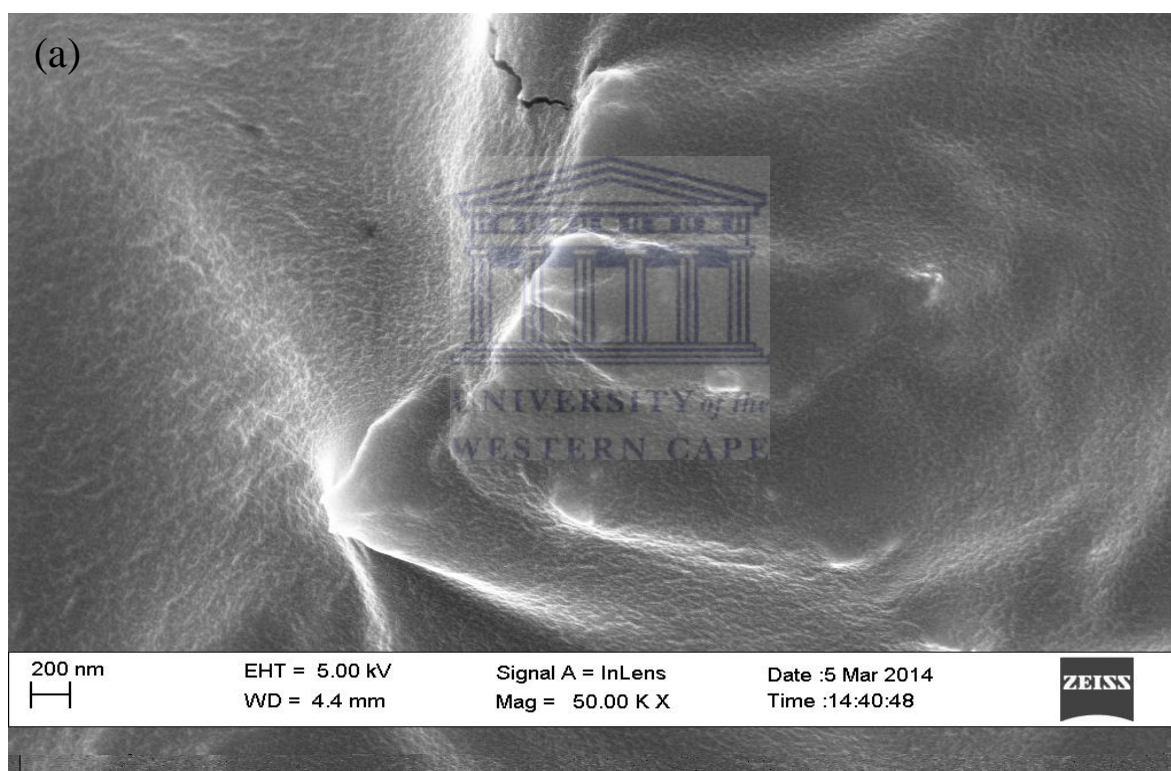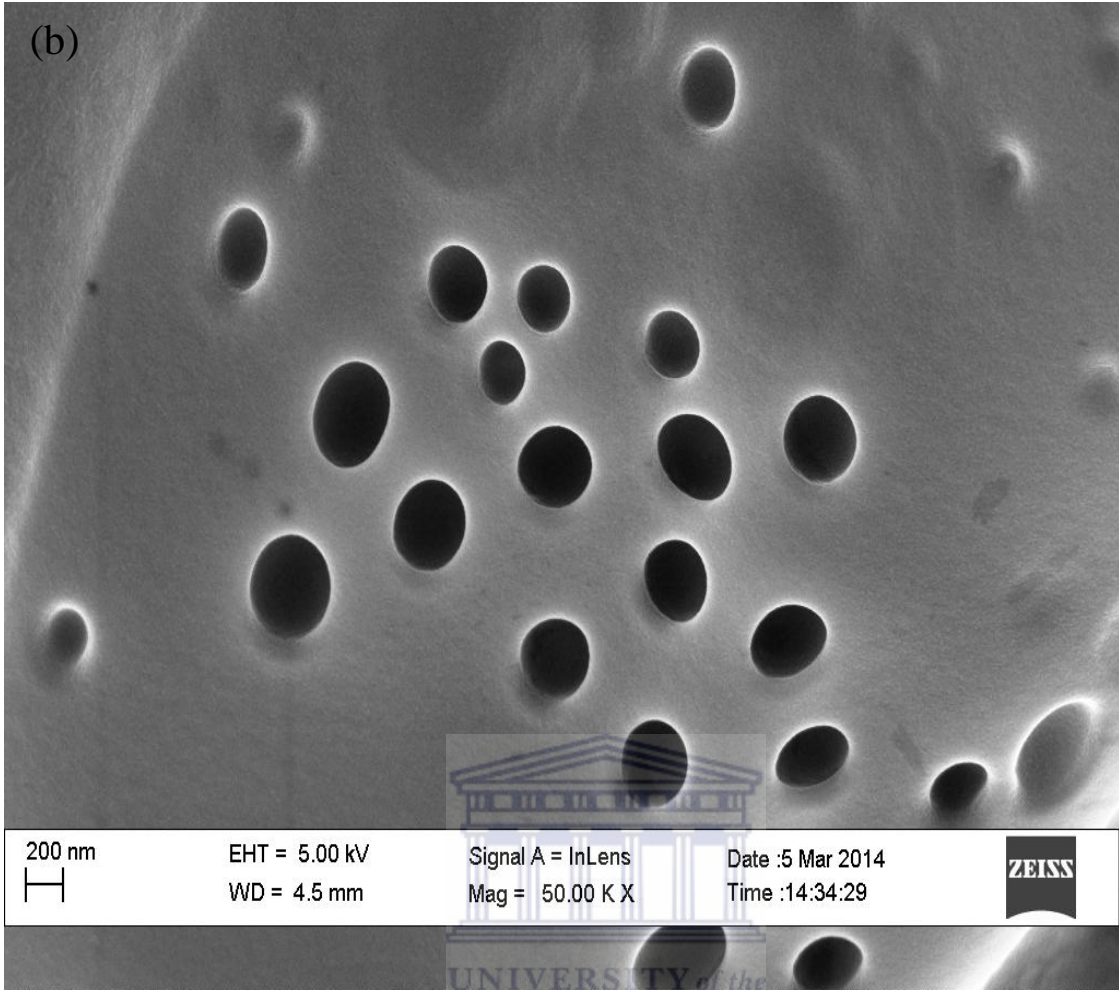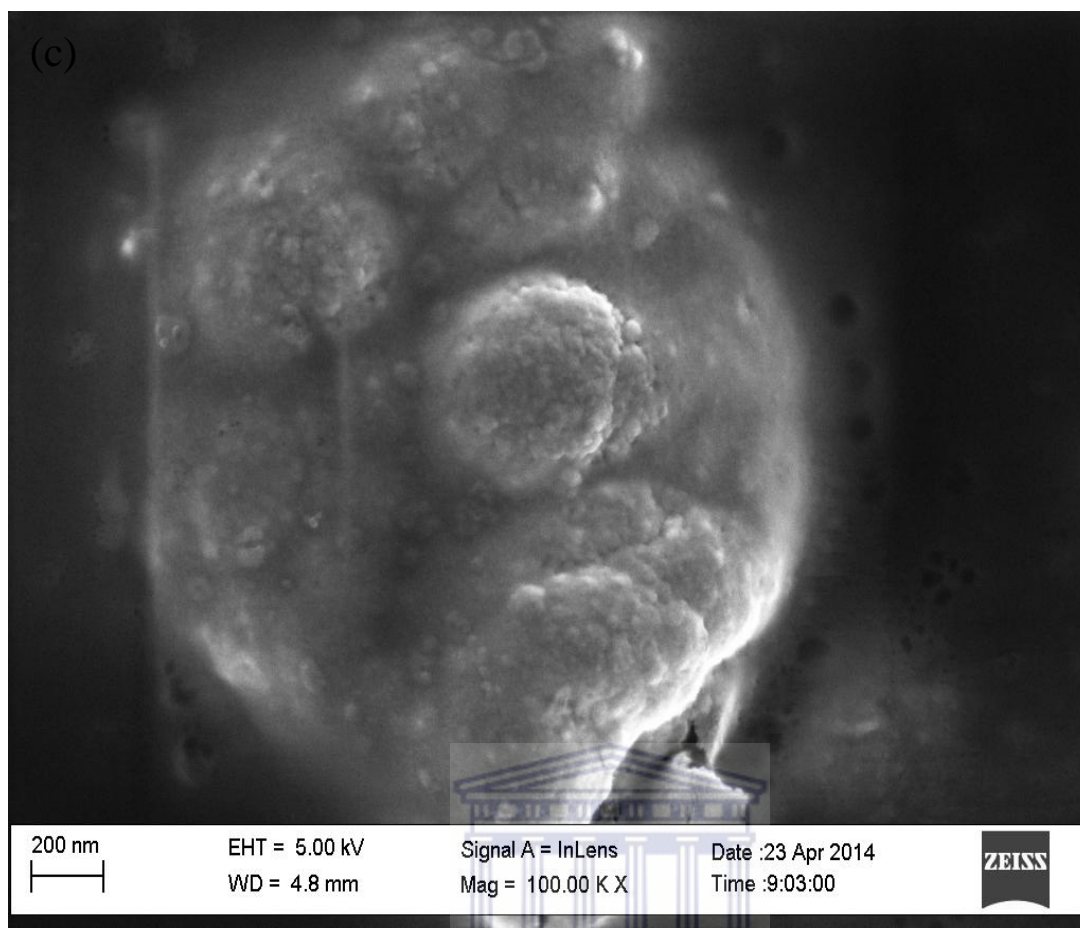
Figure 19. SEM micrographs of (a) Ppy, (b) OvoxPpy and (c) TGA-OsTe$_2$ QDs|OvoxPpy

4.4 Electrochemical characterization of TGA-OsTe$_2$ QDs|OvoxPpy|GCE

During overoxidation process, carbonyl groups such as C=O and $^-$COO$^-$ generated along the polymer backbone. This process usually results in a loss of conjugation and loss of electronic conductivity [151]. The cyclic voltammograms at Figure 20 showed the effect of potential on bare GCE, Ppy|GCE, OvoxPpy|GCE and TGA-OsTe$_2$ QDs|OvoxPpy|GCE. At Figure 21 (curve a), the bare GC electrode showed no redox peaks hence no peak- to- peak separation between potential peaks was observed. However, OvoxPpy|GCE (Figure 21, curve b) showed two broad redox peaks at 289 mV (anodic) and -215 mV (cathodic). On the other hand, TGA-OsTe$_2$ QDs|OvoxPpy|GCE (Figure 21, curve c) showed an increase in the capacitative current with the two redox peaks at 447 mV ($\mathbf{P_a}$) and -271 mV ($\mathbf{P_c1}$). The peak-to-peak separation

between potential peaks (ΔE_p) was 37 mV and 88 mV for OvoxPpy|GCE and TGA-OsTe$_2$ QDs|OvoxPpy|GCE respectively. Due to the resistance of the insulating OvoxPpy film, the direct electron transfer and mass transfer were blocked and thus ΔE_p is lower than TGA-OsTe$_2$ QDs|OvoxPpy|GCE. Apart from its non-conductive property, OvoxPpy|GCE might have enhanced the laoding of the quantum dots and, thus, created significant change in surface area and the kinetics involved [152]. The data obtained from Figure 21 were recorded in Table 6.
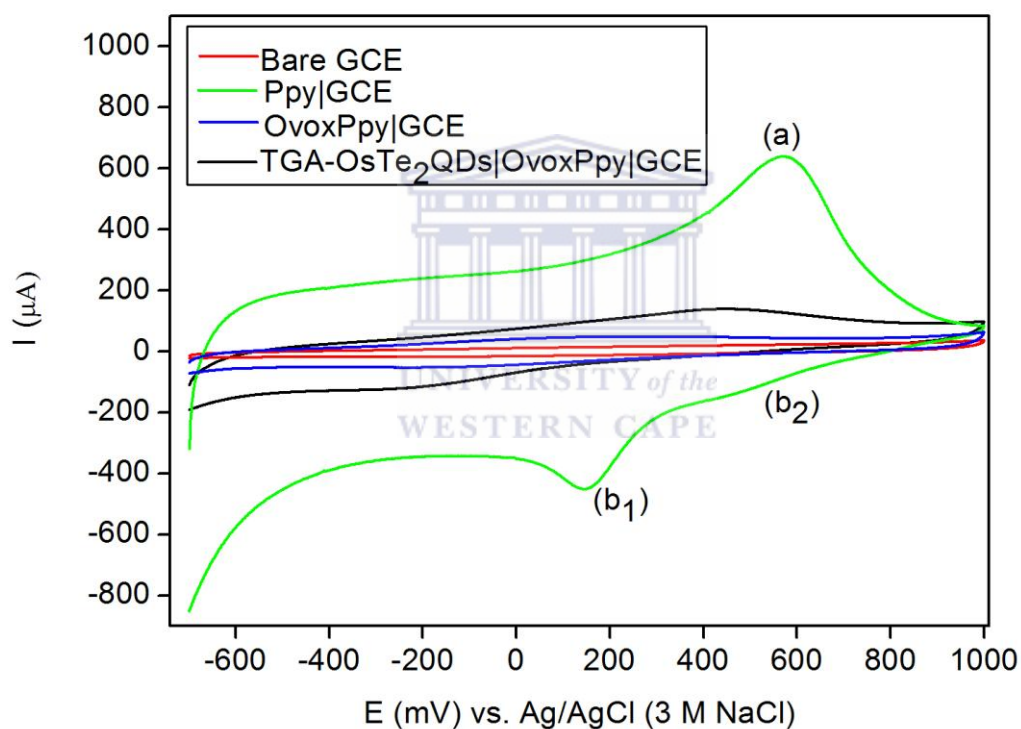
Figure 20.Cyclic voltammograms of bare GCE, Ppy|GCE, OvoxPpy|GCE and TGA-OsTe$_2$ QDs|OvoxPpy|GCE in 0.1 M PBS at 50 mV s^{-1}.
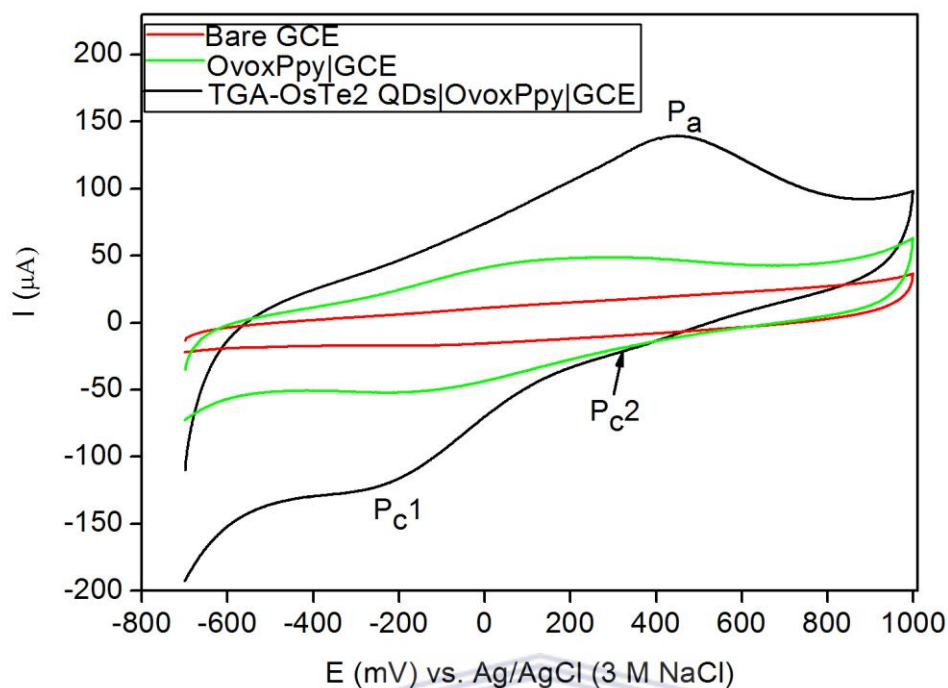
Figure 21.Cyclic voltammograms recorded with (a) bare GCE, (b) OvoxPpy|GCE and (c) TGA-OsTe$_2$ QDs|OvoxPpy|GCE in the presence of 0.1 M PBS (pH 7.0) at scan rate 50 mV s^{-1}.

Table 6. CV data obtained from Figure 21.

Electrode	E_{pa} (mV)	E_{pc} (mV)	I_{pa} (μA)	I_{pc} (μA)	ΔE_p (mV)	I_p (μA)
OvoxPpy|GCE	-215	289	-5.129	4.90	37	-1.04
TGA-OsTe$_2$ QDs|OvoxPpy|GCE	-271	447	-12.32	14.04	88	0.8

Figure 22 shows cyclic voltammogram of modified TGA-OsTe$_2$ QDs electrode with OvoxPpy at different scan rate. As can be seen in Figure 22, when the scan rate was increased, the modified electrode denoted TGA-OsTe$_2$ QDs|OvoxPpy|GCE showed a gradual increase in peak currents as well as the shift in the potential resulting in moderate change in

peak-to-peak separation with each consecutive scan rate change. Based on the results indicated in Figure 22, it may be deduced that TGA-OsTe$_2$ QDs|OvoxPpy nanocomposite film was stable and exhibited reversible electrochemistry. On the other hand, a linear relationship was observed between the cathodic peak current (**P$_c$1**) and the anodic peak current (**P$_a$**) for TGA-OsTe$_2$ QDs|OvoxPpy|GCE (Figure 23). From the linear plots, the surface coverage was also estimated using Brown-Anson model:

$$I_p = \frac{n^2 F^2 \Gamma^*_{\text{TGA-OsTe2 QDs|OvoxPpy}} A v}{4RT} \qquad (29)$$

where $n = 2$ is the number of electrons, F is the faradays constant (96584 C mol^{-1}), Γ^*_{Ppy} is the surface coverage of Ppy film (mol cm^{-2}), A is the area of glassy carbon electrode (0.03 cm^2), v is the scan rate (mV s^{-1}), R is the gas constant (8.314 J mol^{-1} K^{-1}) and T is the temperature (298 K). Compared to surface coverage Γ^*_{ppy}, the surface coverage $\Gamma^*_{\text{TGA-OsTe2QDS|OvoxPpy}}$ was increased to be 3.9695 x 10^{-5} mol cm^{-2} indicating that OvoxPpy is a perfect matrix for loading TGA-OsTe$_2$ QDs [148].
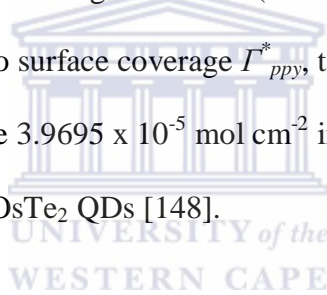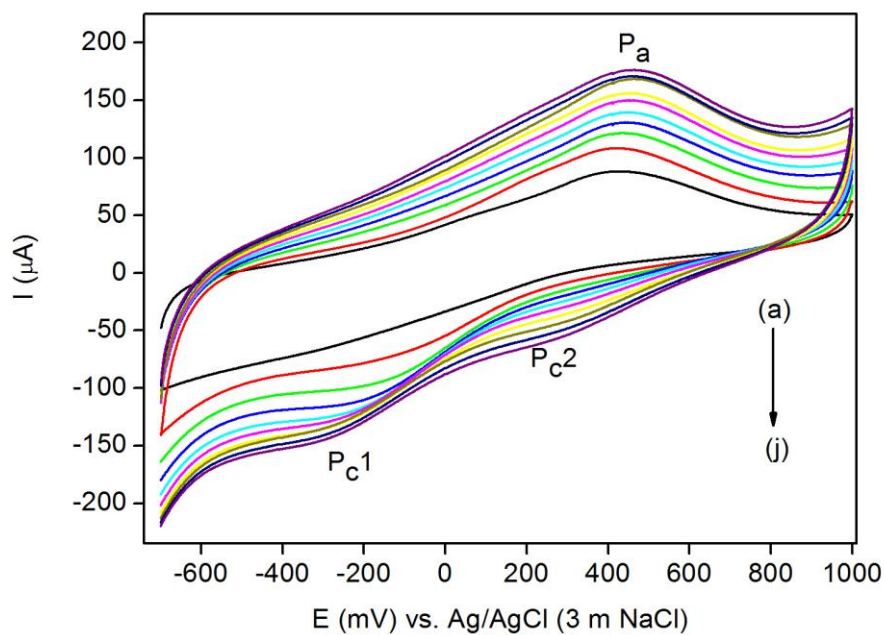
Figure 22. Multiscan voltammograms of TGA-OsTe$_2$ QDs|OvoxPpy|GCE obtained in 0.1 M PBS (pH 7.0) at scan rates: (a) 10, (b) 20 (c) 30, (d) 40, (e) 50, (f) 60, (g) 70, (h) 80, (i) 90, and (j) 100 mV s^{-1}.
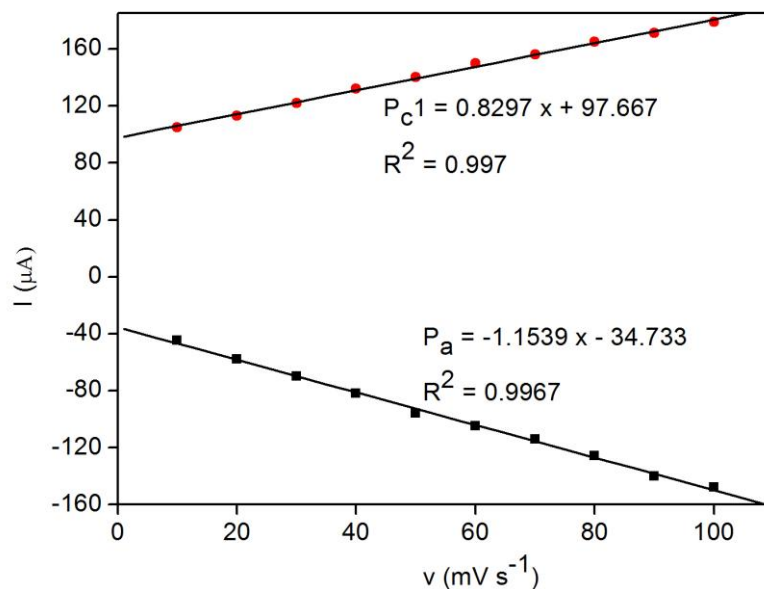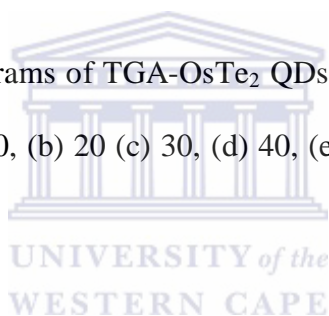
Figure 23. Brown-Anson plots of anodic peak current ($\mathbf{p_a}$) and cathodic peak current ($\mathbf{p_c1}$) for the CV's of TGA-OsTe$_2$QDs|OvoxPpy|GCE shown in Figure 16.

CHAPTER 5

Chapter review

This chapter gives a brief overview on the voltammetric and impedimetric responses of the TGA-OsTe$_2$ QDs based immunosensor towards different concentrations of PSA in biological buffer solution (0.1 M PBS, pH 7.0)

5.0 Results and discussion 2

5.1 Responses of immunosensor to PSA

Cyclic voltammetry results were further confirmed by EIS. The Nyquist plot and the Bode plot were used to investigate changes on the electron transfer process at electrode – solution interface through the biosensor formation and immunocomplex formation upon changes in PSA concentration.
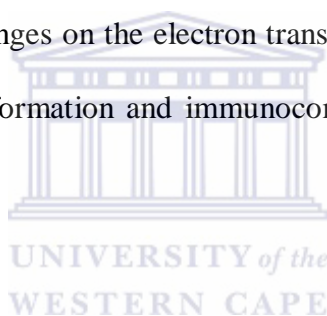
Figure 24 shows a stepwise fabrication of the immunosensor in the frequency range from 100 mHz to 100 kHz: (a) bare GCE (b) TGA-OsTe$_2$ QDs|OvoxPpy|GCE, (c) anti-PSA-antibody|TGA-OsTe$_2$ QDs|OvoxPpy|GCE and (d) BSA- anti-PSA-antibody|TGA-OsTe$_2$ QDs|OvoxPpy|GCE. As mentioned in Section 4.1.1.5.2, the semicircle portion observed at high frequencies in Nyquist plots corresponds to the electron transfer limited process and the diameter of the semicircle is equivalent to the electron transfer resistance. The linear part of the Nyquist plot at lower frequencies corresponds to the diffusion limited process. The Nyquist plot can be further interpreted by fitting with the Randles equivalent circuit (inset Figure 24). The circuit includes resistance of the electrolyte solution (R_s), double layer capacitance (C_{dl}), electron transfer resistance (R_{ct}) and the Warburg impedance (W_s).
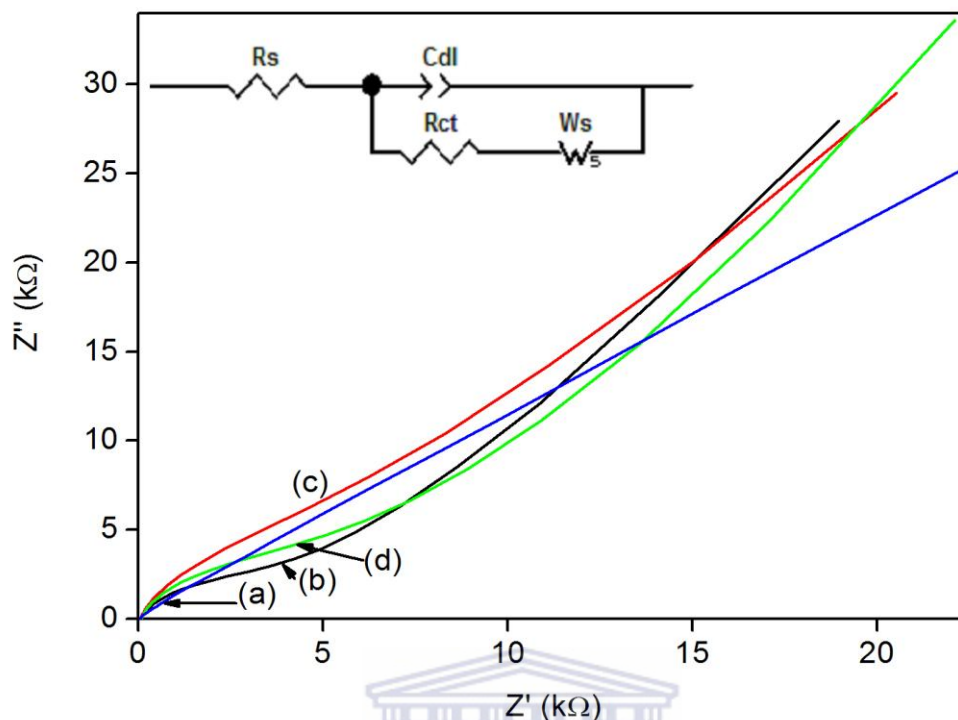
Figure 24: Nyquist plots of the electrochemical impedance spectra of (a) bare GCE, (b) TGA-OsTe$_2$ QDs|OvoxPpy|GCE, (c) anti-PSA-antibody|TGA-OsTe$_2$ QDs|OvoxPpy|GCE and (d) BSA- anti-PSA-antibody|TGA-OsTe$_2$ QDs|OvoxPpy|GCE, within frequency range from 100 mHz to 100 kHz in 0.1 M PBS (pH 7.0).

Table 6: shows the values obtained after fitting the experimental spectra recorded at different steps of the immunosensor fabrication. As observed from the table, the R_s and the W_s remains variant through the modification steps TGA-OsTe$_2$ QDs|OvoxPpy|GCE, electrode after incubation with the antibody and the electrode after blocking with BSA. The C_{dl} depends highly on the dielectric and the insulating features at the electrode or electrolyte interface on the electrode surface and on the thickness of the separating layer. The C_{dl} values indicate changes that occurred during electrode modification process. The bare GCE shows a lower C_{dl} value compared with the TGA-OsTe$_2$ QDs|OvoxPpy|GCE, whereas, it decreased again

after the incubation of the antibody onto TGA-OsTe$_2$ QDs|OvoxPpy|GCE. Upon the blocking of unspecific bindings by BSA onto anti-PSA-antibody|TGA-OsTe$_2$ QDs|OvoxPpy|GCE the C_{dl} value increased again.

The R_{ct} is considered to be the most suitable parameter to be used for sensing the interfacial properties of the immunosensor during fabrication procedure. From Table 7, the bare GCE appears to have high R_{ct} value (1.9079 x 10^6 k Ω) but drastically decreased to 1.804 x 10^4 kΩ after the formation of TGA-OsTe$_2$ QDs|OvoxPpy|GCE. After immobilizing the antibody on to TGA-OsTe$_2$ QDs|OvoxPpy|GCE, the R$_{ct}$ value increased to 2.8403 x 10^5 kΩ as a result of blocking the electrode surface with the antibody molecules. These changes in Rct value strongly shows a successful elaborating of the immunosensor starting from the self assembles monolayer formation to antibody immobilization.
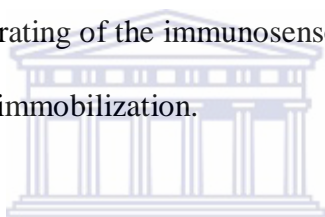
Table 7. Simulated values of all elements in the Randles equivalent circuit for the stepwise fabrication of immunosensor.

Electrode	R_{ct} (kΩ)	C_{dl} (μF)	R_s (kΩ)	W_s (kΩ s$^{-0.5}$)
Bare GCE	1.908 x 10^6	4.970 x 10^{-7}	2.226 x 10^3	3.672 x 10^3
TGA-OsTe$_2$ QDs|OvoxPpy|GCE	1.804 x 10^4	8.45 x 10^{-6}	8.442 x 10^2	1.03 x 10^5
Anti-PSA-antibody|TGA-OsTe$_2$ QDs|OvoxPpy|GCE	2.8403 x 10^5	2.876 x 10^{-6}	2.577 x 10^3	1.960 x 10^6
BSA-Anti-PSA-antibody|TGA-OsTe$_2$ QDs|OvoxPpy|GCE	2.754 x 10^4	5.103 x 10^{-6}	1.676 x 10^3	3.2826 x 10^5

The kinetic parameters of the electron transfer such as frequency at maximum imaginary impedance (ω_{max}), time constant (τ), exchange current (I_o) and the heterogeneous rate constant (k_{et}) were calculated according to equations 24, 25, 26 and 27. From Table 8, it is observed that the bare GC electrode has lower exchange current (1.345×10^{-5} A) compare to the modified electrode TGA-OsTe$_2$ QDs|OvoxPpy|GCE with 7.116×10^{-3} A. A high exchange current at the modified electrode indicate that there is an increase in electron transfer. The exchange further decreased after incubation of the antibody on the surface of TGA-OsTe$_2$ QDs|OvoxPpy|GC electrode suggesting a slower electron transfer between the electrode surface and the electrolyte. The Table also indicates that TGA-OsTe$_2$ QDs|OvoxPpy|GCE has a low time constant 1.5×10^{-2} s rad^{-1} compared to anti-PSA-antibody|TGA-OsTe$_2$ QDs|OvoxPpy|GCE (8.1×10^{-2} s rad^{-1}). This indicates that TGA-OsTe$_2$ QDs|OvoxPpy|GCE had faster kinetics before incubation. To better visualize the whole frequency range, the measured impedance data was plotted in Bode plot diagrams (Figure 25).
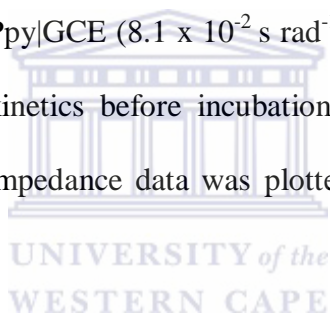
Table 8. Kinetic parameters of the immunosensing system

Electrode	ω_{max} (rad s^{-1})	τ (s rad^{-1})	I_o (A)	k_{et} (cm s^{-1})	F_Φ (Hz)
Bare GCE	1.0545	9.483×10^{-1}	1.345×10^{-5}	4.649×10^{-8}	1.38×10^{2}
TGA-OsTe$_2$ QDs|OvoxPpy|GCE	6.667×10^{2}	1.5×10^{-2}	7.116×10^{-3}	1.229×10^{-5}	1.00×10^{2}
Anti-PSA-antibody|TGA-OsTe$_2$QDs|OvoxPpy|GCE	1.2346×10^{2}	8.1×10^{-2}	4.520×10^{-4}	7.807×10^{-7}	5.35×10^{-1}
BSA-Anti-PSA-antibody|TGA-OsTe$_2$ QDs|OvoxPpy|GCE	7.1428×10^{2}	1.4×10^{-2}	4.662×10^{-3}	5.449×10^{-6}	7.149
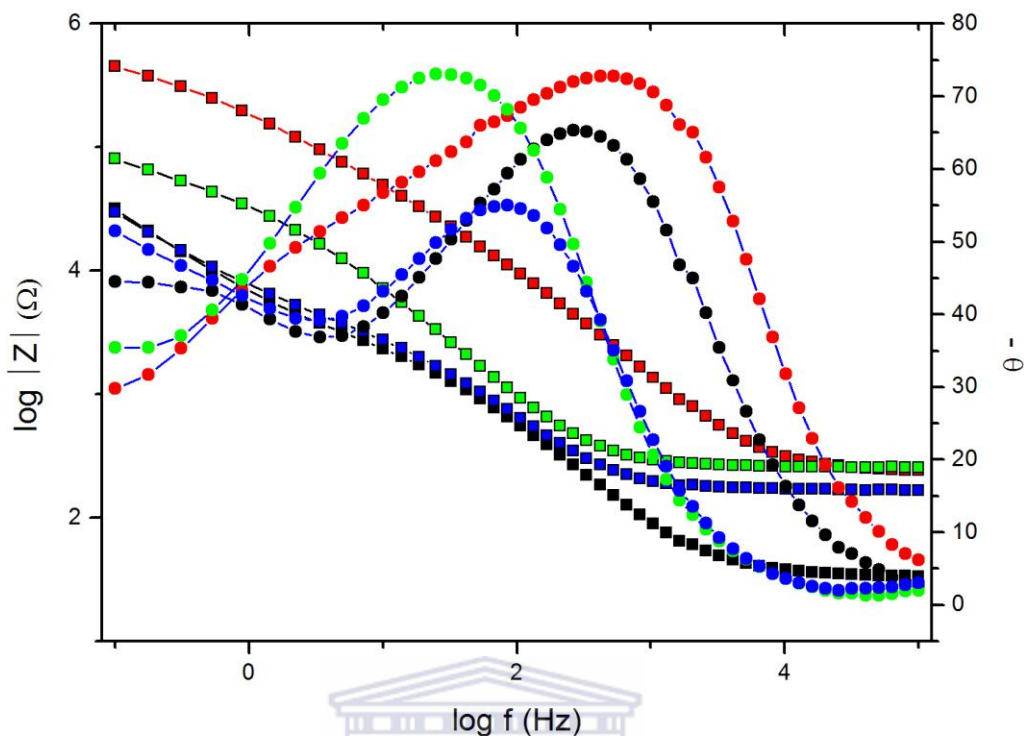
Figure 25. Bode plots of the immunosensing processes measured for each incubation step. Measurements were performed in 0.1 M PBS at 100 mHz to 100 kHz. (Red, black, blue and green colours are for bare GCE, TGA-OsTe$_2$ QDs|OvoxPpy|GCE, Anti-PSA-antibody|TGA-OsTe$_2$ QDs|OvoxPpy|GCE and BSA-Anti-PSA-antibody|TGA-OsTe$_2$ QDs|OvoxPpy|GCE, respectively).

5.2 Selectivity of the developed immunosensor

Selectivity of the proposed immunosensor against non-specific antigen was investigated to confirm that the detected changes are only due to the specific interaction between anti-PSA antibody modified electrode surface and its specific PSA. Figure 24 (d) shows that the R$_{ct}$ changes upon binding BSA to the immunosensor. The slight decrease in the R$_{ct}$ upon immobilizing BSA on the anti-PSA antibody modified electrode indicates that there was no cross-reaction between the anti-PSA antibody and the BSA. The results shows that the recorded impedance changes reflects only the interaction of the antibody and the PSA, the

immunosensor has high selectivity for the detection of PSA in 0.1 M PBA (pH 7.0) and the variation of the impedance as reported in Figure 26, is related to the formation of a specific immunocomplex between the anti-PSA antibody modified electrode and PSA.

After successfully developing the immunosensor as indicated by CV and EIS, it was immersed into 0.1 M PBS solution containing different concentrations of PSA ranging from 0 fg mol^{-1} to 4.207 fg mol^{-1} at room temperature for 1hrto allow antibody-antigen interaction. The immunoreactions between anti-PSA-antibody and the PSA were monitored by impedance spectroscopy in 0.1 M PBS (pH 7.0). Figure 26 shows impedance spectra obtained after immersing the electrode in different concentrations. The R_{ct} depicted in the Nyquist plots increases with PSA concentration, indicating that as the amount of PSA is bound to the antibody modified electrode surface, a large electron transfer resistance will be observed and thus stronger blocking the electron transfer between PBS and the electrode surface. The limit of detection was estimated to be 0.3 fg ml^{-1}. The calibration curve resulting from the R_{ct} values determined at different concentrations of PSA solutions is shown in Figure 27. The linear relation between the R_{ct} values and different PSA concentrations exhibited a linear relation with linear regression equation R_{ct} (kΩ) = -0.0032 (fg ml^{-1}) + 0.812 (correlation coefficient R^2 = 0.9982) suggesting that bonding of PSA with anti-PSA antibody modified electrode was diffusion controlled.
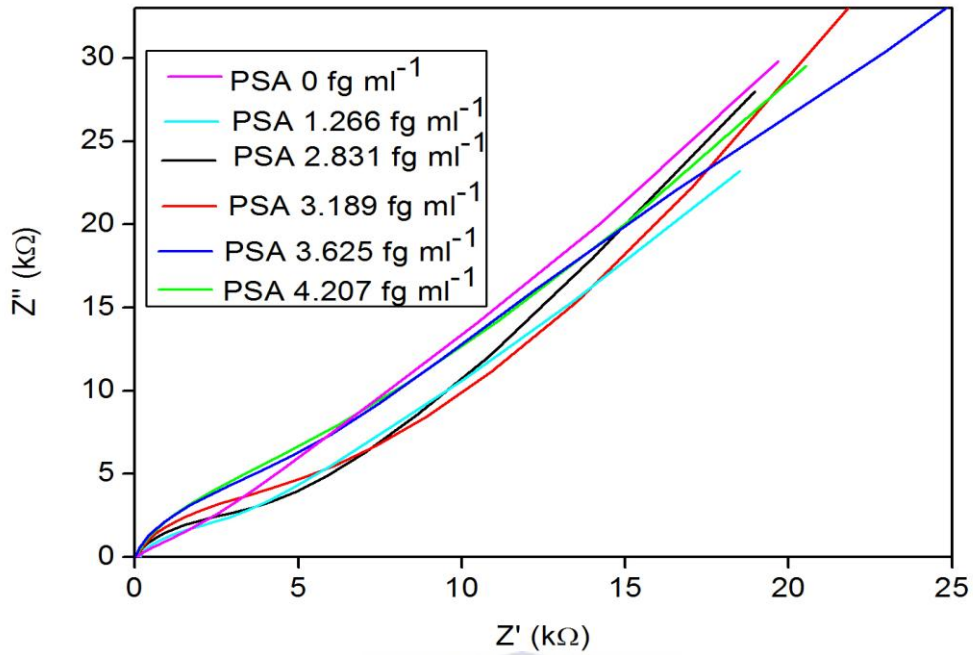
Figure 26: Nyquist plots for the PSA immunosensor. Measurements were performed in 0.1 M PBS at 100 mHz to kHz.

Table 9. Simulated values of all the elements of the Randles equivalent circuit for the PSA detection.

PSA concentration (fg ml^{-1})	R_{ct} (kΩ)	C_{dl} (µf)	R_s (kΩ)	W_s (kΩ s$^{-0.5}$)
0	8.8879 x 10^{-1}	5.103 x 10^{-6}	1.676 x 10^2	5.2826 x 10^5
1.266	4.069 x 10^4	3.904 x 10^{-6}	7.279 x 10^1	6.5811x 10^5
2.831	5.674 x 10^4	3.614 x 10^{-6}	8.939 x 10^1	9.1685 x 10^5
3.189	5.974 x 10^4	3.565 x 10^{-6}	8.948 x 10^1	1.018 x 10^5
3.625	5.917 x 10^4	3.465 x 10^{-6}	9.326 x10^1	1.076 x 10^5
4.207	5.929 x 10^4	1.040 x 10^{-5}	4.907 x 10^1	9.3118 x 10^5

Figure 27: Calibration curve for PSA immunosensor

5.3 Stability of the developed PSA immunosensor.

To check the stability of the proposed PSA immunosensor, the anti-PSA antibody modified electrode was stored at 4℃ for 7 days and tested in 0.1 M PBS (pH 7.0) each day. Over this storage period, the immunosensor kept its 75 % of its initial response indicating that the activity of the immobilized anti-PSA antibody was retained. The stability of the immunosensor was due to the covalent bond formed between the antibody molecule and polymer nanocomposite modified electrode. The impedance of the modified electrode gradually decreases after storage due to the deactivation of the anti-PSA antibody as it is considered unstable when stored [153].
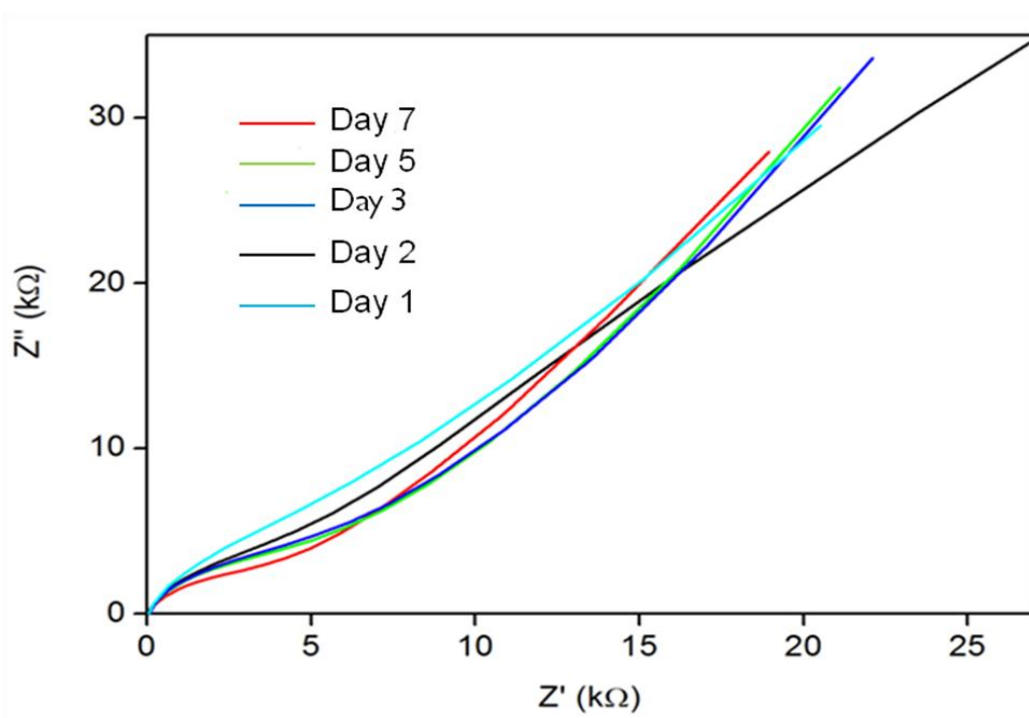
Figure 28. Responses of the PSA immunosensor over a period of one week.

$Y = -0.5811x + 7.655$

$R^2 = 0.9938$
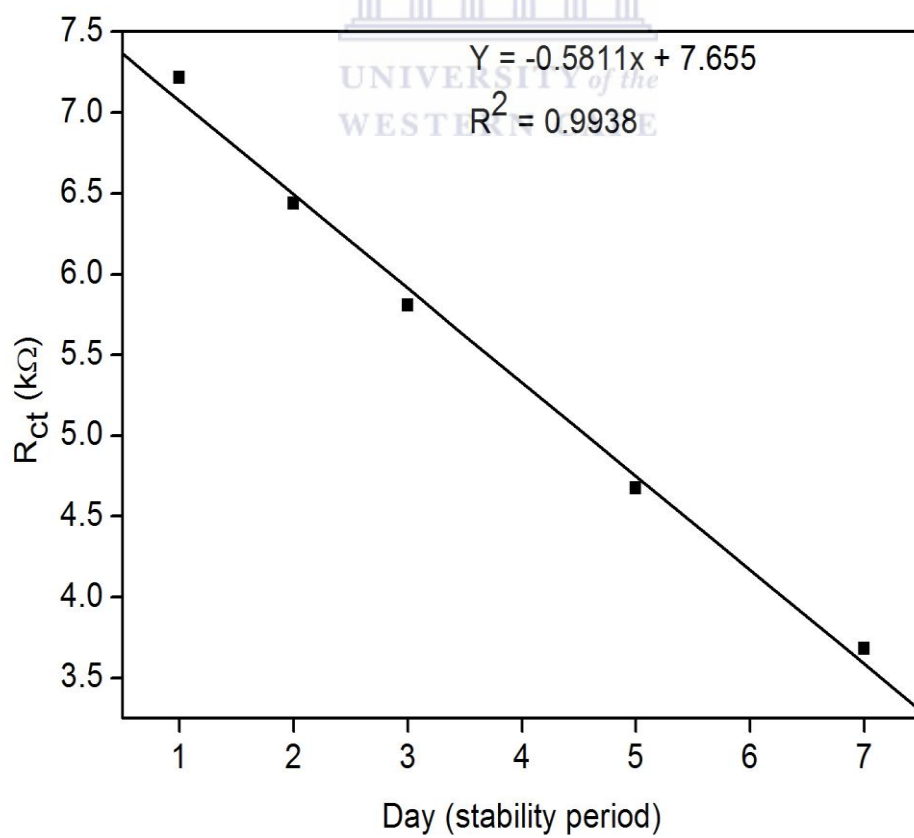
Figure 29. Response stability of the PSA immunosensor.

CHAPTER 6

6.0 Conclusion and recommendations

6.1 Conclusions.

Recently, quantum dots have been proposed as plausible theranostic nanomaterials. In this study, a simple and novel label-free electrochemical immunosensor for the ultrasensitive detection of PSA has been developed and characterized. Highly stable and well dispersed TGA-OsTe$_2$ QDs were successfully prepared by reacting NaHTe and CH$_2$COOHS-Os. In recent years, researchers have developed different types of water soluble QDs that are used in the detection of PSA, namely: CdSe|ZnS and Cu-InS$_2$ QDs to name a few. To our knowledge, OsTe$_2$ QDs are the newly developed (first of its kind) QDs from group 8 transition metal. Due to high surface-to-volume ratio, electro-catalytic activity, good biocompatibility and novel electron transfer properties, TGA-OsTe$_2$ QDs proved to be suitable for PSA immunosensor construction. The prepared quantum dots were characterized by optical absorption spectroscopy and HR-TEM. Compared to traditional organic dyes and Fluorophores, TGA-OsTe$_2$ QDs are superior in fluorescence brightness, tunable fluorescence emission and resistance to photobleaching. They are excited by single light source and absorb energy within narrow emission spectra with different colors. Overoxidized-polypyrrole was synthesized and characterized by electrochemical methods. The nanoporous overoxidized-polypyrrole proved to be an excellent template for the deposition of TGA-OsTe$_2$ quantum dots, which formed a nanocomposite electrode sensor, TGA-OsTe$_2$QDs|OvoxPpy|GCE, with antifouling properties. The sensor electrode exhibited strong electrocatalytic activity towards the detection of PSA.

The Anti-PSA-antibody|TGA-OsTe$_2$QDs|OvoxPpy|GCE bioelectrode exhibits linear behaviour in PSA concentration range of 1.266 fg ml^{-1} to 4.207 fg ml^{-1} with detection limit of 0.3 fg ml^{-1}. This detection limit is an order of magnitude lower than the most sensitive commercially available PSA ELISA kit (0.2 ng ml^{-1}) on the market with dynamic linear range of 0 nm ml^{-1} to 50 ng ml^{-1}. When relating the dynamic linear range from the PSA ELISA kit with prostate cancer stages the following was obtained:

Table 10. PSA ELISA dynamic linear rage for different prostate cancer stages

ELISA dynamic linear range (ng ml^{-1})	Prostate cancer stage
0.2 – 2	I
2 – 3.9	II
≥ 4	III

When comparing the dynamic linear range of the fabricated immunosensor with that of the ELISA, the fabricated immunosensor had the lowest dynamic linear range and proved to be able to detect prostate cancer at an early stage (beginning of stage I). The average analysis time of 30 min is shorter than commercial ELISA (at least 2 h). Compared to recently developed immunosensor, the proposed immunosensor showed high sensitivity of 9.7 μA ng^{-1}. The biocompatible and high catalytic properties of TGA-OsTe$_2$ QDs enhanced the sensitivity of the immunosensor. Consequently, the proposed PSA immunosensor exhibited an excellent stability (75%) and reproducibility over a period of a week. The immunosensor can be used successfully for detection of other biomarkers such as alpha-fetoprotein (liver cancer) and carcinoma antigen 125 (ovarian cancer) and can serves as a valuable tool for clinical cancer diagnostics.

6.2 Outlook for the future

➢ My thesis opens up an entirely new approach in the application of electroanalytical techniques for the detection of PSA by using polymers coupled to quantum dots. Though $OsTe_2$ quantum dots were used for this work, future work is to further establish how other quantum dots would behave is worthwhile.

➢ Chemical methods were used to synthesize quantum dots. For future work, the use of green nanotechnology to synthesize quantum dots will be worthwhile.

➢ New optical and electrochemical approaches have been designed to detect PSA at or below normal (≥ 4 ng ml^{-1}). Most of these approaches which have been validated against cancer patient samples, they have good sensitivity and accuracy for clinically important PSA levels. However, an extensive PSA testing will be necessary on patient samples such as serum or saliva to establish the reliability of clinical sensitivity and selectivity.

➢ A simple, sensitive and reliable detection protocols with microfluidics or other sample handling technologies seem to be necessary for future step to reach point-of-care devise.

References

[1]. Feng D., Lu X., Dong X., Ling Y., Zhang Y. Label-free electrochemical immunosensor for the carcinoembryoic antigen using a glassy carbon electrode modified with electrodeposited Prussian Blue, a graphene and carbon nanotube assembly and an antibody immobilized on gold nanoparticles . *Microchimica Acta*.180:767-774 (2013).

[2]. Ramanaviciene A., Ramanavicius A. Application of polypyrrole for the creation of immunosensor. *Critical Reviews in Analytical Chemistry*.32:245-252 (2002).

[3]. Wang J.J., Myung N.V., Yun M., Monbouquette H.G. Glucose oxidase in polypyrrole on high-surface –area Pt electrodes: a model platform for sensitive electroenzymatic biosensors. *Journal of Electroanalytical Chemistry*. 575:139-146 (2005).

[4]. Chu X, Duan D.X., Shen G.L., Yu R.Q. Amperometric glucose biosensor based on electrodeposition of platinum nanoparticles onto covalently immobilized carbon nanotube electrode. *Talanta*. 71:2040-2047 (2007).

[5]. Liu S., Wollenberger U., Katterle M., Scheller F.W. *Sensors and Actuators B: Chemical*. 113:623-629 (2006).

[6]. Rau J.R., Chen S.C.,Sun H.W. Characterization of a polypyrrole microsensor for nitrate and nitrite ions. *Electrochimica Acta*. 39:2773-2779 (1994).

[7]. Wang M., Wang L., Wang G., Ji X., Bai Y., Li T., Gong S.,Li J. Application of impedance spectroscopy for monitoring colloid Au-enhanced antibody immobilization and antibody-antigen reactions. *Biosensors and Bioelectronics*. 19:575-582 (2004).

[8]. Rubinstein I. Physical Electrochemistry, *Marcel Dekker Inc*., New York (1995).

[9]. Wang L-X., Li X-G., Ynag Y-L. Preparation, properties and applications of pyrroles. *Reactive and Functional Polymers*. 47: 125-139 (2001).

[10]. Hossein E. Studying the characteristics of polypyrrole and its composite. *World Journal of Chemistry*. 2: 67-74 (2007).

[11]. Lee M-I., Kim S.S., Kang Y. Potential zero charge for polypyrrole. *Systematic Materials*. 101: 442-443 (1999).

[12]. Liu A.S., Oliveria M.A.S. Corrosion control of aluminum surface by pyrrole films: influence of electrolyte. *Material Research*. 10:205-209 (2007).

[13]Saville P., Faster T., Faster K. polypyrrole formation and uses. *Define Research and Development Canada-Atlantic*. 1-3 (2005).

[14]. RamanaviciusA., Finkelsteinas A., Cesiulis H., Ramanaviciene A. Electrochemical impedance spectroscopy of polypyrrole based electrochemical immunosensor. *Bioelectrochemistry*.79:11-16 (2010)

[15]. Khalkhali R.A. Effective of dopant on transport properties of polypyrrole conductive/electroactive polymer. *Asian Journal of Chemistry*.17:1449-1455 (2005).

[16]. Braun D. Electronic injection and conduction processes for polymer devices. *Journal of Polymer Science Part B: Polymer Physics*. 41: 2622 (2003).

[17]. Skotheim T.A., Reynolds J.R**.** "Theory of Conjugated Polymers", *Handbook of Conducting Polymers, Conjugated Polymers,* 3rd Edition*,* CRC Press, Taylor & Francis Group. p.1 (2007).

[18]. Özkorucuklu S.P., Şahin Y., Alsancak G. Voltammetric Behaviour of sulfamethoxazole on electropolymerized-molecularly imprinted overoxidized polypyrrole. *Sensors*. 8: 8463-8478 (2008).

[19]. Migdalshi J., Blaz T., Lewenstam A. *Analytica Chimica Acta*. 322 (1996).

[20].Gao Z., Zi M., Chen B. The influence of overoxidation treatment on the permeability of polypyrrole films. *Journal of Electroanalytical Chemistry*. 373 (1994).

[21]. Abate –Shen C., Shen M.M. Molecular genetics of prostate cancer. *Cancer Metastasis*. 20: 2410-2434 (2000).

[22]. Dong J.T. Chromosomal detection and tumor suppressor genes in prostate cancer. *Cancer Metastasis*.20: 173-93 (2001).

[23]. Shmid H.P., Prinkler L., Sturgeon C.M., Semjonow A. Diagnosis of prostate cancer-The clinical use of prostate specific antigen. *EAU Update Series*.1:3-8 (2003).

[24]. Abouelfadel Z., Miller G.J., Glode L.M., Akduman B., Donohue R.E., Nedrow A., Crawford E.D. High Gleason score and low prostate specific antigen levels in a single institution over the past decade. *Clinical Prostate Cancer*. 1: 115-117 (2002).

[25]. Ott J.J., Ullrich A., Miller A.B. The importance of early symptom recognition in the context of early detection and cancer survival. *European Journal of Cancer*. 45: 2743-2748 (2009).

[26]. Magi-Galluzzi C., Epstein J.I. Threshold for diagnosing prostate cancer over time. *Human Pathology*.34:1116-1118 (2003).

[27]. Hernandez D.J. Diagnosing Prostate Cancer: Getting to the Core Question. *Journal of Urology*. 190: 11-12 (2013).

[28]. Schröder F.H., Gosselaar C., Roemeling S., Postma R., Roobol M.J., Bangma C.H. PSA and the Detection of Prostate Cancer After 2005. Part I. *Eau-Ebu Update Series*.4: 2–12 (2006).

[29]. Rumaihi K.A., Jalham K.A., Younes N., Majzoub A.A., Shokeir A.A. The role of an abnormal prostate-specific antigen level and an abnormal digital rectal examination in the diagnosis of prostate cancer: A cross-sectional study in Qatar. *Arab Journal of Urology*.11:355-361 (2013).

[30]. Bandern.H., Trabulsi E.J., Kostakoglu L., Yao D., Vallabhajosula S., Smith-Jones P., Joyce M.A, Milowsky M., Nanus D.M., Goldsmith S.J. Targeting metastatic prostate cancer

with radiolabeled monoclonal antibody J591 to the extracellular domain of Prostate speficic membrane antigen. *Journal of Urology*. 170: 1717–1721 (2003).

[31].El-Shirbiny M.A. Prostate specific antigen. *Advances in Clinical Chemistry*. 31: 100-124 (1994).

[32]. Balk., Ko Y-J., Bubley G.J. Biology of prostate-specific antigen. *Biology of Neoplasia*. 21: 383-391 (2003).

[33].Kobayashi T., Kamato T., Isogawa Y., Kinoshita H., Terai A., Habuchi T., Ogawa O. Ratio of prostate specific antigen minor molecular forms-to-total prostate specific antigen is constant regardless of the pathological condition of the prostate. *Journal of Urology*. 169:121–124 (2003).

[34]. Okegawa T., Kato M., Nuthara K., Higashihara E. Prognostic value of three molecular forms of prostate specific antigen ratios in patients with prostate adenocarcinoma. *Urology*. 57: 936-942 (2001).

[35]. Roddama A.W., Duffy M.J., Hamdy F.C., Ward A.M., Patnick J., Price C.P., Rimmer J., Sturgeon C., White P., Allen N.E. Use of Prostate-Specific Antigen (PSA) Isoforms for the Detection of Prostate Cancer in Men with a PSA Level of 2-10 ng/ml: Systematic Review and Meta-Analysis. *European Urology*. 48: 386–399 (2005).

[36]. Hakimi A.A., Agalliu I., Ho G.Y., Ghavamian R., Yu C., Kattan M.W., Rabbani F. Detection of prostate cancer in an ethnically diverse, disadvantaged population with multiple prostate specific antigen measurements before biopsy. *Journal of Urology*. 187: 1234-1240 (2012).

[37]. Kollmeier M.A., Zelefsky M.J. How to select the optimal therapy for early-stage prostate cancer. *Critical Reviews in Oncology/Hematology*. 83: 225–234 (2012).

[38]. Josić D., Lim Y-P. Analytical and Preparative Methods for Purification of Antibodies. *Food Technology and Biotechnology*. 39: 215–226 (2001).

[39]. Kelley K.W., Lewin H.A. Monoclonal antibodies: Pragmatic application of immunology and cell biology. *Journal of Animal Science*. 63: 288-309 (1986).

[40]. Tang D., Yuan R., Chai Y., Zhang L., Zhong X., Liu Y., Dai J. Preparation and application on a kind of immobilization method of anti-diphtheria for potentiometric immunosensor modified colloidal Au and polyvinyl butyral as matrixes. *Sensors and Actuators B*: *Chemical.* 104:199–206 (2005).

[41]. Gao H., Lu J., Cui Y., Zhang X-X. Electrochemical immunoassay of estrone at an antibody-modified conducting polymer electrode towards immunobiosensors. *Journal of Electroanalytical Chemistry*. 592: 88-94 (2006).

[42]. Pampalakis G., Kelley S.O. An electrochemical immunosensor based on antibody-nanowire conjugates. *Supplementary Material (ESI) for Analyst*. 1-3 (2009).

[43]. Korri-Youssoufi H., Richard C.,Yassar A. A new method for the immobilisation of antibodies in conducting polymers. *Materials Science and Engineering C*. 15: 307-310 (2001).

[44]. Sadik O.A., Xu H. Differential impedance spectroscopy for monitoring protein immobilization and antibody-antigen reactions. *Analytical Chemistry*. 74: 3142-3150 (2002).

[45]. Hodneland C.D., Lee Y-S., Min D-H., Mrksich M. Selective immobilization of proteins to self-assembled monolayers presenting active site-directed capture ligands. *Proceedings of the National Academy of Science*. 5048–5052 (2002).

[46]. Balkenhohl T. Screen-printed electrodes as impedimetric immunosensor for the detection of anti-transglutaminase antibodies in human sera. *Analytica Chemica Acta*. 597:50-57 (2007).

[47]. Rebeski D.E., Winger E.M., Shin Y-K., Lelenta M., Robinson M.M., Vareeka R., Crowther J.R. *Journal of Immunoogical Methods*. 226: 85 (1999).

[48]. Kim J., Grate J.W., Wang P. Nanostructures of enzyme stabilization. *Chemical Engineering Science*. 61 (2006).

[50]. Salimi F., Negahdary M., Mazaheri G., Akbari-dastjerdi H., Ghanbari-kakavandi Y., Javadi S., Inanloo S.H., Mirhashemi-route M. H., Shokoohnia M.H., Sayad A. A novel alcohol biosensor based on alcohol dehydrogenase and modified electrode with ZrO_2 nanoparticles. *International Journal of Electrochemical Sciences*. 7: 7225 – 7234 (2012).

[51]. Monošík R., Streďanský M., Šturdík E. Biosensors — classification, characterization and new trends. *Acta Chimica Slovaca*. 5: 109-120 (2012).

[52]. Pohanka M., Skládal P. Electrochemical biosensors – principles and applications. *Journal of Applied Biomedical Materials*. 6: 57–64 (2008).

[53]. Streďanský M., Pizzariello A., Streďanská S., Miertuš S. Amperometric pH-sensing biosensors for urea, penicillin and oxalacetate. *Analytica Chimica Acta*. 415: 151–157 (2000).

[54]. Jaffrezic-Renault N., Dzyadevych S.V. Conductometric microbiosensors for environmental monitoring. *Sensors*. 8: 2569-2588 (2008).

[55]. Wang M., Cao L., Yan P., Wu N. Fabrication and modeling of ultrasensitive labelfree impedimetric immunosensor for IgG based on poly(o-phenylenediamine) film modified gold electrode. *International Journal of Electrochemical Sciences*. 7: 7927 – 7934 (2012).

[56]. Mostafa G.A.E. Electrochemical biosensors for the detection of pesticides. *The Open Electrochemistry Journal*. 2: 22-42 (2010).

[57]. Zayats M., Raitman O., Chegel V., Kharitonov A., Willner I. Probing antigen-antibody binding process by impedance measurements on ion-selective field-effect transistor devices and complementary surface Plasmon resonance analyses: development of cholera toxin sensors. *Analytical Chemistry*. 74: 4763-4773 (2002).

[58]. Corry B., Uilk J., Crawley C. Probing direct binding affinity in electrochemical antibody-based sensor. *Analytica Chimica Acta*. 496: 103-116 (2003).

[59]. Ding S-J., Chang B-W., Wu C-C., Lai M-F., Chang H-C. Electrochemical evaluation of avidin-biotin interaction of self-assembled gold electrodes. *Electro Chimica Acta*. 1-7 (2005).

[60]. Liu C-C. Electrochemical Sensors. Biomedical Engineering Handbook (second ed.). *Edison Sensor Technology Center*.49 (2000).

[61]. Hill H.A.O., Sanghera G.S (eds). Mediated amperometric enzyme electrodes. Biosensor: A practical approach (eds cass, A.E.G), *Oxford University* (1990).

[62]. Ghindilis A.L., Atanasov P., Wilkinst M.,Wilkins E. Immunosensors: electrochemical sensing and other engineering approaches. *Biosensors and Bioelectronics*.13: 113-131 (1998).

[63]. Ramanavicius A., Finkelsteinas A., Cesiulis H., Ramanaviciene A. Electrochemical impedance spectroscopy of polypyrrole based electrochemical immunosensor. *Bioelectrochemistry*. 79:11–16 (2010).

[64]. Oswald B., Lehman F., Simon L., Terpetsching E., Wolfbeis O.S. Red Laser-induced fluorescence energy transfer in an immunosystem. *Analytical Biochemistry*. 280 (2000).

[65]. Bruice T.C., Benkovic S.J. Chemical basis for enzyme catalysis. *Biochemistry*. 39: 6267-6274 (2000).

[66]. Huber R., Bannet Jr W.S., Schulz G.E. Enzymes as biological catalyst. *Biophysics*. 372-394 (1983).

[67]. Leger C., Bertrand P. Direct Electrochemistry of Redox Enzymes as a Tool for Mechanistic Studies. *Chemical Reviews*.108: 2379–2438 (2008).

[68]. EngvalleE., Perlmann P. Enzyme-linked immunosorbent assay, ELISA III. Quantitation of specific –antibodies by enzyme-labeled anti-immunoglobulin in antigen-coated tubes. *The Journal of Immunology*. 109:129-135(2013).

[69]. Desmyter A., Transue T.R., Ghahroudi M.A., Thi M-H.D., Poortmans F.,Hamers R., Muyldermans R., Wyns L. Crystal structure of a camel single-domain V_H antibody fragment in complex with lysozyme. *Nature Structural Biology*.3: 803 - 811 (1996).

[70]. Albert B., Bray D., Lewis J. et al. Molecular Biology of the cell. 3rd edition. New York: *Garland Science*. 357-389 (1994).

[71]. Reverberi R., Reverberi L. Factors affecting the antigen-antibody reaction. *Blood transfuse*.5:227-240 (2007).

[72]. Ghindilis A.L., Atanasov P., Wilkinst M.,Wilkins E. Immunosensors: electrochemical sensing and other engineering approaches. *Biosensors and Bioelectronics.* 13: 113-131 (1998).

[73]. Gizeli E., Lowe C.R. Immunosensors. *Current Opinion in Biotechnology*.7:66-71(1996).

[74]. Feng D., Lu X., Dong X., Ling Y., Zhang Y. Label-free electrochemical immunosensor for the carcinoembryonic antigen using a glassy carbon electrode modified with electrodeposited Prussian Blue, a graphene and carbon nanotube assembly and an antibody immobilized on gold nanoparticles. *Microchimica Acta*.180:767–774(2013).

[75].Jiang X., Li D., Xu X., Ying Y., Li Y., Ye Z., Wang J. Immunosensors for detection of pesticide residues. *Biosensors and Bioelectronics.* 23: 1577–1587 (2008).

[76]. Talekar S., Waingade S., Gaikwad V., Patil S., Negarekar N. Preparation and characterisation of cross-linked aggregates (CLEAs) of Bacillus anyloliquefaciens alpha amylase. *Journal of Biochemical Technology*. 3: 349-353 (2012).

[77]. Torres M.G., Foresti M.L., Ferreira M.L. Cross-limked enzyme aggregates (CLEAs) of selected lipases: a procedure for the proper calculation of their recovered activity. *AMB Express: A Springer Open Journal*. 3: 1-11(2013).

[78]. Malmiri H.J., Jahanian A.M.J., Berenjian A. Potential applications of chitosan nanoparticles as a novel support in enzyme immobilization. *American Journal of Biochemistry and Biotechnology*. 8 : 203-219 (2012).

[79]. Górecka E., Jastrzębska M. Immobilization techniques and biopolymer carriers. *Biotechnology and Food Science*. 75: 65-86 (2011).

[80]. Hezinger A.F.E., Teßmar J., Göpferich A. Polymer coating of quantum dots – A powerful tool toward diagnostics and sensorics. *European Journal of Pharmaceutics and Biopharmaceutics*. 68: 138–152(2008).

[81]. Hezinger A.F.E., Tebmar J., Gopferich A. Polymer coating of quantum dots- A powerful tool towards diagnostic and sensorics. European *Journal of Pharmaceutics and Biopharmaceutics*. 68: 138-152 (2008).

[82]. Jun Y-w., Koo J-E., Cheon J. One-step synthesis of size tuned zinc selenide quantum dots via a temperature controlled molecular precursor approach, *Chemical Communications*. 14: 1243–1244 (2000).

[83]. Chuan-Liang F., Xinhua Z., Martin S., Anne-Marie C., Jean-Pierre M., Wolfgang K. Graded-Bandgap quantum-dot-modified nanotubes: a sensitive biosensor for enhanced detection of DNA hybridization. *Advanced Materials*. 19: 1933–1936 (2007).

[84]. Li X., Zhou Y., Zheng Z. Glucose biosensor based on nanocomposite films of CdTe quantum dots and Glucose Oxidase. *Journal of American Chemical Society*. 25: 6580-6586 (2009).

[85]. Nikesh V. V., Mahamuni S. Highly photoluminescent ZnSe/ZnS quantum dots. *Semicondiconductor Science and Technology*. 16: 687–690 (2001).

[86]. Lin K.-F., Cheng H.-M., Hsu H.-C., Lin L.-J., Hsieh W.-F. Band gap variation of size-controlled ZnO quantum dots synthesized by sol–gel method. *Chemical Physics Letters*. 409:208–211 (2005).

[87]. Sharma I.D., Sharma V.K., Dhawan S.K., Saini P.K. Modification and designing of electrodeposited polypyrrole film for optoelectronic applications. *Indian Journal of Pure and Applied Physics*. 50: 184-187 (2012).

[88]. Signh K., Chauhan R., Solanki P.R., Basu T. Development of impedimetric biosensor for total cholesterol estimation based on polypyrrole and platinum nanoparticles multi layer nanocomposite. *International Journal of Organic Chemistry*. 4: 262-274 (2013).

[89]. Moon J-M., Kim Y.H., Cho Y. A nanowire-based label-free immunosensor: Direct incorporation of a PSA antibody in electropolymerized polypyrrole. *Biosensors and Bioelectronics*. 57: 157-161 (2014).

[90]. Brahim S., Wilson A.M., Narinesingh D., Iwuoha E., Guiseppi-Elie A. Chemical and biological sensors based on electrochemical detection using conductive electroactive polymers. *Microchimica Acta*. 143: 123-137 (2003).

[91]. Licona-Sanchez T. de J., Alvarez-Romero G.A., Mendoza-Huizar L.H., Galan-Videl C.A. Influence of the cation nature of the sulphate salt on the electrochemical synthesis of sulfate-doped polypyrrole. *International Journal of Electrochemical Sciences*. 6: 1537 – 1549 (2011).

[92]. Shin M.-C., Kim H.-S. Electrochemical characterization of polypyrrole/glucose oxidase biosensor:Part 1. Influence of enzyme concentration on growth and properties of the film. *Biosensors and Bioelectronics*. 11: 1-2(1996).

[93]. Chou N.H., Chou J.C., Sun T.P., Hsiung S.K. Differential type solid-state urea biosensors based on ion-selective electrodes. *Sensors and Actuators B*. 130: 359-366 (2008).

[94]. Diaz A.F., Castillo J.I., Logan J.A., Lee W.Y. Electrochemistry of conductive polypyrrole film. *Journal of Electroanalytical Chemistry*. 129:115- 129 (1981).

[95]. Walle J.L., Vergnolle N., Muscara M.N., Asfaha S., Chapman K., McKnight W., Del-Soldato P., Morelli A., Fiorucci S. Enhanced anti-inflammatory effects of a nitric oxide-releasing derivative of mesalamine in rats. *Gastroenterology*. 117: 557-566 (1999).

[96]. Grande H., Otero T.F., Rodriguez J. Optimization of electrical and redox properties of electrogenerated polypyrroles. *Electrical and Optical Polymer Systems: Fundamental, Method and Application*. 45(1998).

[97]. Bartlett P.W., Whitaker R.G., Electrochemical immobilisation of enzymes. Part II. Glucose oxidase immobilised in poly-N-methylpyrrole. *Journal of Electroanalytical Chemistry*. 224 (1987).

[98]. Detaxis Du Poet P., Miyamoto S. Enzyme Modified Electrodes in Amperometric Biosensors. *Analytica Chimica Acta*. 235 (1990).

[99]. Ugo P., Moretto L.M., Mazzocchin G.A., Guerriero P., Marlin C.R. Electrochemical preparation and characterization of an anion-permiselective composite membrane for sensor technology. *Electroanalysis*. 17: 1168-1173 (1998).

[100]. Arrigan D.W.M. Permiselective behaviour at overoxidized poly[1-(2-carboxyethyl) polypyrrole] films: Dopamine versus ascorbate. *Analytical Communications*. 34: 241-244 (1997)

[101]. Sasso L., Heiskanen A., Diazzi F., Dimaki M., Castillo-León J., Vergan M., Landini E., Raiteri R., Ferrari G., Carminati M., Sampietro M., Svendse W.E., Emnéus J. Doped overoxidized polypyrrole microelectrodes as sensors for the detection of dopamine released from cell populations. *Analyst*. 138: 3651-3659 (2013).

[102]. Hseu C.C., Brajter-Toth A. Electrochemical preparation and analytical applications of ultrathin overoxidized polypyrrole films. *Analytical Chemistry*. 66: 2458-2464 (1994).

[103]. Wang Y.L., Liu Y.S., Zhou L.Y. An alternative aqueous synthetic route to prepare CdTe quantum dots with tunable photoluminescence. *Chinese Chemical Letters*. 23: 359-362 (2012).

[104]. Sun Q., Fu S., Dong T., Liu S., Huang C. Aqueous synthesis and characterization of TGA-capped CdSe quantum dot at freezing temperature. *Molecules.* 17: 8430 – 8438 (2012).

[105]. Zheng S., Huang Y., Cai J., Guo Y. Nano-Copper-MWCNT – modified glassy carbon electrode for selective detection of dopamine. *International Journal of Electrochemical Sciences*. 8: 2296-12307 (2013).

[106]. Bhattacharjya D., Mukhopadhyay I. Controlled growth of polyaniline fractals on HOPG through potentiodynamic electropolymerization. *Langmuir*. 28: 5893-5899 (2012).

[107]. Zhang Z., Li J., Xu R., Xiao D. Electrochemical detection of dopamine in the presence of ascorbic acid using overoxidized polypyrrole/graphene modified electrode. *International Journal of Electrochemical Sciences*. 6: 2149-2161 (2011).

[108]. Mailu S.N., Waryo T.T., Ndangili P.M., Ngece F.R., Baleg A.A., Baker P.G., Iwuoha E.I. Determination of anthraces on Ag-Au alloy nanoparticles/overoxidized – polypyrrole composite modified glassy carbon electrodes. *Sensors*. 10: 9449-9465 (2010).

[109]. Gao X., Zhang Y., Wu Q., Chen H., Chen Z., Lin X. One step electrochemically deposited nanocomposite of chitosan-carbon nanotubes-gold nanoparticles for carcinoembryonic antigenimmunosensor application. *Talanta*. 85: 1980-1985 (2011).

[110]. Farghaly O.A., Hameed R.S.A., Abu-Nawwas A-A.H. Analytical application using morden electrochemical techniques. *International Journal of Electrochemical Sciences*. 9: 3287-3318 (2014).

[111]. Protti P. Amel Electrochemistry: Introduction to morden voltammetric and polarographic analysis techniques. *IV Edition*. 1-3 (2001).

[112]. Luo X., Davis J.J. Electrical biosensor and the label free detection of protein disease biomarker. *Chemical Society Reviews*. 42: 5944-5962 (2013).

[113]. Lee S-J., Pyum S-I. Transport behaviour of electroactive species in ionic compounds: A focus on Li diffusion through transition metal oxide in current flowing condition. *Journal of the Korean Electrochemical Society*. 12:1-10 (2010).

[114]. Brett C.M.A., Brett A.M.D. Electrochemistry: A molecular approach, Plenum Press, *New York and London* (1993).

[115]. Brockris J., Khan S.U.M. Surface electrochemistry: A molecular level approach, Plenum Press. *New York and London* (1993).

[116]. Kumar D.N.T Liu J. Dan T., Wei Q. Suggestion of cyclic voltammetry based electrochemical DNA analysis of DNA-Petrol interaction-novel approach in DNA damage analysis. *International Journal of Engineering Research and applications*. 2: 1111-1116 (2012).

[117].Suroviec A.H. Introduction of Electrochemistry. *Journal of Laboratory Chemical Education*. 3: 45-48 (2013).

[118].Hussam A. Voltammetry: Dynamic electrochemical techniques comprehensive analytical chemistry. 47: 661-689 (2006).

[119].Mirceski V., Guziejewski D., Lisichkov K. Electrode Kinetics measurements with square-wave voltammetry at a constant scan rate. *Electrochemica Acta*. 114: 667-673 (2013).

[120].Miles A.B., Comton R.G. The theory of square –wave voltammetry at uniformly accessible hydrodynamic electrodes. *Journal of Electroanalytical Chemistry*. 487: 75-89 (2000).

[121].Upstone S.L. Ultraviolet/visible light absorption spectrophotometry in clinical chemistry. Encyclopedia of Analytical Chemistry. *John Wiley & Sons Ltd., Chichester*. 1699-1714 (2000).

[122]. So P.T.C., Dong C.Y. Fluorescence spectrophotometry. *Encyclopedia of Life Sciences*. 1-4 (2002).

[123]. Hunag J., Cavanaugh T., Nur B. An introduction to SEM operational principle and geologic applications for shale hydrocarbon reservoirs. *The American Association of Petroleum Geologist.* 102: 1-6 (2013).

[124]. Nixon W.C. General principles of scanning electron microscopy. Philosophical Transactions of the Royal Society of London. *Biological Science.* 261: 45-50 (1971).

[125].Sahu R.K., Mordechai S. Fourier transform infrared spectroscopy in cancer detection. *Future Oncology*. 5: 635-647 (2005).

[126]. Aroui H, Orphal J.,Tchana F.K. Fourier transform infrared spectroscopy of the measurement of spectral line profiles. *Fourier Transform-Material Analysis*. 69-102 (2012).

[127]. Xiao Y., Li C.M., Liu Y. Electrochemical impedance characterization of antibody-antigen interaction with signal amplification based on polypyrrole-streptavidin. *Biosensors and Bioelectronics*. 22: 3161-3166 (2007)

[128]. Daniels J.S., Pourmaud N. Label-free impedance biosensor: Opportunities and challenges. *Electroanalysis*. 1-19 (2007).

[129]. Randviir E.P., Banks C.E. Electrochemical impedance spectroscopy: an overview of bioanalytical applications. *Analytical Methods*. 5: 1098-1115 (2013).

[130]. Muñoz-Berbel X., Godino N., Laczku O., Baldrich E., Muñoz F.X., Campo F.J.D. Impedance-based biosensor for pathogen detection. *Springer Science and Businesss Media, LLC*. 341-344 (2008).

[131].Zheng L., Wang Y.-X., Zhang G.-X., Han Y.-J.luminescent properties dependence of water-solutble CdTe quantum dots on stabilizing agents and reaction time. *Journal of Central South University of Technology*. 17:1148-1154 (2010).

[132].Moradian R., Elahi M., Hadizadeh A., Roshani M., Taghizadeh A.,Sahraei R. Structural, optical and electrical properties of thioglycolic acid-capped CdTe quantum dots thin film. *International Nano Letters*. 3: 1-6 (2013).

[133]. Mozafari M., Moztarzadeh F., Seifalian A.M., Tayebi L. Self-assembly of PbS hallow sphere quantum dots via gas-bubble technique for early cancer diagnosis. *Journal of Luminescence*.133:188-193 (2013).

[134]. Xie R., Li Y., Liu L., Yang L., Xiao D., Zhu J. Aqueous-based route toward Fe:ZnSe semiconductor nanocrystals: synthesis and characterization. *Material Characterization*. 62: 528-587 (2011).

[135]. Hasan Md.M., Hossain E.Md., Mamun M.A., Ehsan M.Q. Study of redox behaviour of Cd(II) and interaction of Cd(II) with proline in aqueous medium using cyclic voltammetry. *Journal of Saudi Chemical Society*. 16: 145-155 (2012).

[136].Rahman M.M., Jeon C.I. Studies of electrochemical behaviour of SWNT-film electrodes. *Journal of Brazilian Chemical Society*. 6:150-1157 (2007).

[137].Bardajee G.R., Hooshyar Z. Synthesis and fluorescence properties investigation of CdSe quantum dots embedded in a biopolymer based on poly(12-dimethyl-aminoethyl)methacrylate grafted onto k-carrogeenan. Colloids and surface A. *Physicochemical Engineering Aspects*. 387:92-98 (2011).

[138]. Oztekin Y., Tok M., Billici E., Mikoliunaite L., Yaziagil Z., Ramanaviciene A., Ramanavicius A. Copper nanoparticles modified carbon electrode for determination of dopamine. *Electrochemica Acta*. 105: 1-7 (2012).

[139]. Sanghari B.J., Kalambate P.K., Karna S.P., Srirastava A.K. Voltammetric determination of sumatriptan based on a graphene/gold nanoparticles/nafion nanocomposite modified glassy carbon electrode. *Talanta*. 120: 1-9 (2014).

[140]. Razavipanah I.,Rounaghi G.H., Zavvar M.H.A. A Glassy Carbon Electrode Modified by polypyrrole and platinum nanoparticles to enhance the catalytic oxidation of methanol. *Analytical Letters*. 47: 117–133 (2014).

[141]. Habelhames F., Nessark B., Girtan M. Electrosynthesis of organic-inorganic compounds (p-n heterojunction). *Material Science in Semiconductor Processing*. 13: 141-146 (2010).

[142]. Huang W., Hao Q., Lei W., Wu L., Xia X. Polypyrrole-hemin-reduce graphene oxide: rapid synthesis and enhanced electrocatalytic activity towards the reduction of hydrogen peroxide. *Material Research Express*. 1: 1-17 (2014).

[143]. Kaplin D.A., Qutubuddin S. Electrochemically synthesized polypyrrole films: effects of polymerization potential and electrolyte type. *Polymer*. 36:1275-1286 (1995).

[144]. Bard A.J., Faulkner L.R. Electrochemical Methods : Fundamentals and applications (2nd edition). Newyork, USA: *John Willey & Sons*, 2000.

[145]. Peik-See T., Pandikumar A., Nay-Ming H., Hong-Ngee L., Sulaiman Y. Simultaneous electrochemical detection of dopamine and ascorbic acid using an iron oxide/reduced graphene oxide modified glassy carbon electrode. *Sensors*. 14:15227-15243 (2014).

[146]. Paramo-Garcia V., Batina N., Ibanez J.G. The effect of pH on the morphology of electrochemically-grown polypyrrole films: An AFM study. *International Journal of Electrochemical Sciences*. 7: 12316-12325(2012).

[147]. Li J., Lin X. Simultaneous determination and serotonin on gold nanoclusters/overoxidized-polypyrrole composite modified glassy carbon electrode. *Sensors and Actuators B: Chemical.* 124: 486-493 (2007).

[148].Su C., Wang L., Xu L., Cheng Z. Synthesis of novel ferrocene-contained polypyrrole derivative and its performance as a cathode material for Li-ion batteries. *Electrochimica Acta*. 104: 302-307 (2013).

[149]. Kalantar-Dehnavi A., Rezaei-Zarchi S., Mazaheri Gh., Negahday M., Malekzadeh R., Mazdapour M. Designing a H_2O_2 biosensor by using modified electrode with nano-composite of nafion/nile blue peroxidise enzyme. *European Journal of Experimental Biology*. 2: 672-682 (2012).

[150]. Beck F., P.B., Oberst, M., Bunsenges Ber., Organic electrochemistry in the solid state-overoxidation of polypyrole. *Journal of Physical Chemistry*. 9: 967-974 (1987).

[151]. Akinyenye, R.O., Nanostructured polypyrrole impedimetric sensors for anthropogenic organic pollutants, unpublished PhD Thesis in Chemistry, University of the Western Cape, South Africa, 2008.

[152]. Mathebe N.G.R., Morrin A.,Iwuoha E.I. Electrochemistry and scanning electron microscopy of polyaniline/peroxidase-based biosensor. *Talanta*. 64: 115-120 (2004).

[153]. Elshafey R., Tlili C., Abulrob A., Tavares A.C., Zourob M. Label-free impedimetric immunosensor for ultrasensitive detection of cancer marker Murine double Minute 2 in brain tissue. *Biosensor and Bioelectronics*. 39: 220-225(2013).